

**Boston University**

**OpenBU**

**<http://open.bu.edu>**

---

Theses & Dissertations

Boston University Theses & Dissertations

---

2018

# Aspects of Higgs physics

---

<https://hdl.handle.net/2144/34770>

*Boston University*

2018

# Aspects of Higgs Physics

Pritchett, Lukas Tueller

---

*Boston University*

BOSTON UNIVERSITY  
GRADUATE SCHOOL OF ARTS & SCIENCES

Dissertation

**ASPECTS OF HIGGS PHYSICS**

by

**LUKAS TUELLER PRITCHETT**

B.S., Brigham Young University, 2013

Submitted in partial fulfillment of the  
requirements for the degree of  
Doctor of Philosophy

2018

© 2018 by  
LUKAS TUELLER PRITCHETT  
All rights reserved

Approved by

First Reader

---

Kenneth D. Lane  
Professor of Physics

Second Reader

---

Andrew Liam Fitzpatrick  
Assistant Professor of Physics

*O be wise; what can I say more?*  
The Book of Mormon — Jacob 6:12

## Acknowledgments

I would first like to thank my adviser, Kenneth Lane. I hoped from the start that I would be able to learn his dedication to thinking about experiments before anything else, and I like to think that I have. I thank him for every argument that he won; I learned something from every one.

I would also like to thank Liam Fitzpatrick for reading this dissertation, and thanks to the rest of my committee, Chris Laumann, Chris Grant, and Claudio Chamon, who helped so graciously at the last minute.

Thank you to Ami Katz for his quantum field theory courses that pushed me to my limit and beyond, to Martin Schmaltz for keeping an eye on me, and the rest of the High Energy Theory group. I also thank Kevin Black, for helping me navigate my final few semesters. Without Mirtha Cabello I couldn't have made it at all, so unlimited thanks to her. Thank you to Manher Jariwala and Nicholas Gross for helping me into the wider world of teaching. Thanks to Manher for giving me the best assignments, and to Nick for giving me free rein to experiment and have fun.

Thanks to Evan Weinberg for always knowing the right time to slack off, and thank you to Manuel Buenabad Najar for many hours of discussion both enlightening and entertaining.

Finally, without my family all of this would be meaningless. Thank you to my parents for showing me both the importance of education and how to use it for good. Thank you to Simon for helping me remember what is most important. And most importantly, thank you to Emily for making these past five years the best of my life.

Lukas Pritchett

# ASPECTS OF HIGGS PHYSICS

LUKAS TUELLER PRITCHETT

Boston University, Graduate School of Arts & Sciences, 2018

Major Professor: Kenneth D. Lane, PhD  
Professor of Physics

## ABSTRACT

The Higgs sector is the collection of fields and particles responsible for the spontaneous symmetry breaking of the electroweak symmetry. It is the keystone of the Standard Model of particle physics. While the Standard Model Higgs sector is in agreement with current experiments alternative models often arise to explain experimental anomalies, or to answer puzzles about the Higgs model itself. In this dissertation I explore two such alternative models of the Higgs sector. The first is a model of a composite Higgs boson that is designed to be “minimally fine-tuned.” I demonstrate how it generates a light Higgs boson with one fine-tuned parameter. The most accessible expected phenomenological signatures of such a model are heavy resonances decaying into weak vector bosons. I compare the predicted behavior of these resonances to recent experiments at the Large Hadron Collider. The second is alternative model attempts to use multiple Higgs to explain a possible 30 GeV resonant excess in dimuon production arising from  $Z$  boson decays. I show that the simplest such model cannot explain the excess, and then argue that all such multiple-doublet models also fail.



# Contents

<b>1</b>	<b>A Composite Higgs Model</b>	<b>1</b>
1.1	Fine-tuning and Renormalization . . . . .	1
1.1.1	Fine-tuning in the Standard Model . . . . .	3
1.2	A Fine-Tuned Composite Model . . . . .	5
1.2.1	Renormalization group analysis and fine-tuning . . . . .	7
1.3	Our new model . . . . .	12
1.3.1	Introduction and UV perspective . . . . .	12
1.3.2	Technicolor interactions . . . . .	17
1.4	Renormalization . . . . .	24
1.4.1	Degrees of freedom and running couplings . . . . .	24
1.4.2	Renormalization group equations . . . . .	26
1.4.3	Mass thresholds . . . . .	34
1.4.4	Running technicolor coupling . . . . .	36
1.5	Renormalization group results . . . . .	38
<b>2</b>	<b>Composite Higgs Phenomenology</b>	<b>41</b>
2.1	Diboson Excesses . . . . .	41
2.2	Other Technicolor States . . . . .	44
2.2.1	Isovectors . . . . .	46
2.2.2	Decays . . . . .	47
2.3	Effective theory for vector mesons . . . . .	48
2.4	Predictions . . . . .	50

2.4.1	Decays . . . . .	50
2.4.2	Production Mechanisms . . . . .	51
2.4.3	Comparison to experiment . . . . .	53
2.4.4	Other signatures . . . . .	55
<b>3</b>	<b>Alternative Higgs Models for a Dimuon Excess</b>	<b>57</b>
3.1	Excess at LEP . . . . .	57
3.1.1	The excess . . . . .	57
3.1.2	Other channels . . . . .	60
3.2	Scalars and Multiple Higgs Doublet Models . . . . .	63
3.2.1	General Multiple Higgs Doublet Models . . . . .	65
3.2.2	Fermion Couplings and the Glashow-Weinberg Theorem . . . . .	67
3.3	Two Higgs Doublet Model – An Instructive Warm-up . . . . .	68
3.3.1	Replicating the signal . . . . .	73
3.3.2	Charged Higgs Decays . . . . .	76
3.4	Three Higgs Doublet Model — Trouble with Triples . . . . .	79
3.4.1	Yukawa couplings and signal . . . . .	83
3.4.2	The charged scalars . . . . .	85
3.4.3	The neutral scalars . . . . .	87
3.5	Conclusions . . . . .	91
	<b>References</b>	<b>94</b>
	<b>Curriculum Vitae</b>	<b>99</b>

# List of Tables

1.1	The predicted masses of the model of Bardeen et al. (Bardeen et al., 1990), where the Higgs boson is a composite of the top quark. It requires very large values of the cutoff $\Lambda$ to produce result even close to realistic. . . . .	11
1.2	Unrenormalized mass values in the ETC-only scheme for two ETC cut-off scales $\Lambda = 20$ TeV and 500 TeV. The pole value of $m_H$ is different due to renormalization, but we cannot say how much without including TC dynamics. Compare to the results of the BHL model in table 1.1	17
1.3	Masses of the fermions and the Higgs boson with $\Lambda_{TC} = 1$ TeV and $\alpha_{TC,IR} = 1.5\alpha_c$ . Compare to table 1.2, which lists the same masses computed without renormalization or TC effects. At $\Lambda_{TC} = 1$ TeV the Higgs mass is unchanged, but both $m_t$ and $m_U$ are raised. . . . .	40
2.1	The significance for a $\sim 2$ TeV excess in each channel as reported by each experiment from Run 1, $\sqrt{s} = 8$ TeV data. The ATLAS significance in the $WH \rightarrow \ell\nu b\bar{b}$ channel is from preliminary Run 2 data. The reported significances are found in the papers cited in the text. . . . .	43
2.2	Principal decay rates of the $\rho_H$ and $a_H$ for $g = 3.862$ and $M_{a_H} = 1.05M_{\rho_H}$ . The width of the the bosons is generically about 10% for this value of $g_T$ . The width varies as $g_T^2$ for fixed $M_{\rho_H}$ . . . . .	51

2.3	Production cross sections at the LHC of the isovector bosons $\rho_H$ and $a_H$ with $\sqrt{s} = 8$ TeV for $g_T = 3.862$ and $M_{a_H} = 1.05M_{\rho_H}$ . The individual DY + VBF contributions are given for $\rho_H$ ; The VBF rates for $a_H$ are very small and not given. As explained in the text, $g_T = 2.73$ gives 75% large cross sections and widths half as large for $\rho_H \rightarrow VV$ . No $K$ -factor has been applied. . . . .	52
2.4	Production cross sections at the LHC of the isovector bosons $\rho_H$ and $a_H$ with $\sqrt{s} = 13$ TeV for $g_T = 3.862$ and $M_{a_H} = 1.05M_{\rho_H}$ . The individual DY + VBF contributions are given for $\rho_H$ ; compare to table 2.3. . . .	52

# List of Figures

1.1	Diagrams that lead to quantum corrections to $m_\phi^2$ in the $\phi^4$ theory of equation 1.1. The corrections are shown up to two-loops, and second order in the coupling constant $\lambda$ . . . . .	2
1.2	The dominant one-loop contributions to the Higgs boson mass corrections. Each diagram contributes to the quadratic divergence $c_H \Lambda^2$ . The top loop dominates the other is stronger than the other fermion loops by a factor of at least $m_t^2/m_b^2$ . . . . .	3
1.3	The Schwinger-Dyson equation for the top mass in the model of Bardeen, Hill, and Lindner. The four-fermion interaction is able to create a mass for the fermion without an explicit mass term. . . . .	6
1.4	The one loop diagrams that make up the $\bar{t}t$ (and $\bar{U}U$ ) propagator in the scalar channel, including only ETC interactions. Both propagators include contributions from both $t$ and $U$ loops. We will include the TC interactions later on. . . . .	14
1.5	The technicolor interaction modifies the four-fermion kernel by adding TC-gluon exchange diagrams. . . . .	18
1.6	The behavior of $\Sigma(0)$ as a function of $\lambda = G\Lambda^2$ in the model of Takeuchi, extended to a more realistic TC $\beta$ function. At a critical value of $\lambda$ , $\Sigma(0)$ jumps from a very small scale to $\mathcal{O}(\Lambda)$ . . . . .	20

1.7	The beta function for $y_t^2$ , in the approximation that the SM gauge couplings do not run, and ignoring TC contributions. There is a fixed point at zero, and one non-zero fixed point. The non-zero fixed point is attractive as $y_t$ runs down to IR scales from $y_t(\Lambda) \gg 4\pi$ . The value of the non-zero fixed point is determined by the strength of the QCD gauge coupling, $g_3$ . . . . .	28
1.8	A figuring detailing which fixed point is dominant for different values of the gauge couplings $\alpha_3$ and $\alpha_{TC}$ . For large $\alpha_{TC}$ the $y_t = 0$ fixed point is overall attractive, but for small $\alpha_{TC}$ the $y_U = 0$ fixed point dominates. . . . .	31
1.9	An illustration of how solutions to the full beta functions undershoot the fixed point values. We have chosen a constant $\alpha_{TC}$ so that the $y_t \neq 0$ fixed point is overall attractive. Both $y_t(\mu)$ and $\lambda(\mu)$ undershoot their non-zero fixed point values before running back up. This lowers the resulting masses relative to the fixed point predictions. . . . .	32
1.10	Another illustration of the undershoot effect. Compare to figure 1.9. The mass of each particle is the scale where the black curve meets its associated running mass. In this figure $m_t$ and $m_H$ are lower than if their running masses ran straight to their fixed-point values. . . . .	33
1.11	The running Yukawa couplings when $\alpha_{TC}$ runs like a step function; $\alpha_{TC}$ is constant and weak in the UV until $\Lambda_{TC}$ , at which point it jumps up to a constant greater than $\alpha_c$ . This causes the dominant fixed point behavior to switch, potentially further lowering the masses relative to their fixed point values. . . . .	35

1.12	The running masses when $\alpha_{TC}$ runs like a step function; compare to figure 1.11. The particle masses are the points where the black curve intersects the running mass curve. . . . .	35
1.13	The results of the RG analysis outlined in section 1.4, showing the masses of the top quark, $U$ technifermion, and the Higgs boson as they depend on $\alpha_{TC,IR}$ (right column), $\Lambda_{TC}$ (left column), and $d_{TC}$ (rows). The colored bands show the variation of each mass as $\Lambda$ is varied between 100 and 10,000 TeV. For almost all cases $m_h$ is between 200 and 400 GeV, and $m_t$ is less than 200 GeV. The lowest values of $m_h$ occur when $d_{TC}$ is large. Increasing $\Lambda$ tends to lower the masses slightly. . . . .	39
2.1	Limits on cross-sections published by ATLAS and CMS from Run 1 data in various channels. A $\sim 2\sigma$ excess is visible around 2 TeV in each. The top row shows the $WZ$ channel with $WH$ in the bottom row. ATLAS data is on the left, CMS on the right. Figures are from the ATLAS and CMS papers cited in the text. . . . .	42
2.2	The two principal production mechanisms for $\rho_H$ and $a_H$ at the LHC. The Drell-Yan contribution (a) comes from the mixing of the $\rho_H, a_H$ with the weak current. The VBF vertex is the same that is used in calculating decay rates. Drell-Yan is the dominant channel for both $\rho_H$ and $a_H$ . . . . .	53
2.3	Production cross-sections for the isovectors with $m_{\rho_H, a_H} = 1800 - 2000$ TeV at $\sqrt{s} = 8$ TeV and 13 TeV. Compare to tables 2.3 and 2.4. The largest cross-sections are Drell-Yan production of $\rho^\pm$ , which decays to $W^\pm Z$ . . . . .	54

3·1	The $m_{\mu\mu}$ invariant mass distributions in the opposite sign muon channel (3·1a) and same sign muon channel (3·1b). The excess is visible at 30 GeV in the opposite sign channel, while none is visible in the same sign channel. This figure is from (Heister, 2016) . . . . .	58
3·2	ALEPH $Z \rightarrow \bar{b}b\mu^+\mu^-$ data with signal plus background model used to extract the 30 GeV signal parameters in Heister’s analysis. This figure is from (Heister, 2016). . . . .	59
3·3	The total dimuon momentum distribution in the low sideband, $2\sigma$ mass window, and high sideband (top, middle, and bottom, respectively). There is no apparent difference in the signal region, and all events have $ p  < 20$ GeV with most events having $ p  \lesssim 5$ GeV. This figure is courtesy of A. Heister, by private communication. . . . .	61
3·4	The angular distribution of the muons in the signal window (3·4a) and sidebands (3·4b). $\theta^*$ is the angle between the dimuon boost axis and the $\mu^-$ . Most events are in the $ \cos\theta^*  > 0.8$ “horns”. . . . .	62
3·5	The opposite-sign dimuon mass distribution in $Z \rightarrow \text{hadrons} + \mu^+\mu^-$ with the $b$ -tag inverted shows no visible evidence for an excess near 30 GeV; figure from (Heister, 2016). . . . .	62
3·6	An example of a lepton-flavor-violating decay of a $\tau$ lepton mediated by some scalar $\phi$ with flavor non-diagonal couplings. This particular decay has a measured width of $< 6.12 \times 10^{-20}$ GeV (Particle Data Group, 2016a), which puts constraints on $y_{\phi,\mu\mu} \times y_{\phi,e\tau}/m_\phi^2$ . Such considerations suggest that off-diagonal Yukawa couplings must be forbidden by a symmetry. . . . .	68



3·7	The possible channels for signal $Z \rightarrow b\bar{b}\mu\bar{\mu}$ events in the 2HDM, shown schematically (not all possible diagrams are included). We assume that only one of the new scalar particles has a mass of 30 GeV. The $Z \rightarrow Z^*h$ and $Z \rightarrow b\bar{b}$ amplitudes are too small to contribute to the observed signal branching ratio. Only the $Z \rightarrow h\eta$ channel . . . . .	73
3·8	An example of a $W^*$ decaying to four leptons through the charged higgs. Though the pairs of muons arising from the neutral scalar vertices may have invariant masses that do not pass the ATLAS cuts ( $50 < M_{\ell\ell} < 120$ GeV for at least one pair), other pairings may. There are enough events of this type that a significant number pass the cuts and constrain the 2HDM. . . . .	78
3·9	Constraints on $\theta_{\pm}$ from bounds on $Z$ decays for $\gamma = 0.5$ and $\beta = 0.1$ . The regions where three constraints are satisfied separately are shown; $B(Z \rightarrow 4\mu)$ must be less than $10^{-6}$ (green region), the signal branching ratio $B(Z \rightarrow 2b2\mu)$ must be in the range $1 - 9 \times 10^{-4}$ (blue region), and the total $Z$ branching ratio to new particles must be less than $9 \times 10^{-4}$ (yellow region). There are two small regions where all three constraints are satisfied. . . . .	84
3·10	The decay rates of a charged Higgs $h^+$ in the 2HDM with $m_{\eta} = 30$ GeV, $m_h = 60$ GeV, and $\beta$ chosen so that $h^+$ and $\eta$ both decay muons much more than other fermions. A charged Higgs heavier than 100 GeV or so decays mainly to a lighter scalar plus a $W$ boson, despite large muon Yukawa couplings. The situation in the 3HDM is similar for at least one charged scalar. . . . .	86

3.11	Bounds on $m_{h_2}$ and $m_{\eta_2}$ from the positivity and unitarity conditions on the 3HDM quartic couplings. Neither coupling can be much more than 100 GeV, putting both in reach of current experiments. The other model parameters used are the same as in figure 3.9 . . . . .	89
------	--	----

## List of Abbreviations

2HDM	.....	Two Higgs Doublet Model
3HDM	.....	Three Higgs Doublet Model
ETC	.....	Extended Technicolor
FCNC	.....	Flavor-changing Neutral Current
IR	.....	Infrared
LEP	.....	Large Electron-Positron Collider
LHC	.....	Large Hadron Collider
RG(E)	.....	Renormalization Group (Equation)
SM	.....	Standard Model
TC	.....	Technicolor
UV	.....	Ultraviolet

## Chapter 1

# A Composite Higgs Model

### 1.1 Fine-tuning and Renormalization

We specify a quantum field theory by choosing a set of fields and then writing down a Lagrangian, which is some function of the fields and their derivatives. Specifically, the Lagrangian is a sum of products of the fields, each of which comes with a coupling constant. For example, the mass term of the Higgs doublet is the term  $m^2 H^\dagger H$  where the coupling constant  $m^2$  is the square of the mass. A Yukawa coupling  $y H \bar{f} f$  is a term involving two fermion fields and one scalar field. The Yukawa coupling constant  $y$  measures the strength of the interaction between the scalar and the fermion, as might be measured in a scattering experiment. The Lagrangian is fully specified by choosing which terms to include and choosing specific values for the coupling constants.

In a classical theory the coupling constant in the mass term is the same as the physical mass one measures in experiments. In a quantum theory, however, the physical quantity is determined by the coupling constant plus quantum corrections that depend on all the other terms in the Lagrangian. One can understand as a result of the path-integral picture of quantum mechanics: transition amplitudes include contributions from the classical trajectories of the particles, but also from trajectories where the particles interact with each other in every possible way as they propagate.

As a concrete example we can consider a theory with a single scalar field  $\phi(x)$  and

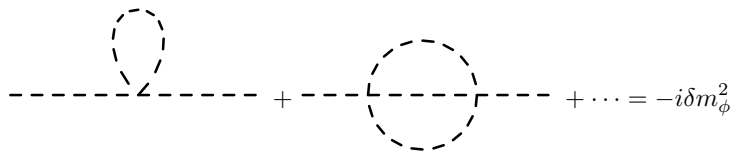


**Figure 1.1:** Diagrams that lead to quantum corrections to  $m_\phi^2$  in the  $\phi^4$  theory of equation 1.1. The corrections are shown up to two-loops, and second order in the coupling constant  $\lambda$ .

the Lagrangian

$$L = \frac{1}{2}(\partial\phi)^2 - \frac{1}{2}m_0^2\phi^2 - \frac{\lambda}{4!}\phi^4 \quad (1.1)$$

When we calculate the observed scalar mass of this theory we get corrections from loop diagrams diagram that involves the quartic coupling  $\lambda$ , as in figure 1.1. These diagrams involve integrals over all possible momenta for the particles in the loops. The integrals are formally divergent; if we introduce a cutoff, a maximum allowed momentum  $\Lambda$ , then we find that the integrals have a quadratic divergence in  $\Lambda$ . Choosing an arbitrary large  $\Lambda$  gives the resulting physical mass

$$m_{\text{phys.}}^2 = m_0^2 - \frac{\lambda}{2(4\pi)^2} \left( \Lambda^2 - m_0^2 \log \frac{\Lambda^2}{m_0^2} \right). \quad (1.2)$$

If  $\Lambda$  is large enough then the observed mass  $m_{\text{phys}}^2$  can be very different from the bare parameter  $m_0^2$  even if  $\lambda$  is a small coupling constant. However, since  $m_0^2$  isn't a physical parameter we can pick whatever value is needed to make our theory predict the experimentally correct value for the mass.

This means, however, that when choosing the parameters of our theory we must consider a high energy scale which will affect the low energy physics. In fact, some physical observables will be quite sensitive to the high energy scale, like the mass in

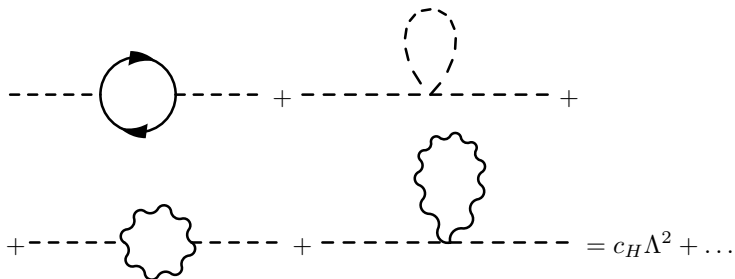


**Figure 1.2:** The dominant one-loop contributions to the Higgs boson mass corrections. Each diagram contributes to the quadratic divergence  $c_H \Lambda^2$ . The top loop dominates the other is stronger than the other fermion loops by a factor of at least  $m_t^2/m_b^2$ .

the example just given. When  $\Lambda$  is much larger than  $m_{\text{phys}}$  if we change  $m_0^2$  by a factor of  $(1 + \delta)$  then  $m_{\text{phys}}^2$  changes by a factor of  $(1 + \delta \frac{\lambda}{2(4\pi)^2} \frac{\Lambda^2}{m_{\text{phys}}^2})$ . This can be a large correction even if  $\delta$  is small if  $\Lambda \gg m_{\text{phys}}$ . Small perturbations in the high energy physics can lead to huge differences in the low energy observables. This is called fine-tuning.

Fine-tuning in a model is generally viewed by theorists as unsatisfactory. If a fine-tuned parameter is so incredibly sensitive to unknown physics, how did that unknown physics happen to produce exactly the value that we see, when a slightly different high-energy value would have produced a wildly different observed value?

### 1.1.1 Fine-tuning in the Standard Model

In the Standard Model the mass of the Higgs boson is a fine-tuned parameter. As the mass of the Higgs boson and the associated symmetry-breaking constant  $v = 246$  GeV are so fundamental to the Standard Model their fine-tuning are viewed as especially unsatisfactory.

The dominant contributions to the Higgs boson quantum mass corrections are shown in figure 1.2. There is a loop involving the a top quark, some loops with  $W$  and  $Z$  bosons, and loops with the Higgs boson itself. All other fermions also contribute, but as we saw the Yukawa couplings of the Standard Model Higgs boson are proportional to the mass of each fermion, and the top quark is nearly 100 times more massive than any other fermion. Considering these diagrams, if the Higgs boson mass is to be natural or not fine-tuned, there must be some new physics at the scale  $\Lambda$  equal to a few TeV (see the introduction to (Schmaltz and Tucker-Smith, 2005) for a good review).

Any theory that removes the fine-tuning of the Higgs mass must somehow remove the effect of the diagrams in figure 1.2. This is typically accomplished by adding new particles whose contribution to the Higgs mass correction cancels out the Standard Model corrections. These extra particles are associated with physics at some new scale  $\Lambda$ . For example, in supersymmetric theory, the correction from the top quark is canceled by additional loop diagrams involving its superpartner, the stop. The new scale is the scale of spontaneous supersymmetry breaking. In theories with composite Higgs the top quark contributions are canceled by other fermionic “top partners” that form a representation of some spontaneously broken symmetry. The new scale is the confining scale of the theory.

While these theories remove contributions quadratic in the cutoff, they do still they still correct the Higgs mass with terms proportional to  $\log \Lambda$ . If the new scale of the theory is large enough, these contributions can still be large enough to make the mass fine-tuned. For supersymmetric theories, as well as many composite Higgs models, the natural cutoff is a few TeV. Hence, almost all natural theories require new particles to appear at or around the TeV scale.

## 1.2 A Fine-Tuned Composite Model

The 2012 discovery of a 125 GeV Higgs boson is beginning to strain most natural models. No other new particles have been discovered that might indicate natural electroweak symmetry breaking. For example, certain Little Higgs theories are constrained to sub percent level fine-tuning (Dercks et al., 2018; Cheung et al., 2018; Reuter et al., 2013), and more general pseudo-Nambu-Goldstone Higgs theories and extra dimension theories are similarly constrained (Bellazzini et al., 2014). Natural supersymmetric theories are also becoming more constrained as experiments exclude higher and higher superpartner mass ranges (Giudice, 2013).

We take this as a sign that the electroweak sector does, in fact, exhibit fine-tuning. To this end, we begin to search for theories that are “minimally fine-tuned.” By this, we mean a theory that involves the smallest possible fine-tuning for  $m_H^2$  and has the fewest number of free parameters that must be fine-tuned to achieve this. In this work we look in particular for a composite model that is minimally fine-tuned in this way. Our model takes inspiration from a model of Bardeen, Hill, and Lindner (BHL) (Bardeen et al., 1990). In this section we will review that model and their analysis. Afterwards we will introduce our model and apply a similar analysis.

The BHL model uses the fact that the top Yukawa coupling is strong to build a model where the Higgs boson is a composite of some physics at a high scale  $\Lambda$ , involving the third generation quarks  $q_L = (t_L, b_L)$  and  $t_R$ . At scales below  $\Lambda$  the interaction is modeled by a four-fermion term,

$$\mathcal{L}_{\bar{t}t} = G \bar{q}_L^{ix} t_{Rx} \bar{t}_R^y q_{Ly} \quad (1.3)$$

where the  $SU(2)_{EW}$  and color- $SU(3)_c$  indices  $i$ , and  $x, y$  are summed over, and  $q_{Li} = (t_L, b_L)_i$ . The theory has an  $SU(2)_{EW} \times U(1)_Y$  gauge symmetry, but  $G$  if given the right strength it can generate a mass term for the top quark via the Nambu-Jona-



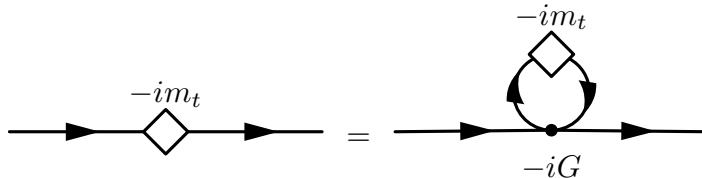


**Figure 1.3:** The Schwinger-Dyson equation for the top mass in the model of Bardeen, Hill, and Lindner. The four-fermion interaction is able to create a mass for the fermion without an explicit mass term.

Lasinio mechanism (Nambu and Jona-Lasinio, 1961). This spontaneously breaks the electroweak symmetry just like a Standard Model Higgs doublet would. We can estimate the required coupling strength in the large- $N_c$ , small gauge-coupling limit.  $G$  must satisfy the mass gap equation of figure 1.3:

$$\begin{aligned} m_t &= -\frac{1}{2}G \langle \bar{t}t \rangle & (1.4) \\ &= 2GN_c m_t \frac{i}{(2\pi)^4} \int d^4l (l^2 - m_t^2)^{-1} \end{aligned}$$

where  $N_c = 3$  is the number of quark colors. The mass arises because the four-fermi interaction generates a top condensate. For this to happen  $G$  must satisfy (assuming  $\Lambda^2 \gg m_t^2$ )

$$\frac{GN_c}{8\pi^2} \left( \Lambda^2 - m_t^2 \log \frac{\Lambda^2}{m_t^2} \right) = 1, \Rightarrow G > G_c = \frac{8\pi^2}{N_c \Lambda^2}. \quad (1.5)$$

In addition to a top quark mass, when equation (1.5) is satisfied we get a mass for the  $SU(2)_{EW}$  vector bosons, and a scalar resonance in the  $\bar{t}t$  channel that acts like a Higgs boson. Using the same approximations as above we can sum the  $\bar{t}t$  bubble diagrams in figure 1.3 and apply equation (1.5) to find that the scalar propagator has

the form

$$\langle \bar{t}t \bar{t}t \rangle (p^2) = \frac{(4\pi)^2}{2N_c} \left[ (p^2 - (2m_t)^2) \int_0^1 dx \log (\Lambda^2 / (m_t^2 - x(1-x)p^2)) \right]^{-1} \quad (1.6)$$

implying a Higgs boson associated with the pole at  $m_H = 2m_t$ . Similar analysis for the weak boson propagators yields the relation  $m_t^2 \log \frac{\Lambda^2}{m_t^2} = \frac{8\pi^2 v^2}{N_c}$  where  $v = 246$  GeV is the experimentally measured electroweak-symmetry-breaking scale. If we take  $\Lambda = 10^{15}$  GeV we get  $m_t \simeq 165$  GeV.

The fine-tuning comes in the relation between  $G^{-1}$  and  $m_t^2$ . In order to satisfy equation (1.5) with  $m_t \simeq v$  with very large  $\Lambda$  the difference  $G^{-1} - G_c^{-1}$  must be very small. However, this is the only fine-tuning required. Once we choose  $G$  correctly to get a small  $m_t$ ,  $m_H$  and  $v$  are automatically small without any additional fine-tuned parameter choices.

Of course, this analysis is very limited. It uses the approximation  $N_c = 3 \gg 1$ , and ignores all gauge couplings, even the strong coupling. It also ignores the fact that the logarithmic terms can be quite large, i.e.  $\log(\Lambda^2/m_t^2) \gg 1$ , which can make ruin calculations that appeared to be perturbative and convergent.

To fix this we need to improve our calculation procedure to remove large logarithms from the analysis. This is accomplished with renormalization group analysis, and it is key to both the analysis of BHL, and our analysis later on.

### 1.2.1 Renormalization group analysis and fine-tuning

In order to improve the predictions from above we must remove the large logarithms from the procedure using what is called renormalization group analysis. The large logarithms arise in parameter corrections when loop diagrams require us to integrate over all momenta from 0 to the cutoff of the theory  $\Lambda$ . Doing these integrals allows us to write the parameter at low energy in terms of a bare parameter at the cutoff.

The bare parameter is then associated with a particular momentum scale,  $\Lambda$ .

What if we instead specify the theory in terms of a different scale and a different associated parameter? For example, we could choose an arbitrary  $\mu^2$  and specify what that when  $p^2 = \mu^2$ , the  $\phi$  propagator looks like  $(p^2 - m(\mu)^2)^{-1}$ . Then when  $p^2$  is close to  $\mu^2$  the propagator will look like  $(p^2 - m(\mu)^2 + \mathcal{O}(\log(p^2/\mu^2)))^{-1}$ , which involves only small logarithms, meaning we can put more trust in our predictions.

Furthermore, the physics of the theory should not depend on the arbitrary  $\mu^2$  scale we chose. We could just as well have specified  $m(\mu')^2$  instead of  $m(\mu)^2$ . We can then define the running mass: for every  $\mu$ ,  $m(\mu)^2$  is the mass parameter specification that gives the physically correct propagator for energies near  $\mu$ . The physical mass is the scale where the propagator has a pole, so that  $m_{\text{phys}}^2 - m(m_{\text{phys}})^2 = 0$ .

Even better, we have already seen that  $m(\mu')^2 \simeq m(\mu)^2 + \mathcal{O}(\log(\mu'/\mu^2))$ , meaning we can compute the running mass at one value in terms of the running mass at values nearby. This leads to a differential equation called the renormalization group equation

$$\frac{dm^2(\mu)}{d\log(\mu)} = \beta(m^2(\mu)) \tag{1.7}$$

The function on the right-hand side is some function of all the parameters in the theory and can be computed by evaluating the loop diagrams used to compute the mass corrections. In general there is one such beta function for every parameter in the theory, and all the coupling constants and parameters depend on an energy scale, or run.

From this perspective, fine-tuning is a question of the relationship between the values of a running parameter at two different scales. If we have a cutoff  $\Lambda$  we can calculate the dependence of  $m_{\text{phys}}^2$  on  $m(\Lambda^2)^2$ . Specifically, the amount of fine-tuning is measured by  $d\log m_{\text{phys}}^2/d\log m(\Lambda^2)^2$ , where values much greater than one indicate severe fine-tuning.

In order to apply renormalization group techniques to the BHL model, we first swap the four-fermion interaction term that generates spontaneous symmetry breaking in favor of scalar Higgs doublet. This is accomplished by adding a non-propagating doublet to the theory at the cutoff and shifting it to absorb the four-fermi term. That is, we start with the Lagrangian and the extra doublet:

$$\mathcal{L}(\Lambda) = \dots + G \bar{q}_L^i t_R \bar{t}_R q_L^i - m_0^2 H_i^\dagger H_i \quad (1.8)$$

then making the shift  $H_i \mapsto H_i + \sqrt{G/m_0^2} \bar{t}_R q_L^i$ , which gives

$$\mathcal{L}(\Lambda) = \dots - m_0^2 H_i^\dagger H_i - y_{t0} (H_i \bar{q}_L^i t_R + \text{h.c.}) \quad (1.9)$$

where  $y_t(\Lambda) = y_{t0} = \sqrt{m_0^2 G}$ . This looks like the Standard Model Higgs doublet mass term and Yukawa term, but the doublet does not have a kinetic term or any quartic self-coupling, meaning at this scale the doublet is a non-propagating degree of freedom.

However, if we begin to compute loop corrections at lower scales we find that the doublet does develop both a kinetic term and a quartic term. It also gets mass corrections that begin to drive the mass down. At a lower scale  $\mu$  the effective Lagrangian becomes

$$\begin{aligned} \mathcal{L}(\mu) = & Z_H(\mu) |D_\mu H|^2 - m_H^2(\mu) - \frac{\lambda_H}{2} (H^\dagger H)^2 + \\ & - y_t(\mu) H_i (\bar{q}_L^i t_R + \text{h.c.}) \end{aligned} \quad (1.10)$$

where

$$\begin{aligned}
Z_H &= \frac{3y_{t0}^2}{(4\pi)^2} \log \frac{\Lambda^2}{\mu^2} \\
m_H^2(\mu) &= m_0^2 - \frac{6y_{t0}^2}{(4\pi)^2} (\Lambda^2 - \mu^2) \\
\lambda_H(\mu) &= \frac{6y_{t0}^2}{(4\pi)^2} \log \frac{\Lambda^2}{\mu^2}
\end{aligned} \tag{1.11}$$

Note that  $Z_H(\Lambda) = 0$ , but becomes non-zero at lower scales. This indicates that the  $H$  field is a non-propagating term at  $\Lambda$ , but as propagating degrees of freedom at lower scales. We will use  $Z_H(\Lambda) \rightarrow 0$  as the condition for compositeness later on. We can also see that at a certain  $\mu$  the Higgs doublet mass term becomes negative, indicating spontaneous symmetry breaking. If we define  $v^2(\mu) = 4m_H(\mu)^2/\lambda(\mu)$  and impose the condition that  $v(246 \text{ GeV}) = v = 246 \text{ GeV}$  then we can see that this quantity is fine-tuned:  $d \log v^2/d \log m_0^2 \simeq \Lambda^2/v^2$ . However, this is the only fine-tuning. The running top mass is  $m_t(\mu) = y_t(\mu)v/\sqrt{2}$  and the Higgs boson mass is  $m_h(\mu)^2 = \lambda(\mu)v^2$ , so once we fix  $v$  the other masses need no more fine-tuning.

Equation (1.11) is still a naive result with large logarithms. To improve the calculation we use the beta functions for each parameter. Since the effective Lagrangian below the cutoff is the same as the Standard Model Lagrangian, we can pull the beta functions from there. The relevant beta functions are (Pendleton and Ross, 1981)

$$(4\pi)^2 \frac{dy_t}{d \log \mu} = y_t \left( (3/2 + N_c)y_t^2 - 8g_3^2 - \frac{9}{4}g_2^2 - \frac{17}{12}g_1^2 \right) \tag{1.12}$$

$$(4\pi)^2 \frac{d\lambda}{d \log \mu} = 12 \left( \lambda^2 + \left( \frac{N_c}{3}y_t^2 - A \right) \lambda + B - \frac{N_c}{3}y_t^4 \right) \tag{1.13}$$

where  $A = \frac{1}{4}g_1^2 + \frac{3}{4}g_2^2$ ,  $B = \frac{1}{16}g_1^4 + \frac{2}{16}g_1^2g_2^2 + \frac{3}{16}g_2^4$ , and the  $g_i$  are the gauge couplings of the Standard Model gauge group. They are also running quantities, though we can ignore exactly how they run for now.

Finally, we must specify boundary conditions. The Standard Model beta functions

$\Lambda$ (GeV)	$10^{19}$	$10^{15}$	$10^{10}$	$10^6$	$10^4$
$m_t$ (GeV)	218	229	255	318	455
$m_h$ (GeV)	239	256	296	391	605

**Table 1.1:** The predicted masses of the model of Bardeen et al. (Bardeen et al., 1990), where the Higgs boson is a composite of the top quark. It requires very large values of the cutoff  $\Lambda$  to produce result even close to realistic.

assume that the kinetic term of each field is normalized at every scale, i.e.  $Z_H(\mu) = 1$ . Since  $Z_H(\mu)$  runs, we can arrange this by redefining  $H_{\mu-d\mu} = H_\mu/Z(\mu - d\mu)$  at each scale, and absorb the factors of  $1/Z_H$  into the other couplings. For example,  $y_t(\mu-d\mu) = (y_t(\mu) + \delta y_t)/(1 + \delta Z_H)$ . The compositeness condition requires  $Z_H \rightarrow 0$  at  $\Lambda$ . We can use the Standard Model beta functions and account for the compositeness condition by requiring the couplings to diverge at  $\Lambda$ ,  $y_t(\Lambda), \lambda(\Lambda) \rightarrow \infty$ .

In addition, since the divergence is meant to come from powers of the Higgs field the ratio  $y_t^4/\lambda$  should remain finite because the Yukawa term couples to one power of the Higgs doublet while  $\lambda$  couples to four. In practice, we use the initial condition  $y_t^2(\Lambda) \simeq \lambda(\Lambda) \simeq 4\pi$ .

The procedure in summary is this:

1. Write down the Standard Model renormalization group equations for  $y_t(\mu)$ ,  $\lambda(\mu)$ , and the gauge couplings.
2. Choose a cutoff scale  $\Lambda$  and specify large values for the Yukawa and Higgs quartic couplings at this scale.
3. Solve the renormalization group equations to get the running couplings at lower scales.
4. Use the result to find the physical pole masses:  $m_t(m_{t,\text{phys}}) = y_t(m_{t,\text{phys}})v/\sqrt{2} = m_{t,\text{phys}}$  and  $m_h(m_{h,\text{phys}})^2 = \lambda(m_{h,\text{phys}})v^2 = m_{h,\text{phys}}^2$  where  $v = 246$  GeV.

Bardeen et al. followed this procedure for their model and got the results summarized in table 1.1. It does produce masses for the Higgs boson and the top quark that are not fine-tuned, assuming that  $v$  is chosen correctly. However, the model produces a top and Higgs that are too heavy, especially for lower cutoffs.

## 1.3 Our new model

### 1.3.1 Introduction and UV perspective

We propose a new candidate for a minimally fine-tuned model. It is inspired by the model of Bardeen et al., and is modified to produce lower masses with lower cutoffs than that model.

To the particles and couplings of the BHL model we add an extra set of fermions, charged under an additional non-abelian gauge interaction. The  $(SU(2)_L, U(1)_Y, SU(3)_c, SU(N)_{TC})$  quantum numbers of the relevant fermions are

$$\begin{aligned} q_L &= \begin{pmatrix} t_L \\ b_L \end{pmatrix} \in (2, \frac{1}{6}, \underline{3}, \underline{1}), \quad t_R \in (\underline{1}, \frac{2}{3}, \underline{3}, \underline{1}), \quad b_R \in (\underline{1}, -\frac{1}{3}, \underline{3}, \underline{1}) \\ T_L &= \begin{pmatrix} U_L \\ D_L \end{pmatrix} \in (\underline{2}, 0, \underline{1}, \underline{d}_{TC}), \quad U_R \in (\underline{1}, \frac{1}{2}, \underline{1}, \underline{d}_{TC}), \quad D_R \in (\underline{1}, -\frac{1}{2}, \underline{1}, \underline{d}_{TC}) \end{aligned} \quad (1.14)$$

where  $d_{TC}$  is the dimension of some representation of the technicolor (TC) gauge group. We refrain here from specifying which group that is, or even if  $d_{TC}$  is the fundamental representation. We ignore light quarks and leptons, and any additional technifermion flavors.

Please note that, while we will use the names “technicolor”, “technifermions”, and “extended technicolor” our theory differs from technicolor and its variants in crucial ways. Much of the conventional wisdom about technicolor will not apply. For example, our technicolor coupling must be small at the extended technicolor scale, as we shall see, whereas in walking technicolor it is large.

The electroweak symmetry breaking comes from a condensate formed from a linear

combination of  $\bar{t}_L t_R$  and  $\bar{U}_L U_R$ . As in the BHL model, we can imagine this occurring as the result of four-fermion interactions from physics at a high scale  $\Lambda$ . We call this the extended technicolor (ETC) sector of the theory. We are agnostic as to its origin or details, except that it involves both quarks and technifermions. We will choose  $\Lambda$  to be of the order of hundreds of TeV or more to avoid issues with flavor-changing neutral currents.

$$\mathcal{L}_{ETC} = G_1 \bar{q}_L^i t_R \bar{t}_R q_L^i + G_2 (\bar{q}_L^i t_R \bar{U}_R T_L^i + \text{h.c.}) + G_3 \bar{T}_L^i U_R \bar{U}_R T_L^i \quad (1.15)$$

This ignores, for now, the mass of the  $b$  and  $D$  fermions. We will take that issue up in a later section.

There are now two gap equations for the two fermion masses,  $m_t$  and  $m_U$ . Each mass has contributions from a top loop and a  $U$  loop, so the Computing the gap equations as in section 1.2, the leading-log gap equations for  $m_t$  and  $m_U$  are of the form

$$\begin{aligned} m_t &= -\frac{1}{2}G_1 \langle \bar{t}t \rangle - \frac{1}{2}G_2 \langle \bar{U}U \rangle \\ &= \frac{G_1 N_c m_t}{8\pi^2} \left( \Lambda^2 - m_t^2 \log \frac{\Lambda^2}{m_t^2} \right) + \frac{G_2 d_{TC} m_U}{8\pi^2} \left( \Lambda^2 - m_U^2 \log \frac{\Lambda^2}{m_U^2} \right) \end{aligned} \quad (1.16)$$

$$\begin{aligned} m_U &= -\frac{1}{2}G_2 \langle \bar{t}t \rangle - \frac{1}{2}G_3 \langle \bar{U}U \rangle \\ &= \frac{G_3 d_{TC} m_U}{8\pi^2} \left( \Lambda^2 - m_U^2 \log \frac{\Lambda^2}{m_U^2} \right) + \frac{G_2 N_c m_t}{8\pi^2} \left( \Lambda^2 - m_t^2 \log \frac{\Lambda^2}{m_t^2} \right) \end{aligned} \quad (1.17)$$

Multiplying equation 1.16 by  $m_U$  and equation 1.17 by  $m_t$ , and requiring the two equations to hold for all  $N_c$  and  $d_{TC}$  we see we must have  $G_2^2 = G_1 G_3$ . Imposing these requirements imply the single fine-tuning condition

$$\frac{G_1 N_c}{8\pi^2} \left( \Lambda^2 - m_t^2 \log \frac{\Lambda^2}{m_t^2} \right) + \frac{G_3 d_{TC}}{8\pi^2} \left( \Lambda^2 - m_U^2 \log \frac{\Lambda^2}{m_U^2} \right) = 1 \quad (1.18)$$

This relation ignores the effect of gauge interactions like the strong interaction and



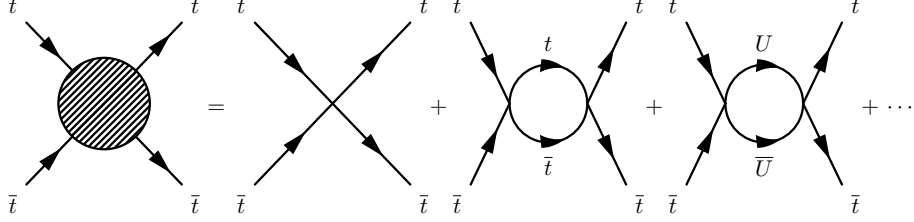


**Figure 1.4:** The one loop diagrams that make up the  $\bar{t}t$  (and  $\bar{U}U$ ) propagator in the scalar channel, including only ETC interactions. Both propagators include contributions from both  $t$  and  $U$  loops. We will include the TC interactions later on.

technicolor, assumes  $N_c, d_{TC} \gg 1$ , and is not renormalized beyond the cutoff  $\Lambda$ . However, it does give us an idea of the fine-tuning involved. Together with the requirement that  $G_2^2 = G_1 G_3$  it implies that only one of the  $G_i$  is independent. Furthermore, once we impose this fine-tuning condition we will see that all the other predicted masses become small without additional fine-tuning. The model thus satisfies part of our minimal fine-tuning condition.

### Scalar and vector poles

When  $G_2^2 = G_1 G_3$  the loop diagrams that make up the  $\langle \bar{t}t \bar{t}t \rangle$  propagator sum geometrically (see figure 1.4), yielding a form with a single pole once the gap equations are applied:

$$\begin{aligned} \langle \bar{t}t \bar{t}t \rangle(p) = m_t^2 & \left[ \frac{N_c m_t^2 (p^2 - 4m_t^2)}{8\pi^2} \int_0^1 dx \log \left( \frac{\Lambda^2}{m_t^2 - x(1-x)p^2} \right) \right. \\ & \left. + \frac{d_{TC} m_t^2 (p^2 - 4m_U^2)}{8\pi^2} \int_0^1 dx \log \left( \frac{\Lambda^2}{m_U^2 - x(1-x)p^2} \right) \right]^{-1} \end{aligned} \quad (1.19)$$

This is of the form  $\langle \bar{t}t \bar{t}t \rangle(p) = A/(p^2 - m_h^2)$ , which is the form we get if  $\bar{t}t$  to  $\bar{t}t$  scattering is mediated by a massive scalar particle. The effect of the strong four-

fermi interactions is to create a massive scalar particle that interacts with  $\bar{t}t$ . The mass of this particle is the value of  $p^2$  where the pole vanishes, so it is the solution to

$$N_c m_t^2 (m_h^2 - 4m_t^2) \int_0^1 dx \log \left( \frac{\Lambda^2}{m_t^2 - x(1-x)m_h^2} \right) + d_{TC} m_U^2 (m_h^2 - 4m_U^2) \int_0^1 dx \log \left( \frac{\Lambda^2}{m_U^2 - x(1-x)m_h^2} \right) = 0 \quad (1.20)$$

or approximately

$$m_h \simeq 2 \sqrt{\frac{N_c m_t^4 + d_{TC} m_U^4}{N_c m_t^2 + d_{TC} m_U^2}} \quad (1.21)$$

We also need to check that the four-fermi terms cause spontaneous electroweak symmetry breaking, and that this massive scalar particle is the Higgs boson we are looking for. In the symmetry unbroken phase gauge invariance requires that the kinetic term for the weak gauge bosons have the form  $(p_\mu p_\nu - p^2 g_{\mu\nu})/g_W^2(p^2)$ , where  $g_W^2(p^2)$  is the effective running coupling of the weak interaction. This form always produces a propagator with a pole at  $p^2 = 0$ , corresponding to massless bosons. However, it is possible for corrections from the four-fermi interactions to produce an effective kinetic term of the form

$$\frac{1}{g_W^2} \langle W_\mu W_\nu \rangle^{-1}(p) = \frac{1}{g_W^2} (p_\mu p_\nu - p^2 g_{\mu\nu}) + \frac{i}{2} \int d^4x e^{ip \cdot x} \langle J_\mu^W(x) J_\nu^W(0) \rangle \quad (1.22)$$

$$= (p_\mu p_\nu - p^2 g_{\mu\nu}) \left( \frac{1}{g_W^2(p^2)} - \frac{f_W^2(p^2)}{p^2} \right) \quad (1.23)$$

which implies a propagator with the form  $A/(p^2 - f_W^2(p^2)g_W^2(p^2))$ . The weak gauge bosons then get a mass that satisfies  $m_W^2 - f_W^2(m_W^2)g_W^2(m_W^2) = 0$ . Additionally, the Fermi constant is the coupling constant between the two gauge currents at low energies, so  $f_W^2(0) = 1/(2\sqrt{2}G_F)$ .

In our theory the gauge currents are

$$J_\mu^\pm = \bar{q}_L \gamma_\mu \tau^\pm q_L + \bar{T}_L \gamma_\mu \tau^\pm T_L \quad (1.24)$$

$$J_\mu^0 = \frac{1}{6}(\bar{q}_L \gamma_\mu q_L + \bar{q}_R \gamma_\mu q_R) + \bar{q}_R \gamma_\mu \tau^3 q_R + \bar{T}_R \gamma_\mu \tau^3 T_R \quad (1.25)$$

$$J_\mu^3 = \bar{q}_L \gamma_\mu \tau^3 q_L + \bar{T}_L \gamma_\mu \tau^3 T_L \quad (1.26)$$

where the  $\tau^i$  are the generators of  $SU(2)$  in the fundamental representation. If we sum all the bubble diagrams in figure 1-3 and apply the gap equation we can compute the propagators for each current. The charged current tells us about the charged weak bosons.

$$\begin{aligned} f_W^2(p^2) = & \frac{1}{(4\pi)^2} \int_0^1 dx x \left[ N_c m_t^2 \log \left( \frac{\Lambda^2}{m_t^2 x - x(1-x)p^2} \right) + \right. \\ & \left. + d_{TC} m_U^2 \log \left( \frac{\Lambda^2}{m_U^2 x - x(1-x)p^2} \right) \right] \end{aligned} \quad (1.27)$$

$$\begin{aligned} g_W^{-2}(p^2) = & g_2^{-2} + \frac{1}{(4\pi)^2} \int_0^1 dx 2x(1-x) \left[ N_c m_t^2 \log \left( \frac{\Lambda^2}{m_t^2 x - x(1-x)p^2} \right) + \right. \\ & \left. + d_{TC} m_U^2 \log \left( \frac{\Lambda^2}{m_U^2 x - x(1-x)p^2} \right) \right] \end{aligned} \quad (1.28)$$

We can produce numerical results as a check on this picture of the model. We fix  $\Lambda$ ,  $m_t$ , and require that  $f_W(0) = (4\sqrt{2}G_F)^{-1/2} \simeq 123$  GeV. The first two requirements combined with the third and equation (1.18) tell us how to choose  $m_U$ . This in turn allows us to determine all the other parameters in the theory using equations (1.20),(1.27), and (1.28). Note that the  $m_t$  and  $m_U$  that appear in all the formulae above are the values of the running masses at the cutoff and are different than the physical pole masses of those particles. We can obtain an approximation  $m_t(\Lambda)$  by using the Standard Model renormalization equations starting at  $m_t(173 \text{ GeV}) = 173$  GeV and running up to  $\Lambda$ . The gauge couplings are chosen so

$\Lambda$	$m_t$	$m_U$	$m_H$
20 TeV	134 GeV	167 GeV	330 GeV
500 TeV	118 GeV	126 GeV	250 GeV
$\Lambda$	$m_W$ (pole)	$m_Z$ (pole)	$\rho$
20 TeV	80.8 GeV	91.0 GeV	1.052
500 TeV	80.6 GeV	93.0 GeV	1.030

**Table 1.2:** Unrenormalized mass values in the ETC-only scheme for two ETC cutoff scales  $\Lambda = 20$  TeV and 500 TeV. The pole value of  $m_H$  is different due to renormalization, but we cannot say how much without including TC dynamics. Compare to the results of the BHL model in table 1.1

that they match their Standard Model values at the scale  $m_Z = 91.17$  GeV.

The results of this numeric calculation are in table 1.2. The value of  $m_H$  is the unrenormalized value defined at the cutoff. We expect the physical pole value to be lower, but we cannot say by how much without more sophisticated calculations. However, we can note that our values for  $m_H$  are already lowered relative the values of BHL for similar cutoffs.

### 1.3.2 Technicolor interactions

Our computation so far has ignored the extra gauge interactions of the technifermions. However, the technicolor interaction is a significant part of the model. The TC gauge group is the set of unbroken ETC symmetries. We expect that not all of the ETC symmetries are broken. Otherwise ETC would be IR free, and it is not clear that such a theory could also be UV free.

We also expect that in the IR the technicolor interaction will be strong enough to spontaneously break the electroweak symmetry by itself, which might invalidate the large- $N$ , ETC-only analysis of the previous sections. Lastly, the TC interaction can have a significant effect on the fermion and Higgs boson masses that arise after spontaneous symmetry breaking. We will see later that it can help to lower the top quark mass relative to the ETC-only result.

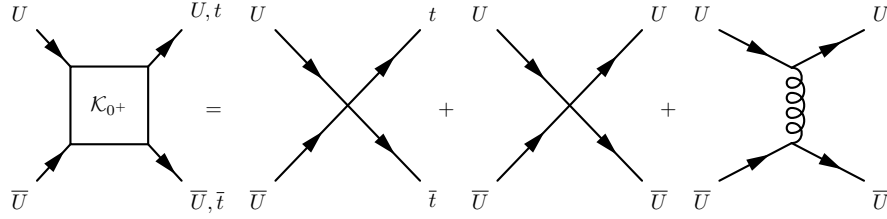


**Figure 1.5:** The technicolor interaction modifies the four-fermion kernel by adding TC-gluon exchange diagrams.

In order that the symmetry breaking be dominated by the higher energy ETC interactions we assume that the TC interaction is weak in the UV, becoming strongly coupled only around the 1 TeV scale. We will also assume that the coupling runs towards an infrared fixed-point in the IR. We will find that this is not strictly necessary, however; the most important feature is the asymptotic freedom with a low strong-coupling scale.

### TC and symmetry breaking

The technicolor interaction is able to break the electroweak symmetry by itself when it becomes strongly coupled. That is the original motivation for technicolor, but as naive technicolor is ruled out (Particle Data Group, 2016a), our model must rely on ETC to dominate the symmetry breaking.

Including TC modifies the gap equation (1.16-1.17) by adding additional components to the four-fermion kernel, as in figure 1.5. The gap equation is the same as the first leading lines of equation (1.16), but computing the expectation values  $\langle \bar{t}t \rangle$  and  $\langle \bar{U}U \rangle$  now involves contributions from the TC interactions. Schematically, the four-fermion vertex on the right-hand side of figure 1.3 is replaced with the more complicated kernel in 1.5.

Computing the  $\langle \bar{t}t \bar{t}t \rangle$  propagator also now uses the four-fermion vertex of figure 1.5

and includes diagrams with TC-gluons being exchanged. These diagrams no longer form a geometric series when summed — even with the  $G_2^2 = G_1 G_3$  condition — so the analysis of the previous section does not work.

The combined ETC + TC kernel has been studied elsewhere, in studies of the dynamical mass function  $\Sigma(p^2)$  in the technifermion propagator  $S^{-1}(p) = \not{p}A(p)^2 - \Sigma(p^2)$ . For a simplified model with only  $G_3 \neq 0$  The Schwinger-Dyson gap equation for  $\Sigma(p^2)$  is (for Euclidean momentum  $p^2 \ll \Lambda^2$ )

$$\Sigma(p^2) = (G\Lambda^2) \int_0^{\Lambda^2} dk^2 \frac{k^2}{\Lambda^2} \frac{\Sigma(k^2)}{k^2 + \Sigma^2(k^2)} + \frac{1}{4\alpha_c} \int_0^{\Lambda^2} dk^2 \alpha_{TC}(M^2) \frac{k^2}{M^2} \frac{\Sigma(k^2)}{k^2 + \Sigma^2(k^2)}. \quad (1.29)$$

Here  $\alpha_c$  is the critical value of the TC coupling  $\alpha_{TC}$  for spontaneous chiral symmetry breaking in a pure-technicolor theory (Cohen and Georgi, 1989). In the ladder approximation it is  $\pi/3C_2(d_{TC})$ . Finally,  $M^2 = \max(k^2, p^2)$ .

In a pure ETC theory  $\Sigma(0) = 0$  when  $\lambda \equiv G\Lambda^2 < 1$ . There is a rapid phase transition at  $\lambda = 1$  which causes  $\Sigma(0)$  to rise to  $\mathcal{O}(\Lambda)$  just above the transition.

In a pure TC theory with  $\alpha_{TC}$  weak in the UV,  $\alpha_{TC}$  reaches  $\alpha_c$  at a scale  $\Lambda_{TC}$ , and we get  $\Sigma(0) \simeq \Sigma(\Lambda_{TC}) = \mathcal{O}(\Lambda_{TC})$ . Additionally,  $\Sigma(p^2)$  falls off as  $\Lambda_{TC}^3/p^2$  when  $\alpha_{TC}$  becomes weak (Lane, 1974).

For constant  $\alpha_{TC}$  (Appelquist et al., 1988) the  $\Sigma(0)$  behaves as it does in the pure ETC theory except that, for  $\alpha_{TC} < \alpha_c$  the phase transition occurred at

$$\lambda_{\alpha_{TC}} = \left( \frac{1 + \sqrt{1 - \alpha_{TC}/\alpha_c}}{2} \right). \quad (1.30)$$

Takeuchi (Takeuchi, 1989) studied the gap equation for a running, asymptotically free TC coupling with beta function  $\beta(\alpha_{TC}) = -b_1\alpha_{TC}^2$  with  $b_1 > 0$ . As long as  $\Lambda_{TC} \ll \Lambda$  (as we expect), he found that  $\Sigma(0) = \mathcal{O}(\Lambda_{TC})$  for  $\lambda < \lambda_{\alpha_{TC}(\Lambda)}$ . At this critical value of  $\lambda$  there is a smooth but rapid transition up to  $\Sigma(0) = \mathcal{O}(\Lambda)$ . The

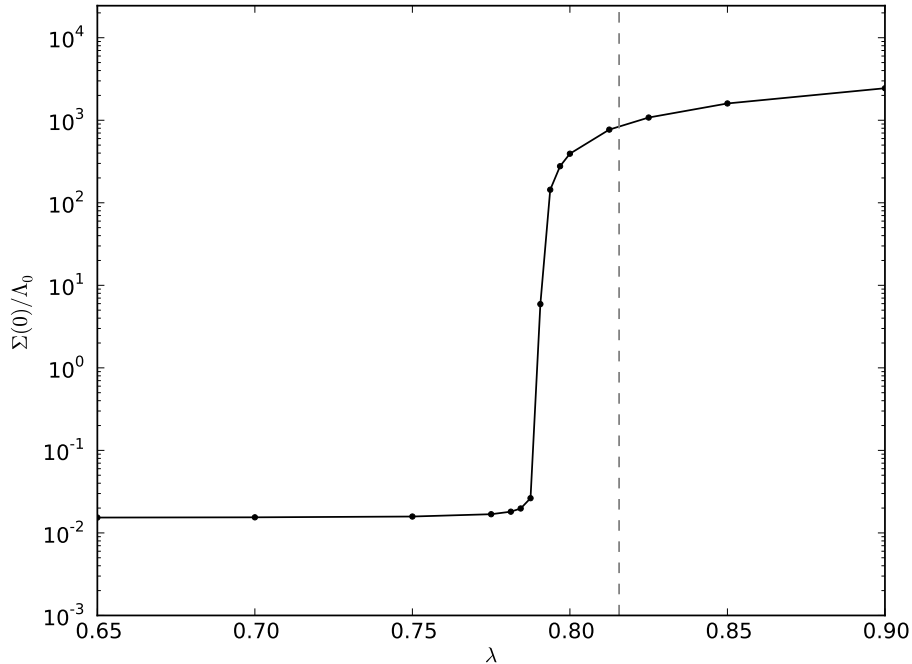


**Figure 1-6:** The behavior of  $\Sigma(0)$  as a function of  $\lambda = G\Lambda^2$  in the model of Takeuchi, extended to a more realistic TC  $\beta$  function. At a critical value of  $\lambda$ ,  $\Sigma(0)$  jumps from a very small scale to  $\mathcal{O}(\Lambda)$ .

transition is more abrupt for small  $\alpha_{TC}(\Lambda)/\alpha_c$  (or equivalently  $\lambda_{\alpha_{TC}} = 1$ ).

We have verified Takeuchi's results for a TC  $\beta$ -function that is more like the one we will use in section 1.4.4. Moreover, we computed the  $p^2$  dependence of  $\Sigma$  for various values of the couplings. For  $\lambda < \lambda_{\alpha_{TC}(\Lambda)}$  we found that  $\Sigma$  is small and falls off approximately as  $1/p^2$  for  $\Lambda_{TC} < p < \Lambda$ . This is the behavior we see from  $\Sigma$  in the pure-TC unbroken phase. On the other hand, at and above the critical value of  $\lambda$ ,  $\Sigma(p)$  rises rapidly to  $\mathcal{O}(\Lambda)$  and then remains nearly constant in  $p$ , which is the behavior of a hard mass as in the broken phase. See figure 1-6, for an example.

In essence, the fine-tuning of our model is picking a value of  $\lambda$  so that  $\Sigma(0)$  is not very small, and not  $\mathcal{O}(\Lambda)$ , but in between at  $\mathcal{O}(m_t)$ . Since the transition between those two phases is very rapid in  $\lambda$ , we have to pick  $\lambda$  very precisely to achieve this.

All together, this is the reassuring result that the TC dynamics do not ruin the

symmetry breaking patterns of the ETC physics that we saw in previous sections. If  $\alpha_{TC}(\Lambda)$  is small compared to  $\alpha_c$  (as it must be for this model to work) then  $\Sigma(0)$  is much smaller than  $\Lambda$  below  $\lambda_{\alpha_{TC}}$  and then rises abruptly above, almost to  $\mathcal{O}(\Lambda)$ . The critical value of  $\lambda_{\alpha_{TC}}$  is smaller than one because TC has the approximate effect of producing an interaction of the same form and sign as the  $G_3$  in the spin-zero channels.

To see why this is in detail, we can use the fact that the TC coupling involved in the EW phase transition is approximately  $\alpha_{TC}(\Lambda)$ . The relevant TC interaction then involves exchange of a technigluon with Euclidean momentum transfer  $\simeq -\Lambda^2$ ,

$$\mathcal{L}_{TC} = -\frac{3\pi\alpha_{TC}(\Lambda)}{2\Lambda^2}\bar{T}\gamma^\mu t_A T \bar{T}\gamma_\mu t_A T, \quad (1.31)$$

where  $T$  is the technifermion doublet and  $t_A$  are the TC generators. Using Fierz identities on both the Lorentz matrices and the TC matrices we get the scalar channel term (among other terms)

$$\mathcal{L}_{TC} = \frac{3\pi C_2(d_{TC})\alpha_{TC}(\Lambda)}{d_{TC}\Lambda^2}\bar{T}T\bar{T}T, \quad (1.32)$$

which combines with the  $G_3$  term in equation 1.15 to give the effective four-fermi coupling

$$\lambda_{eff} = \frac{G_3 d_{TC} \Lambda^2}{8\pi^2} + \frac{3C_2(d_{TC})\alpha_{TC}(\Lambda)}{4\pi} = \lambda + \frac{\alpha_{TC}(\Lambda)}{4\alpha_c}. \quad (1.33)$$

When this effective  $\lambda_{eff}$  equals 1, we have  $\lambda = 1 - \alpha_{TC}(\Lambda)/4\alpha_c \simeq \lambda_{\alpha_{TC}}$ .

### Technicolor bound states

Since the TC interaction becomes strongly coupled and may form a condensate of its own accord at around the TeV scale, we expect that the theory includes many TC bound states, a la QCD. While the details of the TC spectrum are outside the scope



of this dissertation, it does raise some questions we should at least consider.

First, what are the most accessible bound TC states? The lowest-lying states are the Higgs boson  $H$  and the longitudinal modes of the weak bosons,  $W_L^\pm$  and  $Z_L$ . But what are the next modes? What would these look like in a collider experiment? We will address this question in chapter 2, where we will argue that they are isotriplet vector and axial vector technimesons that decay mostly to the Higgs and weak bosons. We will apply this hypothesis to attempt to explain some excesses reported by LHC experiments.

Second, what is the scale of the bound states? The Higgs and weak bosons have masses around  $\mathcal{O}(100 \text{ GeV})$ . The other bound states must have masses greater than approximately 1 TeV to have remained unobserved so far (see, for example, the Particle Data Group experimental review of technicolor (Particle Data Group, 2016a)). Is our theory consistent with this splitting between the lowest lying scalars and the other bound states?

There are roughly three possibilities. One, the other bound states sit around the  $\Lambda_{TC} = \mathcal{O}(\text{few TeV})$  scale as we would expect from a strongly-coupled theory in isolation. Two, the other bound states are as light as the electroweak bosons without any additional fine-tuning due to ETC dynamics. Or three, there is some sort of complex interplay between TC and ETC and we can't say much of anything.

We do not attempt to fully answer this question in this dissertation. However, we can at least rule out the second possibility: the ETC four-fermi terms in equation (1.15) do not have any overlap with isotriplet vector states, so they will not affect the mass of such bound states. If the ETC physics does include other four-fermi terms that do overlap vector states then they will also need to be fine-tuned to create light states. If they are not fine-tuned like the  $G_1, G_2, G_3$  terms then they will not create additional light states without additional fine-tuning<sup>1</sup>. We can tentatively conclude

---

<sup>1</sup>The only other possibility is if whatever UV physics is responsible for the fine-tuned scalar ETC

that in minimally-fine-tuned models the other bound states will have masses of the scale either  $\Lambda$  or  $\Lambda_{TC} \simeq \mathcal{O}(\text{TeV})$ .

---

terms also generates fine-tuned vector terms.

## 1.4 Renormalization

The masses in table 1.2 of section 1.3 are unrenormalized and limited by a large- $d_{TC}$  and  $N_c$  approximation and their calculation ignores the effects of the technicolor interaction entirely. We can improve the mass predictions and remove these limitations using the renormalization group, as in BHL.

A renormalization group treatment also allows us to consider the model from a purely low-energy perspective. Since our UV view of the model is not really a complete model (we don't pretend know to what physics generates the fine-tuned four-fermi interactions), it is helpful to consider what happens with just the IR ingredients and make sure that it is consistent with our claims.

### 1.4.1 Degrees of freedom and running couplings

First we must determine the IR degrees of freedom of our model. As in BHL, we can integrate out the four-fermi terms using a scalar  $SU(2)_L$  doublet:

$$\begin{aligned}
 \mathcal{L}_{ETC} &= -m_0^2 H^\dagger H + G_1 \bar{q}_L t_R \bar{t}_R q_L + G_2 (\bar{q}_L t_R \bar{U}_R T_L + \text{h.c.}) \\
 &\quad + G_3 \bar{T}_L U_R \bar{U}_R T_L \\
 &\mapsto -m_0^2 H^\dagger H - y_{t0} (\bar{q}_L t_R H + \text{h.c.}) - y_{U0} (\bar{T}_L U_R H + \text{h.c.})
 \end{aligned} \tag{1.34}$$

It is important to note that the shift in the scalar doublet required to “complete the square” in this way is only possible when  $G_2^2 = G_1 G_3$ . Otherwise the four-fermi terms cannot be removed with only a single scalar doublet; extra degrees of freedom are required. This corresponds to the fact that the bubble diagrams in the gap equation of section 1.3 can only be geometrically summed to produce a simple scalar pole when  $G_2^2 = G_1 G_3$ .

Assuming that a single scalar Higgs doublet is sufficient, the only other additional degrees of freedom we need are the technifermions,  $U$  and  $D$ , and the gauge bosons

of the technicolor interaction. Everything else is just as in the Standard Model. (However, for now we will ignore all the Standard Model fermions except for  $(t_L, b_L)$ , and  $t_R$ .)

The effective Lagrangian at low energies is like the Standard Model. The interaction terms are

$$\begin{aligned} \mathcal{L}_{IR} = & \mathcal{L}_{\text{kinetic}} + \mathcal{L}_{\text{gauge}} - m_0^2 H^\dagger H \\ & - y_t (\bar{q}_L^i t_R H^i + \text{h.c.}) - y_U (\bar{T}_L^i U_R H^i + \text{h.c.}) \\ & - \frac{\lambda}{2} (H^\dagger H)^2 \end{aligned} \tag{1.35}$$

If we assume the doublet mass coefficient  $m_0^2$  is tuned so that it generates the correct Higgs vacuum expectation value  $\langle H \rangle = (v/\sqrt{2}, 0)^T$ , with  $v = 246$  GeV, then the couplings of interest are the Yukawa couplings  $y_t$  and  $y_U$  and the Higgs quartic coupling. (Note: this definition of the Higgs field is different from the one of the Standard Model; the SM Higgs gets a vacuum expectation value in its lower component). These determine the masses  $m_t$ ,  $m_U$ , and  $m_H$ , respectively, via the pole equations

$$y_t(m_t)v/\sqrt{2} = m_t, \tag{1.36}$$

$$y_U(m_U)v/\sqrt{2} = m_U, \tag{1.37}$$

$$\text{and } \lambda(m_h)v^2 = m_h^2. \tag{1.38}$$

The composite nature of the Higgs boson can be enforced in the UV behavior of the couplings. If the IR couplings become strongly coupled as they run to the UV that is an indication that the theory is breaking down and that additional degrees of freedom must be added. We can also recall the BHL analysis and imagine the Higgs propagator term  $Z_H(\mu)$  vanishing at  $\Lambda$ , causing the other couplings to diverge. Hence, the compositeness condition of our theory is a boundary condition on the

running couplings imposed at the cutoff  $\Lambda$ . Specifically, we will require that the Yukawa couplings and the quartic coupling become non-perturbative:

$$y_{t,U}^2(\Lambda), \lambda(\Lambda) \gg 4\pi. \quad (1.39)$$

### 1.4.2 Renormalization group equations

We can use the IR Lagrangian to compute the renormalization group equations for the running couplings. They are like the Standard Model results modified by the extra technifermions. For the Yukawa couplings they are

$$(4\pi)^2 \frac{dy_t^2}{d \log \mu} = 2y_t^2 \left( (3/2 + N_c)y_t^2 + d_{TC}y_U^2 - z_c \right), \quad (1.40)$$

$$(4\pi)^2 \frac{dy_U^2}{d \log \mu} = 2y_U^2 \left( N_c y_t^2 + (3/2 + d_{TC})y_U^2 - z_{TC} \right), \quad (1.41)$$

where  $z_c$  and  $z_{TC}$  are functions of the Standard Model running gauge couplings,  $g_1, g_2$  and  $g_3$ , and the technicolor gauge coupling  $\alpha_{TC} = g_{TC}^2/(4\pi)$ . Specifically, these are

$$z_c = 8g_3^2 + \frac{9}{4}g_2^2 + \frac{17}{12}g_1^2 \quad (1.42)$$

$$z_{TC} = \frac{1}{2}(4\pi)^2 \frac{\alpha_{TC}}{\alpha_{\text{crit}}} + \frac{9}{4}g_2^2 + \frac{3}{4}g_1^2. \quad (1.43)$$

The Higgs quartic coupling has the beta function

$$(4\pi)^2 \frac{d\lambda}{d \log \mu} = 12 \left[ \lambda^2 + \lambda \left( \frac{N_c}{3}y_t^2 + \frac{d_{TC}}{3}y_U^2 - A \right) + B - \frac{N_c}{3}y_t^2 - \frac{d_{TC}}{3}y_U^2 \right] \quad (1.44)$$

with

$$A = (g_1^2 + 3g_2^2)/4 \quad (1.45)$$

$$B = (g_1^4 + 2g_1^2g_2^2 + 3g_2^4)/16 \quad (1.46)$$

The gauge couplings also run. At one loop the beta functions for the Standard Model gauge couplings are

$$(4\pi)^2 \frac{dg_i^2}{d \log \mu} = -2c_i g_i^4 \quad (1.47)$$

with

$$c_1 = -\frac{1}{6} - \frac{20}{3}N_g, \quad c_2 = \frac{43}{6} - \frac{4}{3}N_g, \quad c_3 = 11 - \frac{4}{3}N_g \quad (1.48)$$

where  $N_g$  specifies the number of quark / lepton generations. The Standard Model value is 3, but it is not obvious that we should use that number in a model that doesn't explicitly contain those particles. However, we will find that the outcome of the analysis depends very little on this choice, and we use  $N_g = 3$ . Since we expect the technicolor interaction to become confining and perhaps also approach a non-trivial fixed point, we need a beta function beyond the one-loop approximation we used for the Standard Model couplings. We will specify the form for the technicolor beta function later on.

### Fixed points

The renormalization group flow to be controlled largely by the fixed points of the beta functions. Since we can learn quite a bit about the model from looking at the fixed points, we do so now. We will assume that only the strong gauge coupling and the technicolor coupling are significant, and that they both run slowly enough at low scales that we can treat them as constants,  $g_3^*$  and  $\alpha_{TC}^*$ .

To get an idea of how the fixed points affect the masses we first examine the top Yukawa coupling by itself. In this case and with the assumptions above the beta

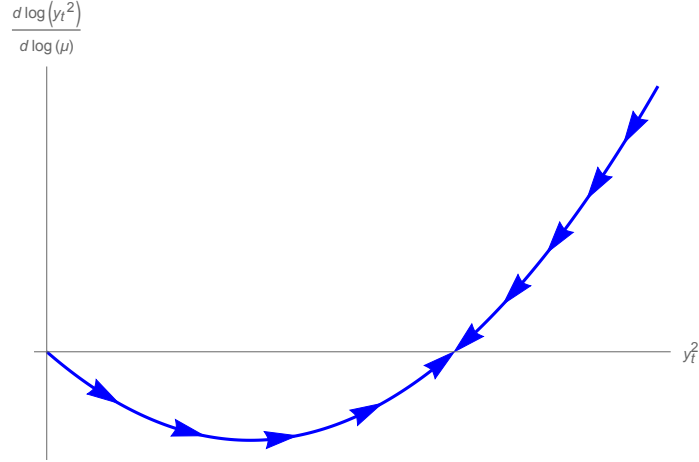


**Figure 1.7:** The beta function for  $y_t^2$ , in the approximation that the SM gauge couplings do not run, and ignoring TC contributions. There is a fixed point at zero, and one non-zero fixed point. The non-zero fixed point is attractive as  $y_t$  runs down to IR scales from  $y_t(\Lambda) \gg 4\pi$ . The value of the non-zero fixed point is determined by the strength of the QCD gauge coupling,  $g_3$ .

function is simple:

$$(4\pi)^2 \frac{dy_t^2}{d \log \mu} = 2y_t^2 \left( (3/2 + N_c)y_t^2 - 8g_3^{*2} \right). \quad (1.49)$$

This has a fixed points at  $y_t^2 = 0$  and  $y_t^2 = 8g_3^{*2}/(3/2 + N_c)$ , as illustrated in figure 1.7. The trivial fixed point is attractive for increasing  $\log \mu$  and the non-trivial one is repulsive. We can also see that as  $y_t^2 \rightarrow \infty$ ,  $dy_t^2/d \log \mu \rightarrow \infty$ , so there is also a UV attractor at infinity.

When we start with  $y_t^2(\Lambda) \gg 4\pi$  and then run  $\log \mu$  down, the Yukawa coupling is attracted towards the non-trivial fixed point. When  $y_t^2$  is much larger than the fixed point value it runs like  $y_t^2(\mu) \simeq y_t(\Lambda)^2 + \frac{3/2+N_c}{(4\pi)^2} y_t(\Lambda^2) \log(\mu/\Lambda)$ . When  $y_t^2$  is smaller it decays towards the fixed point value like  $y(\mu)^2 \simeq y_t^{*2} + (y_t^2(\mu_R) - y_t^{*2})(\mu/\mu_R)^{(3/2+N_c)/(4\pi)^2}$ .

The result is that  $y_t(m_t)$ , and hence the physical value of  $m_t$ , is not fine-tuned, given the correct value of the vacuum expectation value  $v$ . The Yukawa coupling at

weak couplings is a marginal coupling and so does not run at tree level. Any quantum corrections due to interactions with small couplings only change the running of the Yukawa coupling by a small amount. Hence, we expect the Yukawa coupling to run very little and not be fine-tuned.

At one-loop the  $y_t$  beta function does not depend on the quartic coupling  $\lambda$ , and so the beta function for  $\lambda$  also has two approximate fixed points that depends on  $y_t^{*2}$ . They are

$$\lambda_{\pm}^* = \frac{-N_c \pm \sqrt{12N_c + N_c^2}}{6} y_t^{*2}. \quad (1.50)$$

The larger fixed point is IR-attractive. Moreover, if  $\lambda(\Lambda) \gg 4\pi$  then  $\lambda$  will run down towards  $\lambda_+^*$  in the IR, generating a Higgs mass without any additional fine-tuning just as we saw for the top.

### More fixed points

All of the analysis above is found in Bardeen et al. (Bardeen et al., 1990). If we include the technifermion Yukawa coupling the fixed point structure of the beta functions becomes more complex. If we again assume that the strong gauge and technicolor couplings do not run and that the other gauge couplings are negligible then the Yukawa beta functions are governed by four fixed points:

$$y_t^2 = 0, \quad y_U^2 = 0 \quad (1.51)$$

$$y_t^2 = z_c/(3/2 + N_c), \quad y_U^2 = 0 \quad (1.52)$$

$$y_t^2 = 0, \quad y_U^2 = z_{TC}/(3/2 + d_{TC}) \quad (1.53)$$

$$(1.54)$$



and

$$\begin{aligned} y_t^2 &= \frac{1 + \frac{2}{3}d_{TC}(z_c - z_{TC})}{\frac{3}{2} + N_c + d_{TC}}, \\ y_U^2 &= \frac{1 + \frac{2}{3}N_c(z_{TC} - z_c)}{\frac{3}{2} + N_c + d_{TC}} \end{aligned} \quad (1.55)$$

There is also a UV-attractor at  $y_t^2, y_U^2 \rightarrow \infty$ .

The trivial fixed point is always IR-repulsive. Which of the other three is attractive or repulsive depends on the parameters  $z_c, z_{TC}, N_c, d_{TC}$ .

When  $z_{TC} > (1 + \frac{3}{2}d_{TC})z_c$  the  $y_t^2 = 0$  solution has two attractive eigenvectors, while the  $y_U^2 = 0$  solution has one repulsive and one attractive eigenvector. The reverse is true when  $z_c > (1 + \frac{3}{2}N_c)z_{TC}$ . In both of these cases the third non-trivial fixed point — with  $y_t^2, y_U^2 \neq 0$  — has unphysical negative values for  $y_t^2$  or  $y_U^2$  and has one repulsive eigenvector.

In the limited region where  $z_c < (1 + 3/2N_c)z_{TC}$  and  $z_{TC} < (1 + 3/2d_{TC})z_c$  the third fixed point has positive values for both  $y_t^2$  and  $y_U^2$  and both of its eigenvectors are attractive. The other two non-trivial fixed points have one repulsive eigenvector in this case. Figure 1.8 illustrates the overall fixed point structure.

This suggests that for a given set of parameters the renormalization flow will end up approaching the single fixed point that has two attractive eigenvectors. The existence of the  $y_t^2 = 0$  attractive fixed point offers hope for lowering the mass of the top quark relative to the Bardeen model; this hope is realized, as we shall see in the final results.

Solving the RG equations with constant gauge couplings demonstrates that couplings do flow to the attractive fixed point, albeit indirectly. When the Yukawa couplings are comparable at the cutoff and one of the couplings is zero at the fixed point the flow tends to undershoot the non-zero fixed point value before flowing slowly back towards it. This tends to produce lower values of the associated physical mass

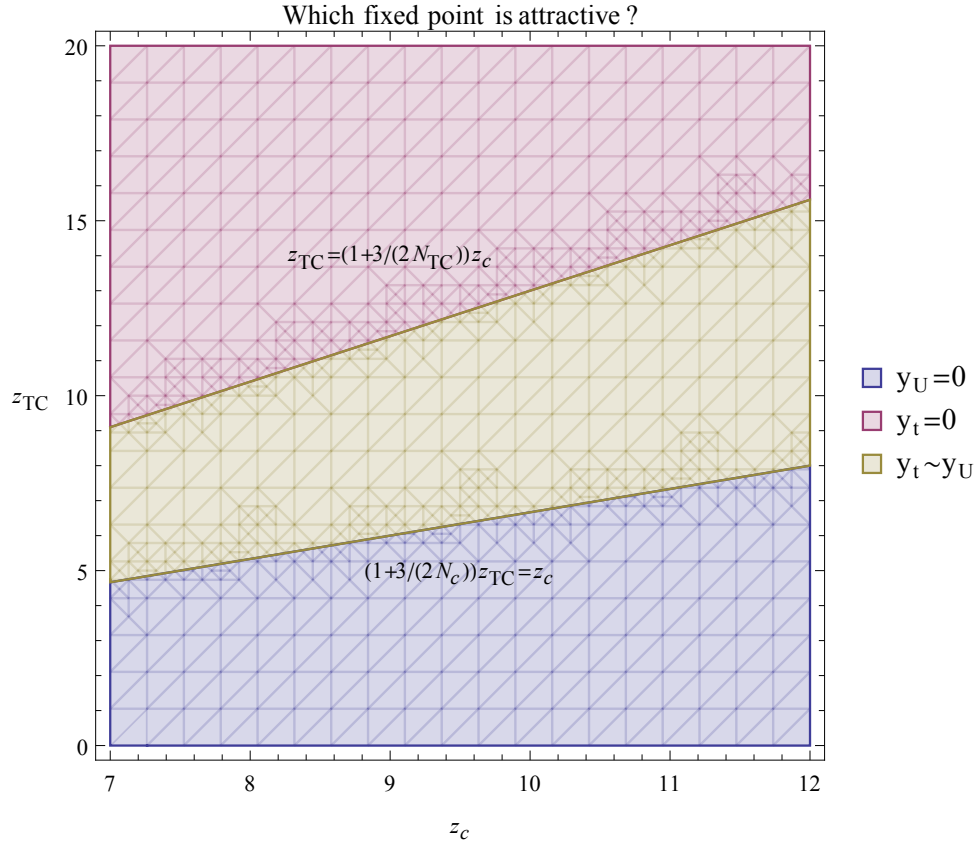


**Figure 1·8:** A figuring detailing which fixed point is dominant for different values of the gauge couplings  $\alpha_3$  and  $\alpha_{TC}$ . For large  $\alpha_{TC}$  the  $y_t = 0$  fixed point is overall attractive, but for small  $\alpha_{TC}$  the  $y_U = 0$  fixed point dominates.

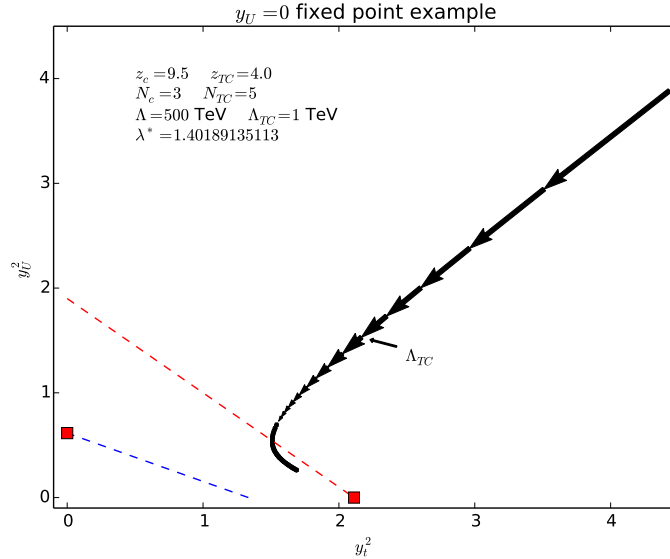


**Figure 1-9:** An illustration of how solutions to the full beta functions undershoot the fixed point values. We have chosen a constant  $\alpha_{TC}$  so that the  $y_t \neq 0$  fixed point is overall attractive. Both  $y_t(\mu)$  and  $\lambda(\mu)$  undershoot their non-zero fixed point values before running back up. This lowers the resulting masses relative to the fixed point predictions.

than the fixed-point prediction, as illustrated in figures 1-9 and 1-10.

In the same approximation, the RG equation for  $\lambda$  has two fixed points whose values are determined by the fixed point values of  $y_t^2$  and  $y_U^2$ . There are two fixed points for  $\lambda$  for each fixed point of the  $y_t, y_U$  equations. One of the  $\lambda$  fixed points is always positive and the other negative, and the positive one is always IR-attractive. This again means that  $\lambda$  will run down from its large value at the cutoff towards the positive fixed point.

Whether the fixed-points are perturbative (i.e. have  $y_{t,U}^2, \lambda \lesssim 4\pi$ ) depends on the gauge coupling strengths and the number of quark colors and technicolors. The known values of  $z_c = 8g_3^2 \simeq 11$  and  $N_c = 3$  are consistent with the perturbativity of all the fixed-points and the  $y_U = 0$  fixed point is perturbative for all values of  $z_{TC}$  and  $d_{TC}$ . The  $y_t = 0$  fixed point can be non-perturbative in  $y_U$  if  $\alpha_{TC}/\alpha_{crit.} \geq (3 + 2d_{TC})/4\pi$ .

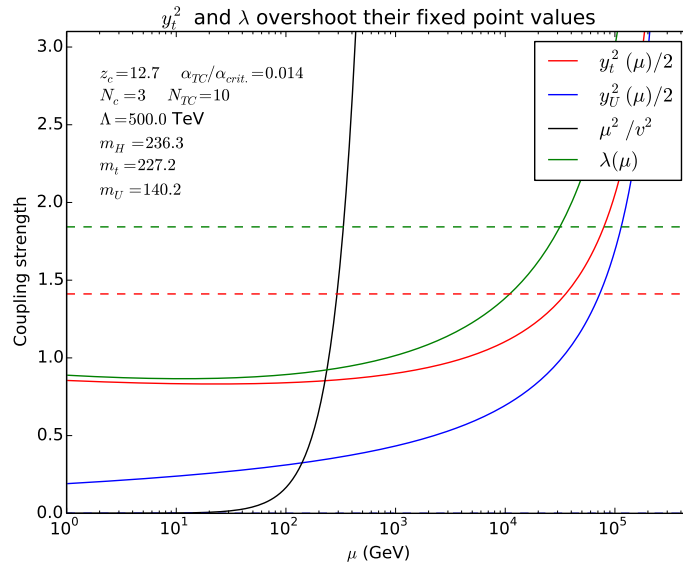


**Figure 1.10:** Another illustration of the undershoot effect. Compare to figure 1.9. The mass of each particle is the scale where the black curve meets its associated running mass. In this figure  $m_t$  and  $m_H$  are lower than if their running masses ran straight to their fixed-point values.

For  $d_{TC} = 10$  this means we need  $\alpha_{TC}/\alpha_{crit.} \lesssim 1.8$  for the theory to be perturbative.

### Running gauge couplings

So far we have assumed that all the gauge couplings are constant or negligible. This is clearly not a good approximation, especially since the technicolor coupling is required to run from a small value at  $\Lambda$  to a value strong enough to confine at  $\Lambda_{TC} \simeq 1$  TeV.

However, if the gauge couplings run slowly compared to the Yukawa couplings we can consider a sort of adiabatic approximation. In this scheme we expect the Yukawa couplings at any scale to run towards the fixed point that is dominant and attractive, as determined by the values of the gauge couplings at that scale.

For example, if the technicolor gauge coupling is very weak at the cutoff then the couplings will be attracted to the  $y_U = 0$  fixed-point initially. Then if the strength of the technicolor coupling surpasses the strength of the QCD coupling the behavior will switch and the couplings will be attracted to the  $y_t = 0$  fixed-point.

This hypothetical behavior is demonstrated in figures 1-12 and 1-12, where the technicolor coupling is approximated as a step-function for simplicity. We can see in those figures how  $m_t$  is lower than it would have been in the BHL model (which has only the single attractive fixed point), but also higher than it would be if  $y_t$  were attracted to  $y_t = 0$  the whole time.

This is still an approximation, of course, but it helps us to understand the behavior we see when we solve the full RG equations. The full results are not too different from these approximate ones.

#### 1.4.3 Mass thresholds

Renormalization group equations are the result of Feynman diagrams where off-shell particles run in closed loops. So far we have ignored the masses of the virtual particles, but this is not necessarily appropriate. For example, the contribution of a quark loop

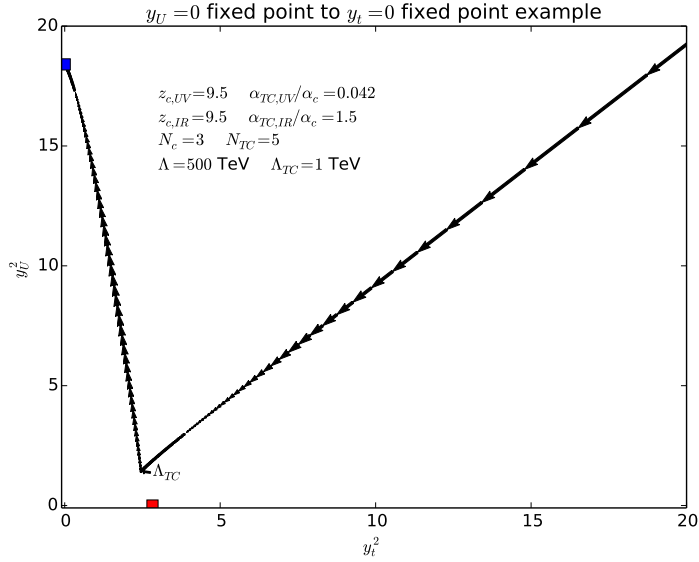


**Figure 1-11:** The running Yukawa couplings when  $\alpha_{TC}$  runs like a step function;  $\alpha_{TC}$  is constant and weak in the UV until  $\Lambda_{TC}$ , at which point it jumps up to a constant greater than  $\alpha_c$ . This causes the dominant fixed point behavior to switch, potentially further lowering the masses relative to their fixed point values.

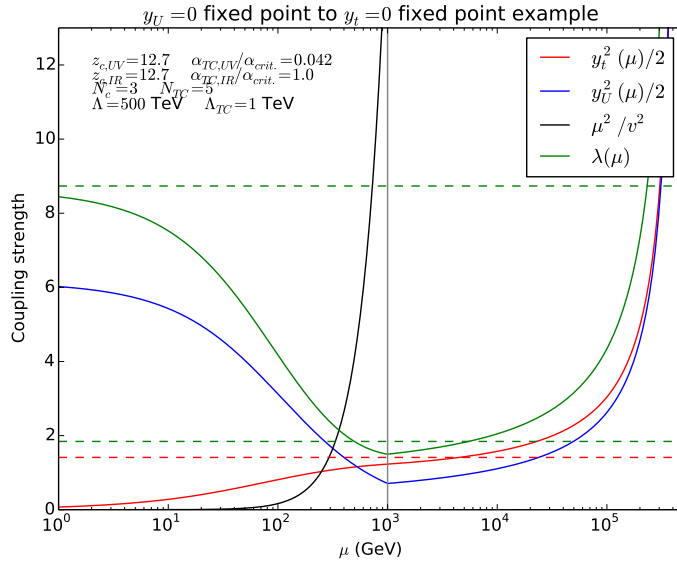


**Figure 1-12:** The running masses when  $\alpha_{TC}$  runs like a step function; compare to figure 1-11. The particle masses are the points where the black curve intersects the running mass curve.

to a photon propagator is diminished when the four-momentum of the photon is not sufficient to create a quark anti-quark pair. That is, when  $p^2 < (2m_q)^2$ . Thus, at scales well below  $2m_t$ , contributions to the RG equations from top loops should vanish. Likewise for contributions from the up technifermion.

If the up technifermion is significantly heavier than the top quark this can affect the top quark mass prediction. At scales below the technifermion mass the beta function for the top Yukawa changes to the same for as in the BHL model. It will be attracted towards the non-trivial fixed-point value where it may have been attracted to zero under the full RG equations. It is possible for this to affect the top mass prediction (or whichever fermion ends up lighter). We do not expect it to be a large effect since the change is only active over the energy range  $[m_t, m_U]$ , which we expect to be relatively small. However, our calculations do account for it, for completeness' sake.

To account for the changing RG equations without knowing the physical masses beforehand we calculate the physical masses of the fermions with a guess for where to cut out the fermion loops. We can then repeat the calculation with those results as the new guess for the cut-out points. As we repeat this process the guess and the resulting mass begin to converge. Once the guesses and the results are close enough to each other we use the resulting masses as the final result. In practice this algorithm converges after only a few iterations.

#### 1.4.4 Running technicolor coupling

We have left the technicolor coupling unspecified so far. Since it is an integral part of the RG equations, we correct that now.

We have only a few requirements on the running of the TC coupling. First, it should be weakly coupled at our ETC cutoff. We want EWSB to be driven largely by ETC and not technicolor, so it should be comparably weak at that scale. Second, it

should be strong and confining at a low scale  $\Lambda_{TC}$ . The mass scale of the lowest-lying vector mesons of the TC interaction should be  $\sim 1$  TeV or greater to explain why they have not yet been observed (Particle Data Group, 2016a).

We will assume that the technicolor interaction becomes confining at the critical scale  $\alpha_{TC,crit} = \pi/3C_2(R)$  (Cohen and Georgi, 1989), and we call the scale where the coupling reaches this value  $\Lambda_{TC} \lesssim 1$  TeV. The technicolor coupling enters the Yukawa RG equations proportionally to  $a_{TC} = \alpha_{TC}/\alpha_{crit}$  so we only need to specify that ratio. This allows us to remain agnostic about which gauge group defines the interaction and which representation the technifermions live in.

The requirement that  $\alpha_{TC}$  be weak at  $\Lambda$  while the ETC interaction at the same scale is strong enough to trigger symmetry-breaking may seem inconsistent. However, the couplings  $G_i$  that cause the symmetry-breaking are essentially independent of the ETC gauge coupling. As in the electroweak theory at low energies, they are of the form  $g_{ETC}^2/M_{ETC}^2$ , where  $M_{ETC} \propto g_{ETC}$  times a Goldstone boson decay constant. Thus the gauge couplings  $g_{TC}(\Lambda) \simeq g_{ETC}(\Lambda)$  may be weak while the four-fermion couplings are “strong” enough to trigger symmetry-breaking as required.

For simplicity, we use an RG equation for  $a_{TC}$  that allows both an IR fixed point and asymptotic freedom:

$$\frac{da_{TC}}{d \log \mu} = \beta_0 a_{TC}^2 (a_{TC} - a^*) \quad (1.56)$$

where  $\beta_0$  can be chosen so that  $a(\Lambda_{TC}) = 1$  and  $a(\Lambda)$  is as small as we’d like, as long as the IR fixed point value  $a^*$  is greater than 1 (and hence  $\alpha_{TC}^* > \alpha_{crit}$ ).

Ultimately the physical masses are not very sensitive to the exact for we use for  $\alpha_{TC}$  as long as the coupling becomes large around  $\Lambda_{TC}$ . This is expected from the fixed-point analysis from above. As long as the coupling causes the dominant fixed-point to switch at some point the running masses will have roughly the same behavior



as in figures 1.11 and 1.12.

## 1.5 Renormalization group results

The plots in figure 1.13 summarize the results of the renormalization group analysis. There are many parameters to the theory that can be adjusted, but most choices yield similar results.

The predicted Higgs mass tends to be in the range 150 to 300 GeV, with the lowest values occurring as  $\alpha_{TC}(\Lambda) \rightarrow 0$ . The top mass, on the other hand ranges from around 50 to 100 GeV with larger values occurring at lower  $\alpha_{TC}(\Lambda)$ . The  $U$  mass follows the same pattern as the Higgs mass, but is usually less than the Higgs mass. In nearly every case we investigated the Higgs was heavier than both the top quark and the  $U$  technifermion.

This dependence of the masses on  $\alpha_{TC}(\Lambda)$  is expected based on the fixed point analysis of section 1.4.2. The larger  $\alpha_{TC}$  is the more the  $y_t = 0$  fixed point will dominate the RG flow, leading to a lighter top and a heavier  $U$  technifermion.

The examples in figure 1.13 have values of  $d_{TC}$  that range from 5 to 25. Smaller values of  $d_{TC}$  produce higher masses across the board. Large  $d_{TC}$  lowers  $m_U$  because the attractive fixed-point value of  $y_U$  has  $d_{TC}$  in the denominator, see equation 1.53. Large  $d_{TC}$  lowers  $m_t$  by increasing the threshold value of  $z_{TC}$  that causes the  $y_t \neq 0$  fixed point to become attractive (recall section 1.4.2). This means  $y_t$  runs towards zero over a longer range, lowering its final value. Once  $m_t$  and  $m_U$  are lowered  $m_H$  is lowered as well, since its fixed point value depends on those two masses.

Raising  $\Lambda_{TC}$  also raises  $m_H$  and  $m_U$  and lowers  $m_t$ .  $\Lambda_{TC}$  approximately marks the scale where  $\alpha_{TC}$  becomes strongly coupled, and when  $\alpha_{TC}$  is strongly coupled the  $y_t = 0$  fixed point dominates the RG evolution. The higher  $\Lambda_{TC}$  the more time  $m_t$  has to run towards 0, and the more time  $m_U$  has to run to its non-zero fixed point.

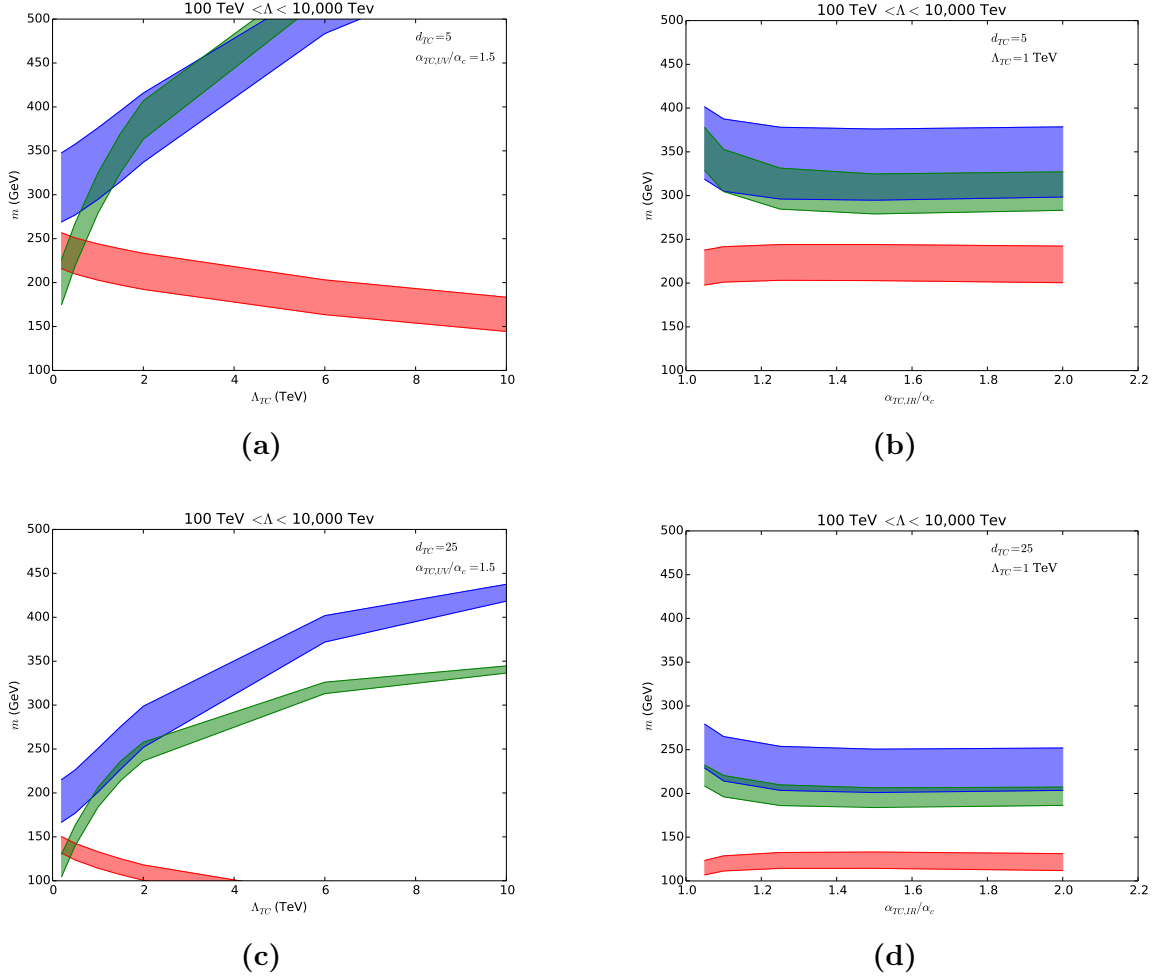


**Figure 1.13:** The results of the RG analysis outlined in section 1.4, showing the masses of the top quark,  $U$  technifermion, and the Higgs boson as they depend on  $\alpha_{TC,IR}$  (right column),  $\Lambda_{TC}$  (left column), and  $d_{TC}$  (rows). The colored bands show the variation of each mass as  $\Lambda$  is varied between 100 and 10,000 TeV. For almost all cases  $m_h$  is between 200 and 400 GeV, and  $m_t$  is less than 200 GeV. The lowest values of  $m_h$  occur when  $d_{TC}$  is large. Increasing  $\Lambda$  tends to lower the masses slightly.

$\Lambda$	$m_t$	$m_U$	$m_H$
20 TeV	187 GeV	263 GeV	338 GeV
500 TeV	154 GeV	229 GeV	256 GeV

**Table 1.3:** Masses of the fermions and the Higgs boson with  $\Lambda_{TC} = 1$  TeV and  $\alpha_{TC,IR} = 1.5\alpha_c$ . Compare to table 1.2, which lists the same masses computed without renormalization or TC effects. At  $\Lambda_{TC} = 1$  TeV the Higgs mass is unchanged, but both  $m_t$  and  $m_U$  are raised.

When  $\Lambda_{TC} = 1$  TeV, for example,  $m_t$  ranges from 0 to 50 GeV. More realistic masses like  $m_t \gtrsim 100$  GeV require smaller  $\Lambda_{TC}$ , closer to 200 GeV.

All of the reported resulting masses are insensitive to  $\Lambda$ , as expected. Once the electroweak scale is set by a single fine tuning (i.e. setting  $v = 246$  GeV) all of the other fermion masses and the Higgs mass are naturally around the 100 – 300 GeV range, even with  $\Lambda$  as high as thousands of TeV.

However, no choice of parameters seems to be able to produce a Higgs mass as low as 125 GeV, and obtaining a realistic value of  $m_t \simeq 173$  GeV requires very large technicolor representations. The model accomplishes the goal of producing a light Higgs and top quark without other light top partners, it cannot produce a Higgs that is light enough to model the real world.

## Chapter 2

# Composite Higgs Phenomenology

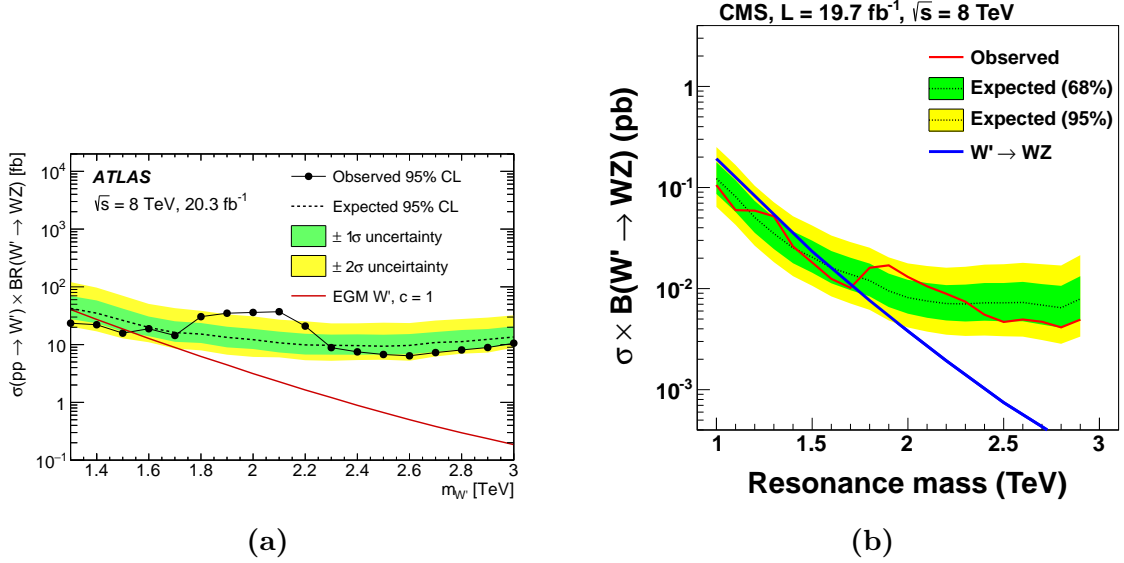
In the previous chapter we introduced a model for “minimally fine-tuned” composite Higgs. While that model did not work to describe a realistic Higgs boson mass, we will use the basic idea as inspiration in this chapter. Specifically, we will investigate the next-lightest bound states implied by that sort of model. We will show that such states can plausibly explain an excess that was possibly observed in diboson production at LHC experiments.

In the first section we will review the relevant LHC Run 1 experimental results. In the second section we will present the general properties of the bound states of a fine-tuned composite Higgs sector, especially the lowest-lying isotriplet vectors. Then we will introduce an effective Lagrangian and calculate production sections / branching ratios, and compare those predictions to experiment.

### 2.1 Diboson Excesses

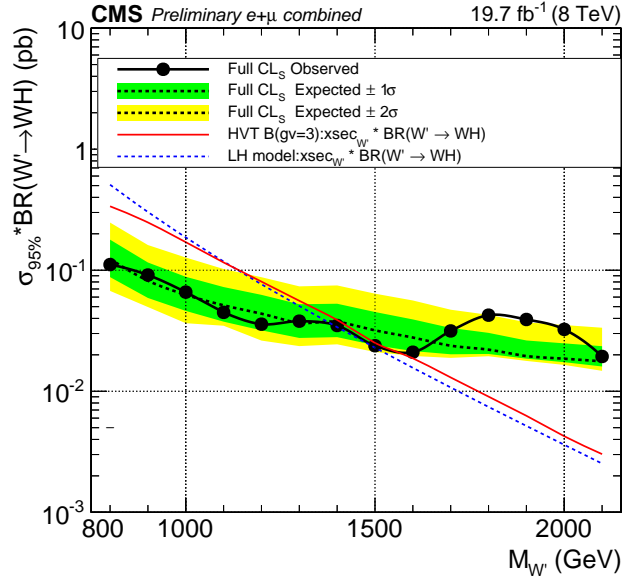
In 2014 and 2015 the ATLAS and CMS collaborations at the LHC both reported excesses in the production of pairs of weak bosons that have an invariant mass of approximately 2 TeV (ATLAS Collaboration, 2015b; CMS Collaboration, 2014a; CMS Collaboration, 2014b). The excess was observed in various channels in  $\sqrt{s} = 8$  TeV data: the ATLAS data is non-leptonic, i.e. both vector bosons decay to  $\bar{q}q$  jets, while the CMS signal appears in both semi-leptonic data and dijet data.

The original signal had a significance of  $\simeq 3\sigma$ , depending on the channel and the



(a)

(b)



(c)

**Figure 2.1:** Limits on cross-sections published by ATLAS and CMS from Run 1 data in various channels. A  $\sim 2\sigma$  excess is visible around 2 TeV in each. The top row shows the  $WZ$  channel with  $WH$  in the bottom row. ATLAS data is on the left, CMS on the right. Figures are from the ATLAS and CMS papers cited in the text.

	“ $WW$ ” $\rightarrow JJ$	“ $WW$ ” $\rightarrow \ell\nu J$	$WH \rightarrow \ell\nu b\bar{b}$
ATLAS	$3.2\sigma$	$< 1\sigma$	$1.5 - 2\sigma$
CMS	$2.2\sigma$	$1.8\sigma$	$2.2\sigma$

**Table 2.1:** The significance for a  $\sim 2$  TeV excess in each channel as reported by each experiment from Run 1,  $\sqrt{s} = 8$  TeV data. The ATLAS significance in the  $WH \rightarrow \ell\nu b\bar{b}$  channel is from preliminary Run 2 data. The reported significances are found in the papers cited in the text.

analysis with the highest significance in the dijet searches. ATLAS also searched in the semi-leptonic channel but reported no significant excess (ATLAS Collaboration, 2015c; ATLAS Collaboration, 2015d).

Both ATLAS and CMS also looked for resonant production of a vector boson in association with a Higgs boson (CMS Collaboration, ; ATLAS Collaboration, 2015a). CMS reported a  $2\sigma$  excess near 1.8 TeV in  $WH \rightarrow \ell\nu b\bar{b}$ . ATLAS looked for  $WH$  and  $ZH$  in semi-leptonic modes in Run 1 data but saw no excess.

The ATLAS non-leptonic  $WZ$  excess was initially estimated to correspond to a signal cross section times branching ratio of 3 fb (Brooijmans and Pollard, 2015; Brehmer et al., 2015). Overall the statistics of the excesses was sparse in the 8 TeV data, around 5 to 10 events. See (Brehmer et al., 2015) for a good overview of the experimental results and significances.

The analyses bin the events into  $WW$ ,  $WZ$ , and  $ZZ$  “pots”, and events appear in all three, though there may be as much as 30% spillover between them. The ATLAS analysis identifies a  $V$ -jets as a  $W$  if its mass is within 13 GeV of  $m_W = 82.4$  GeV, and likewise for a  $Z$ . In the non-leptonic CMS data a  $V$ -jet is considered a  $W$ -jet candidate if  $65 < M_V < 105$  GeV and a  $Z$ -candidate if  $70 < M_V < 110$  GeV.

The significances of the excesses in the various channels in the Run 1 data is summarized in table 2.1. CMS combined its semi-leptonic and non-leptonic data and still obtained a  $2\sigma$  effect at 1.8 TeV.

More recent analyses of Run 2,  $\sqrt{s} = 13$  TeV data did not observe the excesses. Both ATLAS and CMS put an upper limit on the cross section for  $pp \rightarrow V' \rightarrow WZ$  of about 10 fb for a 2 TeV resonances, and 8 – 10 fb for a 1.8 or 1.9 TeV resonance (CMS Collaboration, 2018a; ATLAS Collaboration, 2018a). CMS reports an upper bound on  $\sigma(pp \rightarrow V' \rightarrow WH, ZH)$  of 4-5 fb for  $WH$  and about 6 fb for  $ZH$  when  $M_{V'} = 2$  TeV (CMS Collaboration, 2017b). We will cover these Run 2 analyses in more detail at the end of this chapter.

The non-observation of the excesses in the Run 2 data may be evidence that the excesses were statistical anomalies of the Run 1 data. However, it is also possible that the Run 1 excesses were statistical up-fluctuations of a real signal that is not yet observable in the Run 2 data.

If the latter is true, then we argue that a plausible explanation is that the resonances are the lightest vector and axial-vector triplet bound states of strong interactions responsible for the compositeness of the Higgs boson  $H$ .

## 2.2 Other Technicolor States

Any composite Higgs model requires new degrees of freedom at high energies to describe the constituents of the Higgs. Often, and in technicolor-like models like the one of the previous chapter, the extra particles are fermions with additional strongly-coupled gauge interactions between them.

Strong interactions will create other bound states besides the Higgs boson. These extra states should be active around the scale where the Technicolor interaction becomes strong. This scale is usually assumed to be of the order up to  $\sim 10$  TeV so that the electroweak breaking is not fine-tuned.

In the model of the previous chapter we presented a model where the Higgs boson and longitudinal modes of the weak bosons are composites. Their mass is made light

by a fine-tuned interaction like extended technicolor (ETC). The ETC interaction had an unbroken subgroup interaction like technicolor (TC) that became confining at the scale  $\Lambda_{TC} \simeq 1$  TeV. While the symmetry-breaking pattern of that model is different from the usual technicolor pattern, we expect that the other bound states will be more typical.

Since these technicolor bound states participate in the weak interaction they can potentially affect measured electroweak precision observables. The most common and well-measured of these are the  $\rho$  parameter (Veltman, 1977) and the Peskin-Takeuchi parameters  $S$ ,  $T$ , and  $U$  (Peskin and Takeuchi, 1992). The  $\rho$  parameter is a ratio of weak boson masses  $m_W^2/m_Z^2 \cos^2 \theta_W \simeq 1$ , while the Peskin-Takeuchi parameters measure corrections to the weak current propagators.

The  $\rho$  parameter and the  $T$  parameter are linked via  $\rho \simeq 1 + \alpha T$ . They are protected from large corrections in theories that have a custodial symmetry (Sikivie et al., 1980). The custodial symmetry the  $SU(2)_L \times SU(2)_R \simeq SO(4)$  global symmetry of the Standard Model Higgs sector. We can see that the Standard Model Higgs sector has a such a symmetry by noting that we can write the Higgs Lagrangian in terms of a bidoublet  $\Sigma_P$  where

$$\Sigma = \begin{pmatrix} i\sigma_2 H^* & H \end{pmatrix}. \quad (2.1)$$

The custodial symmetry acts on  $\Sigma_P$  via  $\Sigma_P \mapsto U_L \Sigma_P U_R^\dagger$ . In the case where the Higgs is composite the symmetry is implemented in the underlying technifermions via

$$T_{L,R} = \begin{pmatrix} U_{L,R} \\ D_{L,R} \end{pmatrix} \mapsto U_{L,R} \begin{pmatrix} U_{L,R} \\ D_{L,R} \end{pmatrix}. \quad (2.2)$$

As long as this symmetry is not badly broken in the technicolor sector then the new bound states will not cause excluded corrections to  $\rho$  and  $T$ .

We expect, then, that the new states should organize into isoscalars and isotriplets



of the custodial isospin symmetry. The Higgs boson and the longitudinal modes of the weak bosons,  $W_L^\pm$  and  $Z_L$ , are the lightest bound states of the technifermions. We assume that they are made light by fine-tuning the strength of the ETC coupling, as explained in the previous chapter.

### 2.2.1 Isovectors

The next lightest bound states after the Higgs and weak Goldstone modes should be isovector and isoscalar bosons analogous to the  $\rho$ ,  $\omega$ , and  $a_1$  mesons. In this chapter we will concentrate on the isovectors and show how they can be responsible for the Run 1 excesses. We will call the parity-odd vector isotriplet  $\rho_H^{\pm,0}$  and the parity-even axial-vector isotriplet  $a_H^{\pm,0}$ .

While the custodial isospin symmetry protects  $\rho$  and  $T$  we also consider the Peskin-Takeuchi  $S$  parameter.  $S$  is not protected by the custodial symmetry. However, the technivector contribution to  $S$  can be appropriately small if  $M_{a_H} \simeq M_{\rho_H}$  and  $g_{\rho_H} \simeq g_{a_H}$ , where  $g_{a_H, \rho_H}$  measure the couplings of those bosons to the weak current. See (Lane and Martin, 2009) for references arguing this. The masses of  $a_H$  and  $\rho_H$  in a technicolor-like theory can be expressed as  $m_{\rho_H} = g_{\rho_H} f$  where  $f \simeq \Lambda_{HC}$ . From the earliest days of technicolor, the mass of the technirho in a one-doublet model was estimated (naively) to be  $\sim 1.8$  TeV (Dimopoulos, 1980; Dimopoulos et al., 1981). We will hence search for a theory with an approximate parity symmetry that will help enforce  $g_{\rho_H} = g_{a_H}$  and  $m_{a_H} \simeq m_{\rho_H}$ .

This means that the vector triple  $\rho_H$  and the axial vector triplet  $a_H$  should have similar masses. If they are to explain the diboson excesses of section 2.1 we must have  $m_{a_H} \simeq m_{\rho_H} \simeq 2$  TeV.

### 2.2.2 Decays

The technivectors  $\rho_H$  and  $a_H$  must decay primarily to the Higgs boson and the longitudinal modes of the weak bosons, as those are the only lighter technihadrons. The production mechanisms of  $\rho_H$  and  $a_H$  are the Drell-Yan (DY) process, induced by mixing with the photon and weak bosons, and weak vector boson fusion (VBF). In section 2.4.2 we will find production times decay rates of a few femtobarns, dominated by Drell-Yan.

Since the underlying dynamics are strongly-coupled we expect to see large widths, dominated by decays involving longitudinally polarized weak bosons  $V_L$ . The Run 1 diboson data favors  $\Gamma(\rho_H) \lesssim 200$  GeV, though a somewhat greater width is still allowed.

The parity and isospin symmetries of the theory tell us quite a bit about the decays of  $\rho_H$  and  $a_H$ . The approximate parity symmetry further constrains which decays are allowed. The longitudinal modes of the weak bosons  $V_L$  are axial vectors, and so the vector  $\rho_H$  should decay to  $V_L V_L$ , while the  $a_H$  is an axial vector and should decay to  $V_L V_T$  (where  $V_T$  is a weak boson with transverse polarization) or  $V_L H$ .

For nearly degenerate  $\rho_H$  and  $a_H$  and a light Higgs the decay rates  $\rho_H \rightarrow V_L V_L$  and  $a_H \rightarrow V_L H$  are identical. That is, they are precisely identical in the Wigner-Weyl mode of the electroweak symmetry in which  $(H, \vec{\pi})$  form a degenerate quartet, where the  $\pi$ 's are the pseudoscalar Goldstone modes eaten by the weak bosons. Furthermore,  $V_L V_T$  modes are suppressed relative to  $V_L V_L$  modes because for a highly boosted weak boson  $V_{L\mu} = \partial_\mu \pi / m_V$ , and  $m_V \propto gv$ . Hence, decays of  $\rho_H / a_H$  involving  $V_T$  will be suppressed by a factor of  $g^2$  relative to ones involving  $V_L$ . We can conclude that  $a_H \rightarrow V_L H$  will dominate  $a_H \rightarrow V_L V_T$ .

The approximate  $SU(2)$  isospin symmetry of the theory acts on both the weak bosons and the for Run 1 and Run 2 and scenarios and compare those to the actual

results. technivectors. This constrains the decays somewhat. In particular, an  $I = 1, I_3 = 0$  particle cannot decay into two  $I = 1, I_3 = 0$  bosons, and so  $\rho^0 \rightarrow Z_L Z_L$  is strongly suppressed. Likewise, two  $I = 0$  particles cannot arise from an  $I = 1$  particle so  $\rho^0 \rightarrow HH$  is suppressed.

All together this suggests that  $\text{Br}(\rho^\pm \rightarrow W_L^\pm Z_L) \simeq \text{Br}(\rho^0 \rightarrow W_L^+ W_L^-) \simeq 1$  and  $\text{Br}(a^\pm \rightarrow W_L^\pm H) \simeq \text{Br}(a^0 \rightarrow Z_L H) \simeq 1$ . Hence we can potentially account for the Run 1 excesses by hypothesizing that the  $WZ$  and  $WW$  events come from a 2 TeV  $\rho_H$  and that the  $WH$  events come from a 2 TeV  $a_H$ .

In the next section we will present an effective Lagrangian for  $\rho_H$  and  $a_H$ , and use it to compute production cross-sections and decay rates. Then we will compare our calculations to the Run 1 and Run 2 data, and make predictions for future experiments.

### 2.3 Effective theory for vector mesons

We use the effective Lagrangian for  $\rho_H$  and  $a_H$  that was derived by Lane and Martin in (Lane and Martin, 2009), adapted to the case of a single technidoublet with no light pseudo-Goldstone bosons, and with couplings chosen to cancel the  $\rho_H$  and  $a_H$  contributions to  $S$ . Similar Lagrangians were derived in (Marzocca et al., 2012) and (Bellazzini et al., 2012). The Lagrangian is obtained from the Hidden Local Symmetry (HLS) approach, describing the  $\rho_H$  and  $a_H$  isovectors as  $SU(2)_L \times SU(2)_R$  gauge bosons.

In order to derive an effective theory for the technivectors we use the Hidden Local Symmetry (HLS) formalism introduced in (Bando et al., 1988), which was introduced to derive a phenomenological Lagrangian for the QCD  $\rho$  meson with some success (Bando et al., 1985). The whole derivation is that of (Lane and Martin, 2009), and so we give only a overview in this section.

The idea of the HLS formalism is to treat the global  $SU(2)_L \times SU(2)_R$  symmetry of the technicolor interactions as a local symmetry. The  $\rho_H$  and  $a_H$  are then treated as the vector and axial vector combinations of the requisite “gauge bosons.” This symmetry — in addition to the Standard Model gauge group  $SU(2)_{EW} \times U(1)_Y$  — is then spontaneously broken to  $U(1)_{EM}$ , yielding the weak bosons along with massive  $\rho_H$  and  $a_H$ . We will take the two extra gauge couplings  $g_L$  and  $g_R$  to be equal, in view of the approximate parity symmetry of our intended theory.

The  $\rho_H$  mass in (Lane and Martin, 2009) is nominally given by  $m_{\rho_H} = \frac{1}{2}g_{\rho_H}f_{\rho_H}$  where  $f_{\rho_H}$  is the HLS decay constant (analogous to the decay constant of a pseudo-Goldstone boson composite Higgs). The coupling  $g_{\rho_H} \simeq g_{a_H}$  is the coupling of the  $\rho_H/a_H$  meson to the weak current, and is related to the HLS gauge couplings. If we take  $f_{\rho_H} = 1 \text{ TeV} \simeq 4v$ , where  $v = 246 \text{ GeV}$  is the Higgs vacuum expectation value, then  $g_{\rho_H} = 4$  for  $M_{\rho_H} = 2 \text{ TeV}$ .

The result of the work in (Lane and Martin, 2009) is the following interaction terms, showing only terms the terms most relevant for technivector decays:

$$\mathcal{L}(\rho_H \rightarrow VV) = -i \frac{g^2 g_T v^2}{2M_{\rho_H}^2} (\rho_{T\mu\nu}^0 W_\mu^+ W_\nu^- + (\rho_{T\mu\nu}^+ W_\mu^- - \rho_{T\mu\nu}^- W_\mu^+) Z_\nu / \cos \theta_W) \quad (2.3)$$

$$\begin{aligned} \mathcal{L}(a_H \rightarrow VV) = & i \frac{g^2 g_T v^2}{2M_{\rho_H}^2} (a_{T\mu}^0 (W_{\mu\nu}^+ W_\nu^- - W_{\mu\nu}^- W_\nu^+) \\ & - [a_{T\mu}^+ (W_\nu^- Z_{\mu\nu} - W_{\mu\nu}^- Z_\nu) - \text{h.c.}] / \cos \theta_W) \end{aligned} \quad (2.4)$$

where  $V_{\mu\nu}$  means  $\partial_\mu V_\nu - \partial_\nu V_\mu$  and we have assumed that all the technivectors have very close to the same mass,  $M_{\rho_H}$ . We can also calculate the couplings of the  $a_H$  to the Higgs boson, as we expect them to be stronger than the  $a_H VV$  couplings.

$$\mathcal{L}(a_H \rightarrow VH) = gg_T v (a_\mu^+ W_\mu^- + a_\mu^- W_\mu^+) H + \frac{gg_{\rho} v}{\cos \theta_W} a_\mu^0 Z_\mu H \quad (2.5)$$

We can note how the  $a_H VV$  couplings all have at least one factor of  $W_{\mu\nu}$  or

$Z_{\mu\nu}$  term. Since the longitudinal part of a massive boson is  $V_L = i\partial_\mu\pi/m$  for some pseudoscalar Goldstone mode  $\pi$ ,  $V_{\mu\nu} = V_{T\mu\nu} + i[\partial_\mu, \partial_\nu]\pi/m = V_{T\mu\nu}$ . That is, those terms will couple the  $a_H$  to at least one transverse weak boson. We have already argued that those decays are much smaller than decays with two longitudinal modes.

The  $a_H VH$  couplings can be derived from the fact, already mentioned in section 2.2.2 that the decay rates of  $\rho_H \rightarrow W_L W_L$  and  $a_H \rightarrow V_L H$  should be identical.

## 2.4 Predictions

With the effective theory we can calculate production cross-sections, branching ratios, and decay widths, and then compare to experimental data.

### 2.4.1 Decays

The  $\rho_H$  decays, as expected, primarily to  $V_L V_L$ . The branching ratios  $B(\rho_H^\pm \rightarrow W^\pm Z)$  and  $B(\rho_H^0 \rightarrow W^+ W^-)$  are both nearly 100%. Note that neither the  $\rho_H^0$  nor the  $a_H^0$  decays to  $ZZ$  in our model. This is because both the  $\rho, a_H^0$  and  $Z$  are isospin  $I = 1, I_3 = 0$  states, and an isospin-conserving theory forbids such decays. Hence, our model predicts that the  $ZZ$  signals claimed by ATLAS and CMS in the Run 1 data must have been one or two misidentified  $Z$ -bosons. (Another possibility is the production of an  $I = 0$  scalar technimeson, like the QCD  $f_0$ , which could decay to  $ZZ$ . We do not explore this possibility). We will see later that the Run 2 data is consistent this prediction.

Since the  $\rho_H$  decays to longitudinal modes and the  $\rho_H$  is much heavier than the weak bosons, the associated decay amplitudes pick up factors proportional to the energy of the weak bosons  $E/M_W \propto M_{\rho_H}/M_W$ , one for each longitudinally polarized boson. These two factors of  $M_{\rho_H}$  cancel the  $1/M_{\rho_H}^2$  from the coupling in equation 2.3, and the factors of  $1/M_W$  cancel against the  $g^2 v^2$ . Hence the decay rates for the

$M_{\rho_H}$	$\Gamma(\rho_H \rightarrow VV)$ (GeV)	$\Gamma(a_H \rightarrow VH)$ (GeV)	$\Gamma(a_H \rightarrow VV)$ (GeV)
1800	178	184	0.82
1900	188	196	0.78
2000	198	208	0.74

**Table 2.2:** Principal decay rates of the  $\rho_H$  and  $a_H$  for  $g = 3.862$  and  $M_{a_H} = 1.05M_{\rho_H}$ . The width of the the bosons is generically about 10% for this value of  $g_T$ . The width varies as  $g_T^2$  for fixed  $M_{\rho_H}$ .

heavy  $\rho_H$  are

$$\Gamma(\rho_H^0 \rightarrow W^+W^-) \simeq \Gamma(\rho^\pm \rightarrow W^\pm Z) \simeq \frac{g_T^2 M_{\rho_H}}{48\pi} \quad (2.6)$$

As noted earlier, the  $a_H \rightarrow VH$  decay rate rate should be identical to this, and from equation (2.5) we find

$$\Gamma(a_H^0 \rightarrow ZH) \simeq \Gamma(a_H^\pm \rightarrow W^\pm H) \simeq \frac{g_T^2 M_{a_H}}{48\pi} \quad (2.7)$$

We recall that CMS reported a  $2\sigma$  excess in the  $WH$  channel, though ATLAS did not. If this signal is real it must be due to the  $a_H$ .

For comparison, the much weaker decay rate of  $a_H$  to pairs of weak bosons is

$$\Gamma(a_H^0 \rightarrow W^+W^-) \simeq \Gamma(a_H^\pm \rightarrow W^\pm Z) \simeq \frac{g_T^2 M_W^2 M_{a_H}^3}{24\pi M_{\rho_H}^4} \quad (2.8)$$

Table 2.2 lists the cumulative decay rates for  $M_{\rho_H} = 1800, 1900,$  and  $2000$  GeV with  $M_{a_H} = 1.05M_{\rho_H}$ . For these calculations we fix  $g_T = 1900 \text{ GeV}/2v = 3.862$ . This yields widths for the new particles near 200 GeV, which is compatible with the Run 1 experimental data. For this value of  $g_T$  the widths are generically 10% of the particle mass.

#### 2.4.2 Production Mechanisms

The main production mechanisms of the technivectors are Drell-Yan (DY) production and Vector Boson Fusion (VBF), as illustrated in figure 2.2. The DY channel proceeds

$M_{\rho_H}$ (GeV)	$\sigma_{DY+VBF}(\rho^\pm)$ (fb)	$\sigma_{DY+VBF}(\rho^0)$ (fb)	$\sigma(a^\pm)$ (fb)	$\sigma(a^0)$ (fb)
1800	$1.53 + 0.36$	$0.74 + 0.18$	0.71	0.37
1900	$1.05 + 0.24$	$0.50 + 0.12$	0.51	0.27
2000	$0.73 + 0.15$	$0.36 + 0.075$	0.36	0.17

**Table 2.3:** Production cross sections at the LHC of the isovector bosons  $\rho_H$  and  $a_H$  with  $\sqrt{s} = 8$  TeV for  $g_T = 3.862$  and  $M_{a_H} = 1.05M_{\rho_H}$ . The individual DY + VBF contributions are given for  $\rho_H$ ; The VBF rates for  $a_H$  are very small and not given. As explained in the text,  $g_T = 2.73$  gives 75% large cross sections and widths half as large for  $\rho_H \rightarrow VV$ . No  $K$ -factor has been applied.

$M_{\rho_H}$ (GeV)	$\sigma_{DY+VBF}(\rho^\pm)$ (fb)	$\sigma_{DY+VBF}(\rho^0)$ (fb)	$\sigma(a^\pm)$ (fb)	$\sigma(a^0)$ (fb)
1800	$7.61 + 3.67$	$3.74 + 1.93$	4.65	2.23
1900	$5.74 + 2.62$	$2.81 + 1.37$	3.16	1.69
2000	$4.37 + 1.90$	$2.16 + 0.99$	2.39	1.27

**Table 2.4:** Production cross sections at the LHC of the isovector bosons  $\rho_H$  and  $a_H$  with  $\sqrt{s} = 13$  TeV for  $g_T = 3.862$  and  $M_{a_H} = 1.05M_{\rho_H}$ . The individual DY + VBF contributions are given for  $\rho_H$ ; compare to table 2.3.

through the mixing of the  $\rho_H$  and  $a_H$  with the weak current. The VBF channel proceeds through the same interactions as the  $\rho_H, a_H$  decays.

The cross sections for the dominant decay modes are listed in tables 2.3 and 2.4 and figure 2-3 for  $M_{\rho_H} = 1800 - 2000$  GeV,  $M_{a_H} = 1.05M_{\rho_H}$ , and  $g_T = 3.862$ . The DY and VBF rates for  $\rho_H$  are given separately. The VBF rates for  $a_H$  are very small.

The cross sections were computed at both  $\sqrt{s} = 8$  TeV and 13 TeV, in anticipation of LHC Run 2, and they exhibit the following patterns:

- $\sigma_{DY}(a_H) \simeq 0.5\sigma_{DY}(\rho_H)$
- $\sigma_{DY}(13 \text{ TeV}) = 5 - 6 \times \sigma_{DY}(8 \text{ TeV})$
- $\sigma_{VBF}(a_H) \lesssim 0.01\sigma_{VBF}(\rho_H)$
- $\sigma_{VBF}(\rho_H) \simeq 0.25\sigma_{DY}(\rho_H)$  at  $\sqrt{s} = 8$  TeV, rising to about  $0.5\sigma_{DY}(\rho_H)$  at 13 TeV.

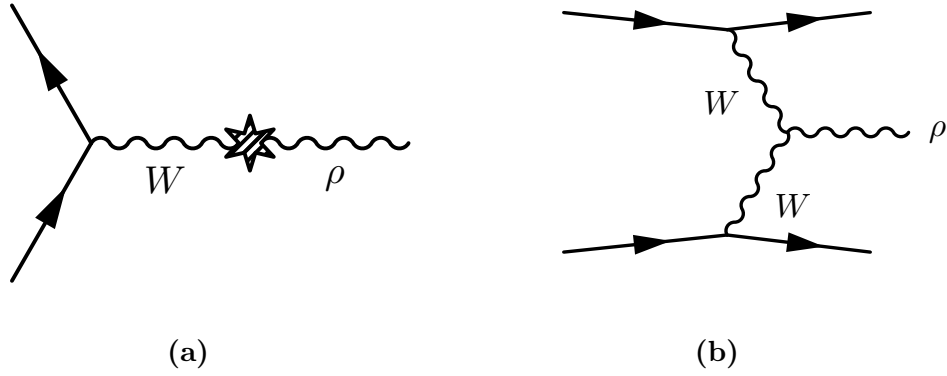


**Figure 2.2:** The two principal production mechanisms for  $\rho_H$  and  $a_H$  at the LHC. The Drell-Yan contribution (a) comes from the mixing of the  $\rho_H, a_H$  with the weak current. The VBF vertex is the same that is used in calculating decay rates. Drell-Yan is the dominant channel for both  $\rho_H$  and  $a_H$ .

- $\sigma(\rho_T^\pm) \simeq 2\sigma(\rho_H^0)$  uniformly. This is strongly dominated by  $\rho^+$  over  $\rho^-$  for both DY and VBF and is a consequence of the proton parton distribution functions.

The Drell-Yan cross sections vary roughly as  $1/g_T^2$  for fixed  $M_{\rho_H}$ . On the other hand, the VBF rate for  $\rho_H \rightarrow VV$  varies as  $g_T^2$ . Then, e.g.,  $g_T = 2.73$  instead of 3.862 gives a 75% larger production rate for  $\rho_H \rightarrow VV$  and a  $\rho_H$  width half as large.

### 2.4.3 Comparison to experiment

The largest predicted cross-section at  $\sqrt{s} = 8$  TeV is the  $WZ$  channel, proceeding mainly through a  $\rho^\pm$ . At  $M_\rho = 2$  TeV this amounts to a total cross-section times branching ratio for  $WZ$  of about 0.88 fb. This is smaller than the estimated  $WZ$  cross section from (Brooijmans and Pollard, 2015).

The predicted  $\sqrt{s} = 13$  TeV cross-sections are significantly larger, by five or six times. This brings them in just under the upper-bounds from ATLAS and CMS analyses of the 13 TeV data. At  $M_{\rho_H} = 2$  TeV we predict a total cross section for the  $WZ$  channel of 6.27 fb, increasing to 11.28 fb at  $M_{\rho_H} = 1.8$  TeV. The various



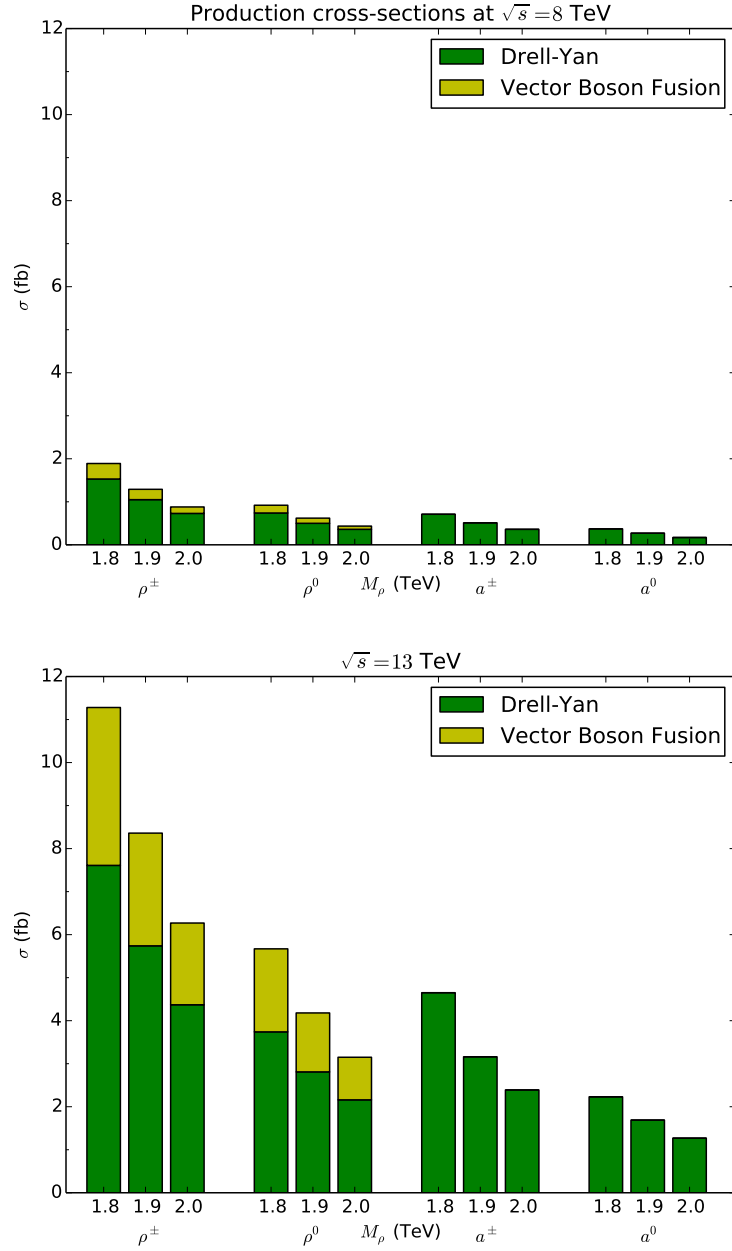


**Figure 2.3:** Production cross-sections for the isovectors with  $m_{\rho_H, a_H} = 1800 - 2000$  TeV at  $\sqrt{s} = 8$  TeV and 13 TeV. Compare to tables 2.3 and 2.4. The largest cross-sections are Drell-Yan production of  $\rho^\pm$ , which decays to  $W^\pm Z$ .

CMS and ATLAS analyses report an upper limit for  $\sigma(pp \rightarrow \rho_H \rightarrow WZ)$  of about 10 fb (CMS Collaboration, 2018a; ATLAS Collaboration, 2018a; CMS Collaboration, 2018b). One ATLAS analysis (ATLAS Collaboration, 2018b) reports an upper bound on Drell-Yan production of  $\rho_H \rightarrow WZ$  2 to 3 fb at  $M_\rho = 2$  TeV, along with a VBF upper bound of 10 fb. At  $M_\rho = 1.9$  TeV the upper bound increases to 9 fb DY and 10 fb VBF. Almost all of these bounds are just above the predicted ones in table 2.4.

One CMS Run 2 analysis (CMS Collaboration, 2017b) reports an upper limit on  $\sigma(pp \rightarrow a \rightarrow WH, ZH)$  of 4 to 5 fb for  $WH$  and about 6 fb for  $ZH$ . This is just above the predicted cross sections for  $a_H$  in table 2.4.

Our model predicts that there are no  $ZZ$  signal events. This was possibly in conflict with the Run 1 data, which assigned a non-negligible number of events to the  $ZZ$  channel ((ATLAS Collaboration, 2015b; CMS Collaboration, 2014b), etc.). However, there is significant overlap between the  $WW$ ,  $WZ$ , and  $ZZ$  bins, so it is possible that the reported  $ZZ$  events were mis-assigned. Since the 13 TeV data does not exhibit the excess it has nothing to say about  $ZZ$  versus other channels.

Our model predicts cross-sections below the observed upper limits for both the 8 TeV and 13 TeV data. If the excesses are real and explained by our model (a big if!) it must mean that the 8 TeV excesses were statistical up-fluctuations. The 13 TeV data is not strong enough yet to rule out our model. More data is required.

In the meantime, we present a few other predictions that can be used to identify our model in the case that additional Run 2 data starts to bear out our predictions.

#### 2.4.4 Other signatures

In this section we present a few phenomenological signatures of our model beyond just cross-sections and branching fractions.

First, as mentioned above, decays of  $\rho_H, a_H$  to  $ZZ$  are isospin-violating and so their rates are very small. Therefore we expect that channel to have next to no signal

in future data. This seems to be borne out by Run 2 data ()

Second, there should be significant numbers of events in semi-leptonic  $VV$  events as in all other channels. Their spotty evidence in the  $\sqrt{s} = 8$  TeV data must have been a consequence of low statistics. The  $\ell\nu\bar{q}q$  events should have  $\sigma(\ell^+)/\sigma(\ell^-) \simeq 2$ , as a consequence of  $\sigma(\rho^+) \simeq 2\sigma(\rho^-)$ .

Third, the  $\rho_H$  width is almost entirely due to strong-interaction decays to  $VV$  and is about 200 GeV with our parameters. Presumably, it would be best measured in semi-leptonic events.

Fourth, the  $\rho_H \rightarrow VV$  decays involve a pair of longitudinally-polarized weak bosons. Boosted longitudinal vector bosons tend to produce quark subjects that have more equal momenta along the parent  $V$ -direction than do boosted  $V_T$ . There may be other ways of eventually distinguishing  $V_L$  from  $V_T$ . See, (Cui et al., 2011), e.g.

Note that a measurement of the  $\rho_H$  width is in effect a measurement of  $VV$  polarizations. A large width can be due only to strong dynamics, and hence emission of  $V_L V_L$ . A small width is more likely to be an electroweak decay involving  $V_L V_T$  or  $V_T V_T$ .

Fifth, the  $VH$  decay should strengthen with more data, and it should have a large width as it comes from the strong decay  $a_H \rightarrow V_L H$ . In our model  $\Gamma(a_H) \simeq \Gamma(\rho_H)$ .

Sixth, we can look for forward jets in the detector to distinguish the  $\rho_H$  from the  $a_H$ . The  $\rho_H$  has a significant vector boson fusion production cross-section, which comes along with forward jets. The  $a_H$  is produced almost entirely through Drell-Yan processes, which does not produce forward jets. Hence, we predict that there will be no forward jets associated with  $WH$  signal events, but forward jets with  $VV$  events.

## Chapter 3

# Alternative Higgs Models for a Dimuon Excess

### 3.1 Excess at LEP

In a 2016 paper Heister analyzed archived data from the ALEPH experiment at LEP and found apparent evidence for a narrow dimuon ( $\mu^+\mu^-$ ) resonance at 30 GeV (Heister, 2016).

The purpose of this chapter is to present models where the resonance is a new scalar particle with mass 30 GeV. Our conclusion will suggest that general models of this type are not viable, and that this intriguing experimental signature calls for more theoretical attention. In the first section we review the experimental data and analysis. In the subsequent sections we introduce multiple Higgs doublet models to explain the signal. After showing that a two Higgs doublet model (2HDM) cannot explain the signal without also introducing excluded  $Z$  decays, we introduce a three Higgs doublet model (3HDM). The three Higgs doublet model can explain the signal, but is excluded by other unavoidable constraints. Finally we argue that the constraints that rule out the three Higgs doublet model exclude out all models for the resonance with new light scalars.

#### 3.1.1 The excess

The data in which the excess appears is from the LEP collider taken between 1992 and 1995. The LEP collider was a circular electron-positron collider that ran from

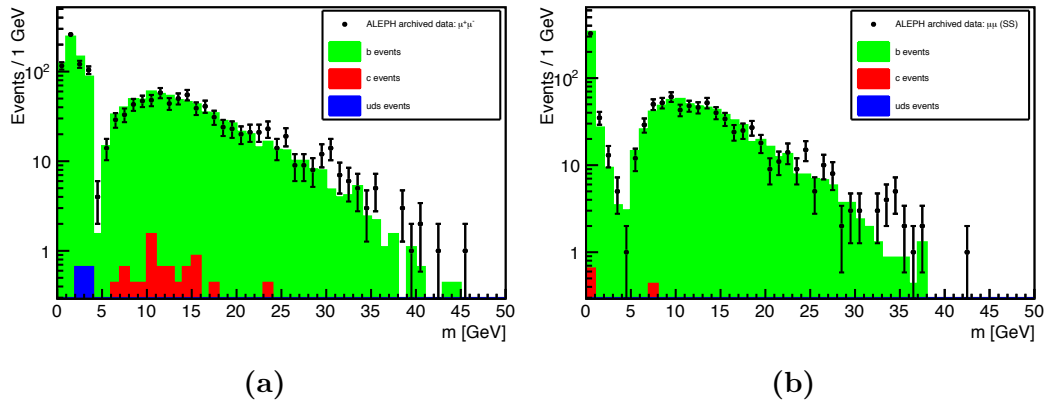


**Figure 3.1:** The  $m_{\mu\mu}$  invariant mass distributions in the opposite sign muon channel (3.1a) and same sign muon channel (3.1b). The excess is visible at 30 GeV in the opposite sign channel, while none is visible in the same sign channel. This figure is from (Heister, 2016)

1989 to 2000 (Schael et al., 2006). Its tunnel now houses the Large Hadron Collider. During the relevant period it operated at a beam center-of-momentum energy of 91 GeV, allowing it to act as a factory for  $Z$  bosons. The opposing electron and positron beams collide and produce  $Z$  bosons at rest.

The ALEPH experiment was designed to measure the mass and decays of the  $Z$  bosons in detail (ALEPH Collaboration, 1990). The relevant dataset comprises 1.9 million hadronic decays of  $Z$ -bosons. The analysis in question looked at decays of the form  $Z \rightarrow \bar{q}q\ell\ell'$ .

The result was an excess in the channel  $Z \rightarrow \bar{b}b\mu^+\mu^-$ , as illustrated in figure 3.1. The apparent excess forms a narrow peak around a dimuon invariant mass of around  $m_{\mu^+\mu^-} = 30$  GeV. According to (Heister, 2016) this has a local significance of  $2.6\sigma$ , or  $5.4\sigma$  depending on the benchmark method used. The second method requires using the look-elsewhere effect, which reduces the reported significance by  $1.4 - 1.6\sigma$ .

The resonant peak in figure 3.2 corresponds to  $32 \pm 11$  signal events. Fitting a Breit-Wigner peak to the signal yields a width of 1.78 GeV. This width measurement

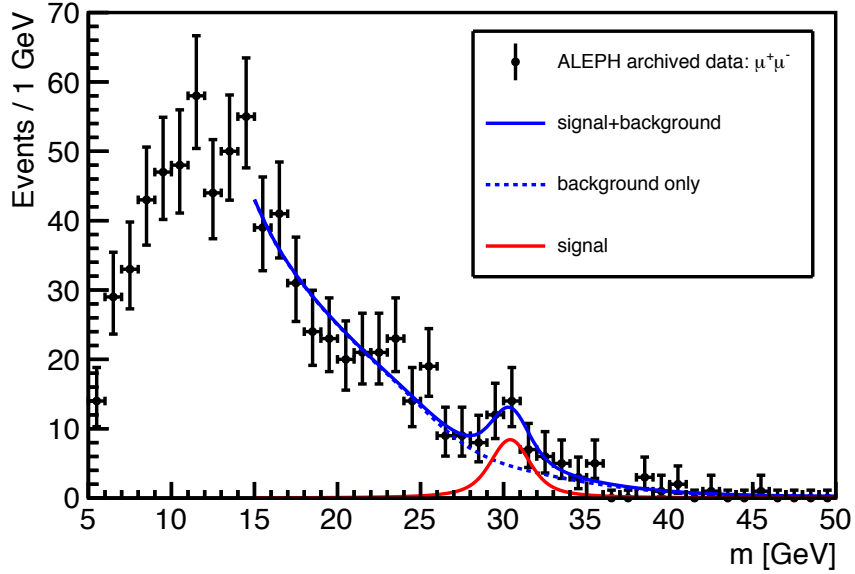


**Figure 3-2:** ALEPH  $Z \rightarrow \bar{b}b\mu^+\mu^-$  data with signal plus background model used to extract the 30 GeV signal parameters in Heister’s analysis. This figure is from (Heister, 2016).

is close to the dimuon mass reconstruction performance of the ALEPH experiment at 30 GeV, so it is theoretically likely to be at least as narrow as the mass. Using the  $b$ -tag and muon-ID efficiencies in (Heister, 2016) this yields the branching ratio

$$B(Z \rightarrow \bar{b}b X(\rightarrow \mu^+\mu^-)) = (2.77 \pm 0.95) \times 10^{-4}. \quad (3.1)$$

If this signal does arise from a process of the form  $Z \rightarrow \bar{b}bX$ ,  $X \rightarrow \mu^+\mu^-$ , we cannot say from the data whether it is emitted from the  $Z$  — as in  $Z \rightarrow Z^*X$  with  $Z^* \rightarrow \bar{b}b$  — or from one of the  $b$ -quarks, or if there are two new particles  $Z \rightarrow XY$  with  $Y \rightarrow \bar{b}b$ .

Since the  $Z$  bosons at LEP are produced at rest we know the total momentum of the system. The ALEPH data allows us to reconstruct the momentum of the dimuon, which must be the same as the momentum of the two  $b$  quarks. The dimuon (and  $\bar{b}b$ ) momentum distribution of the background and signal is plotted in figure 3-3. There

is no noticeable narrow peak at any particular momentum. In the signal region most events have  $|\vec{p}^\dagger|$  around 5 GeV. When  $m_Z = 91.17$  GeV and  $m_{\mu^+\mu^-} = 30$  GeV this corresponds to a  $\bar{b}b$  mass of  $m_{\bar{b}b} = 60.5$  GeV.

Figure 3.4 shows the distribution of the angle  $\theta^*$  between the dimuon boost axis and the  $\mu^-$ , in both the signal region and the sideband. Most of the events are at large  $|\cos\theta^*| \simeq 1$  and have the muons close to a  $b$ -jet. Presumably, most of these events are semi-leptonic  $b$  decays. There is also a smaller component of the distribution that is isotropic that appears in both the signal and sideband regions.

The decay angle ( $\cos\theta^*$ ) distribution for muons in the dimuon rest frame, where  $\theta^*$  is the angle between the dimuon boost axis and the  $\mu^-$  is shown in figure 3.4 for the signal region, a mass range of  $2\sigma$  around the fitted mean mass  $m_{\mu^+\mu^-} = (30.40 \pm 3.85)$  GeV. There is a clear preference for forward-backward production, i.e., with each muon close to a  $b$ -jet. This looks like semi-leptonic  $b + \bar{b}$  decay, and presumably most of these events are just that. There is a smaller, approximately isotropic component for  $|\cos\theta^*| < 0.8$ . This could indicate a different — scalar — production mechanism. However, figure 3.4b shows the angular distribution in the sidebands, with  $m_{\mu^+\mu^-} = 15 - 50$  GeV and excluding the signal region. It does not appear substantially different from figure 3.4a, though the ratio of events at  $|\cos\theta^*| > 0.8$  to those in between is greater than in figure 3.4b.

### 3.1.2 Other channels

Of the other  $Z$  decay channels investigated, only the channel  $Z \rightarrow \bar{b}be^+e^-$  shows any excess. That channel shows a small excess of  $8.0 \pm 4.5$  events near  $m_{e^+e^-} = 30$  GeV, with a significance of only  $\simeq 1.5\sigma$ . This is significantly lower than in the dimuon channel. We will ignore it for the remainder of this chapter.

The same-sign channel,  $Z \rightarrow \bar{b}b\mu^\pm\mu^\pm$  shows no excess near 30 GeV (see figure 3.1), nor does the opposite-sign electron-muon data,  $Z \rightarrow \bar{b}be^\pm\mu^\mp$ .

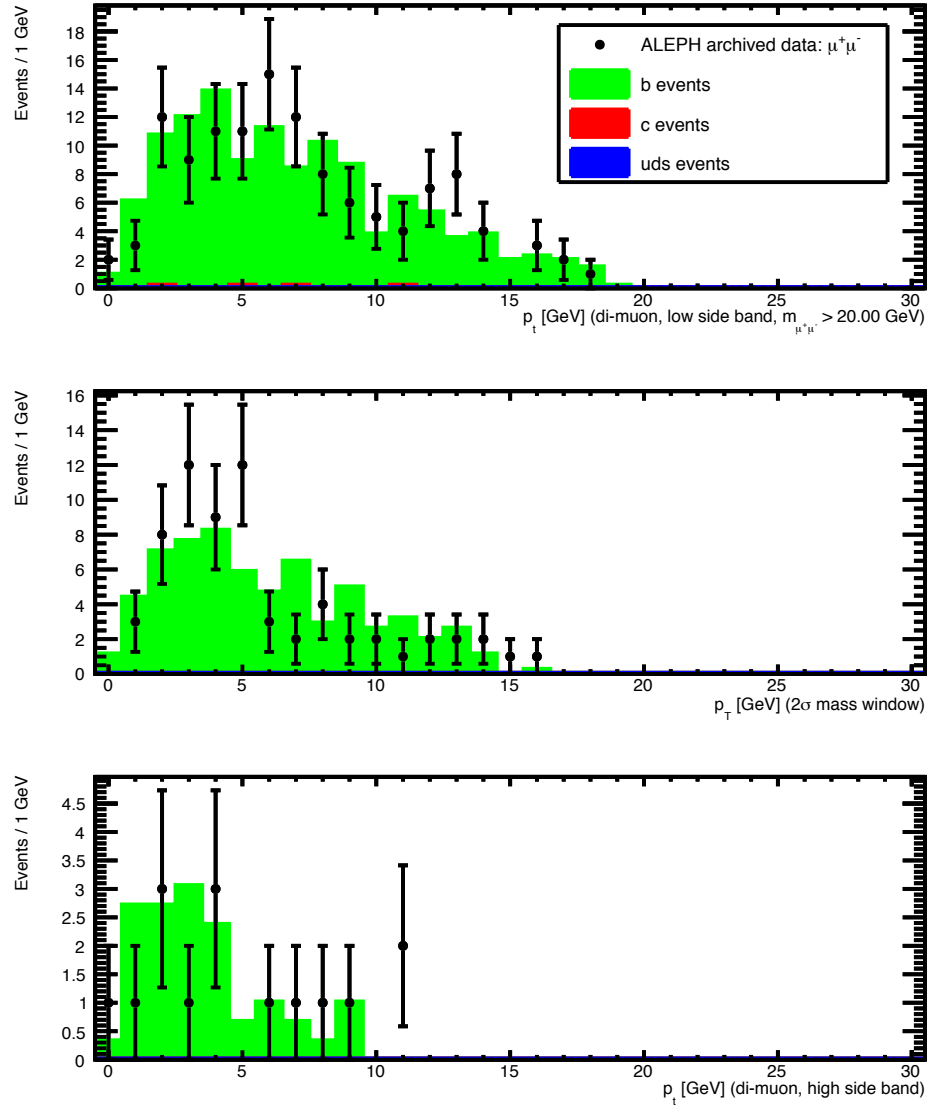


**Figure 3-3:** The total dimuon momentum distribution in the low sideband,  $2\sigma$  mass window, and high sideband (top, middle, and bottom, respectively). There is no apparent difference in the signal region, and all events have  $|p| < 20$  GeV with most events having  $|p| \lesssim 5$  GeV. This figure is courtesy of A. Heister, by private communication.



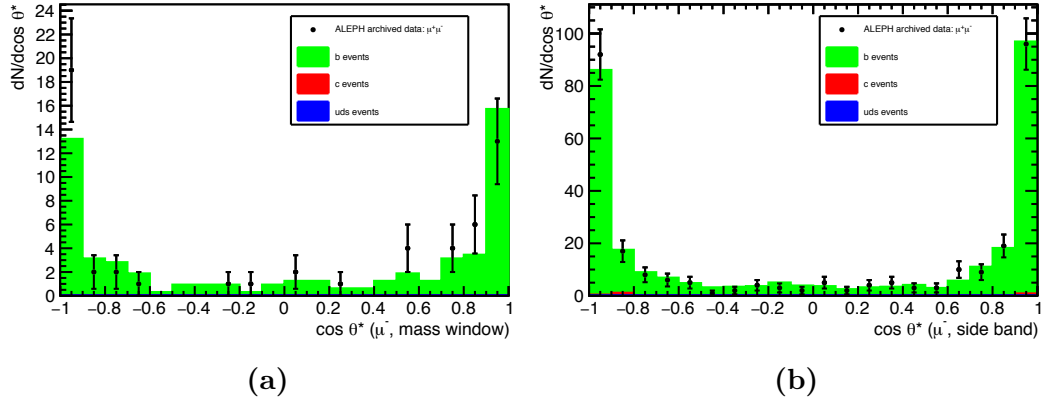


**Figure 3-4:** The angular distribution of the muons in the signal window (3-4a) and sidebands (3-4b).  $\theta^*$  is the angle between the dimuon boost axis and the  $\mu^-$ . Most events are in the  $|\cos\theta^*| > 0.8$  “horns”.

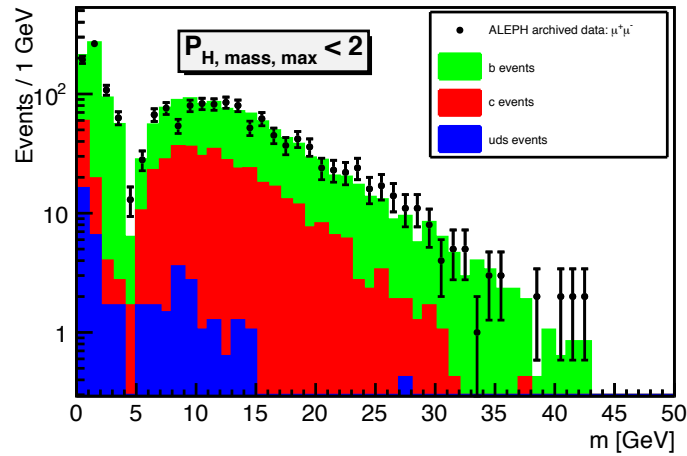


**Figure 3-5:** The opposite-sign dimuon mass distribution in  $Z \rightarrow$  hadrons +  $\mu^+\mu^-$  with the  $b$ -tag inverted shows no visible evidence for an excess near 30 GeV; figure from (Heister, 2016).

The apparent signal seems to be associated with  $b$  production. If the analysis is performed with its  $b$ -tag inverted then the excess disappears, as in figure 3.5, suggesting that there is not an associated  $\bar{q}q\mu^+\mu^-$  signal for  $q \neq b$ .

## 3.2 Scalars and Multiple Higgs Doublet Models

Let us briefly survey the sorts of models that could possibly explain the experimental signal. We will make a few assumptions as we do so. First, we will assume that the signal events are actually comprised of two  $b$  quarks and two muons, and not muons plus something that fakes  $b$ -jets. Second, we will assume that the signal really does appear only in the  $b$  channel, as the data suggests.

Finally, we will assume that the signal is actually a resonance. That is, there is a new particle with a narrow width that decays into a muon pair. We considered models of the opposite type, where a new particle decays to a muon plus a  $b$  quark (or something that fakes a  $b$  jet), with the excess bump being a kinematic edge. Our investigations of models of this type yielded no candidates that could plausibly generate the required resonant signal.

We also reject the possibility that the signal is an anomaly in semi-leptonic  $b$ -decays. If it were so, we should see the signal in the  $e^+e^-$  and even the  $e^\pm\mu^\mp$  channels as well as in the  $\mu^+\mu^-$  channel, but we do not.

If the signal does come from a process like  $Z \rightarrow XY$  with  $X \rightarrow \mu^+\mu^-$  and  $Y \rightarrow \bar{b}b$  we must explain why we do not see a resonant peak in the  $m_{\bar{b}b}$  mass distribution in figure 3.3. One possibility is that  $Y$  is an off-shell  $Z$  boson that then decays to  $\bar{b}b$ . Another possibility is that  $Y$  is another new particle with mass very close to  $m_Z - m_{\mu^+\mu^-}$ . The model we will ultimately construct has both channels, though only the one where  $Y$  is a new scalar particle is non-negligible. We will see this in detail in section 3.3.1.

This leaves us with two general possibilities. Since muons are spin  $\frac{1}{2}$  a pair of them must arise from the decay of either a spin 0 or a spin 1 particle.

Other authors have considered the possibility of a new spin 1 vector boson as the 30 GeV vector boson, in (Ko et al., 2016). While this explanation is not inherently implausible, we do not pursue that avenue further, and instead focus on models with a spin 0 particle.

Again, we have a few general possibilities. The spin 0 scalar field must couple to a scalar muon-anti-muon operator. The left-handed muon transforms under the Lorentz group and the gauge groups  $SU(2)_L$  and  $U(1)_Y$  as  $\mu_L \in ((\frac{1}{2}, 0), \underline{2}, -\frac{1}{2})$ , while the right-handed muon transforms as  $\mu_R \in ((0, \frac{1}{2}), \underline{1}, -1)$ . This means there is only one possible  $\mu\bar{\mu}$  terms that a new scalar could couple to:

$$\bar{\mu}_R \mu_L \in ((0, 0), \underline{2}, \frac{1}{2}) \quad (3.2)$$

$$(3.3)$$

A scalar field that couples  $\bar{\mu}_R \mu_L$  must have the same quantum numbers as the Standard Model Higgs doublet. This stands to reason, as  $\bar{\mu}_L \mu_R$  by itself is a mass term, and the Higgs doublet is how the mass terms in the Standard Model arise in a gauge-invariant way.

Since the Standard Model Higgs doublet contains the 125 GeV Higgs boson as its only physical degree of freedom, we must add at least one additional doublet field to get the 30 GeV resonance we are looking for.

It is worth noting that a Higgs doublet has an additional attractive feature for our purposes. Since Higgs bosons have couplings to fermions that are proportional to the mass of the fermion, it is easy to explain why the signal should appear mainly in the  $b\bar{b}$  channel. If the  $b$  quark is the most massive fermion a 30 GeV Higgs-type boson can decay to, then that decay rate should be the strongest by at least a factor

of  $(m_b/m_c)^2 \simeq 15$ .

On the other hand, it takes some doing to make a Higgs-type boson to decay significantly to muons. If the hypothetical 30 GeV boson can decay to the  $\tau$  then that rate will be larger by a factor of  $(m_\tau/m_\mu)^2 \simeq 280$ . We will see that we must arrange a model with lepton flavor non-universality so that a Higgs boson can decay to muons but not taus, avoiding this problem.

We are thus lead to the so-called multiple Higgs doublet models. The simplest examples are Two Higgs Doublet Models (2HDM). The 2HDMs have been studied extensively, mostly in the context of supersymmetric theories of the Standard Model, where the second Higgs doublet is required to avoid chiral anomalies. However, almost all of the typical 2HDMs have very specific, flavor-universal fermion couplings. Our model is different, so only some of the standard 2HDM results apply to the model that we will build.

We will first review the basics of general multiple Higgs doublet models, then deduce the sort of fermion couplings needed to explain the observed signal.

### 3.2.1 General Multiple Higgs Doublet Models

In the Standard Model there is one scalar field  $H$  that transforms as a doublet under the  $SU(2)_L$  gauge group, and has a weak hypercharge of  $Y_H = +\frac{1}{2}$ . The potential for this field has the form

$$V(H) = -m_0^2(H^\dagger H) + \frac{\lambda}{2}(H^\dagger H)^2 \equiv \frac{\lambda}{2} \left( (H^\dagger H) - \frac{v^2}{2} \right)^2 \quad (3.4)$$

When  $m_0^2$  and  $\lambda$  are both positive the minimum for this potential has a nonzero value for  $|H|$ , and so the field acquires a vacuum expectation value,  $\langle H \rangle = (0, v/\sqrt{2})^T$ .

We can then write

$$H = \begin{pmatrix} G^+ \\ (v + h + iG_Z)/\sqrt{2} \end{pmatrix} \quad (3.5)$$

The  $G^+$  and  $G_Z$  fields are the Goldstone modes that are eaten by the vector bosons to give them mass. The remaining degree of freedom is the scalar field  $h$ . It gets a mass  $m_h^2 = \lambda v^2$ .

Since the field is a doublet we can also write the Yukawa terms (e.g.)

$$\mathcal{L}_{\text{yuk}} = y_\mu \bar{L}_\mu^i \mu_R H^i + \text{h.c.} \quad (3.6)$$

$$\rightarrow \frac{y_\mu v}{\sqrt{2}} \bar{\mu} \mu \equiv m_\mu \bar{\mu} \mu \quad (3.7)$$

In a more general model there are multiple scalar doublet fields,  $H_a$ . If the scalar sector of the potential has a non-trivial global minimum then at least some of the fields get vacuum expectation values (vevs), and the gauge symmetry can be broken down to  $U(1)_{EM}$ .

The extra fields contained in the doublets mix to form a collection of massive scalar bosons. If there are  $N$  doublets and the Higgs sector is  $CP$  conserving there will be  $N$  physical neutral scalars,  $N - 1$  physical neutral pseudoscalars, and  $N - 1$  physical charged scalars. One linear combination of the neutral scalars must be the 125 GeV Higgs boson observed at the LHC. Additionally, we need one combination of scalars or pseudoscalars to have a mass of 30 GeV and decay to muons. We need the rest to either be massive enough or to have the right couplings to have escaped searches for additional Higgs bosons.

We must also ensure that the 125 GeV scalar has couplings to other particles that are close to the values predicted by the Standard Model. The ratios between the measured couplings of  $H(125)$  and the Standard Model predictions are currently all consistent with one (CMS Collaboration, 2015).

### 3.2.2 Fermion Couplings and the Glashow-Weinberg Theorem

The most general Yukawa couplings are

$$\begin{aligned}
\mathcal{L}_Y = & \sum_{f,f',a} \bar{L}_f^i \Gamma_{\ell,ff'}^a \ell_R H_a^i + \text{h.c.} \\
& + \bar{D}_{L,f}^i \Gamma_{d,ff'}^a d_R H_a^i + \text{h.c.} \\
& + \bar{U}_{L,f}^i \Gamma_{u,ff'}^a u_R (i\sigma_2)_{ij} H_a^{\dagger j} + \text{h.c.}
\end{aligned} \tag{3.8}$$

After spontaneous symmetry breaking, these turn into non-diagonal mass terms for the leptons and quarks. The mass matrix is  $M_{\ell,u,d} = \sum_a v_a \Gamma_{\ell,u,d}^a / \sqrt{2}$ . This matrix is not necessarily hermitian but can be diagonalized by separate rotations of the right-handed and left-handed fermions. That is,  $M = P m_{\text{diag}} Q^\dagger$ .

However, for multiple doublets and generic Yukawa couplings  $\Gamma$  the transformation that diagonalizes the mass matrix does not also diagonalize the couplings of the fermions to the neutral physical bosons. That is,  $P^\dagger \Gamma^a Q$  is not diagonal for any general  $\Gamma^a$  even though  $\sum_a P^\dagger v_a \Gamma^a Q$  is. This implies that each of the neutral bosons can act as a flavor-changing neutral current (FCNC), the existence of which is largely ruled out. Quark FCNCs are well-studied, and bounds on lepton-flavor violating decays of the  $\tau$  and  $\mu$  leptons constrain interactions like the one in figure 3-6.

Glashow and Weinberg proved (Glashow and Weinberg, 1977) that a necessary and sufficient condition for a multiple Higgs doublet model to not introduce FCNCs is that there must be a basis for the doublets where all flavors of fermion that share the same quantum numbers must couple to a single doublet. In the Standard Model with lepton flavor-universality this implies that all leptons must couple to one doublet, all the up-type quarks couple to one doublet, and all the down-type quarks couple to one doublet.

This requirement is too strict for our model; if the muons couple to the same scalar

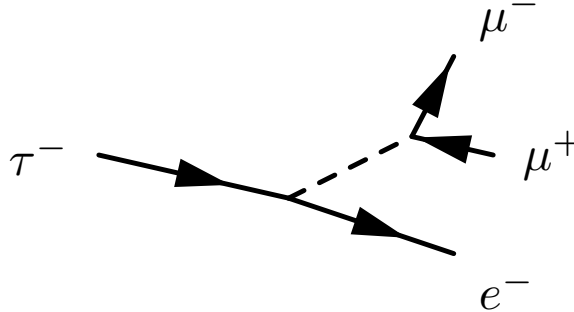


**Figure 3-6:** An example of a lepton-flavor-violating decay of a  $\tau$  lepton mediated by some scalar  $\phi$  with flavor non-diagonal couplings. This particular decay has a measured width of  $< 6.12 \times 10^{-20}$  GeV (Particle Data Group, 2016a), which puts constraints on  $y_{\phi,\mu\mu} \times y_{\phi,e\tau}/m_\phi^2$ . Such considerations suggest that off-diagonal Yukawa couplings must be forbidden by a symmetry.

as the taus then the branching ratio to muons will be tiny, suppressed by a factor of at least  $(m_\mu/m_\tau)^2 \simeq 1/285$ . We can get around this requirement by introducing additional global symmetries so that the muon has different quantum numbers than the taus. This will require extra symmetries for the Higgs doublets as well. We will use a scheme where one doublet couples to the muons only, and other doublets couple to all the other fermions.

### 3.3 Two Higgs Doublet Model – An Instructive Warm-up

We will start by investigating the minimal model with a scalar resonance, a two Higgs doublet model (2HDM). We will see that this model is too simple to be able to both explain the 30 GeV signal and avoid known bounds on  $Z$  branching ratios and Higgs searches. However, since other models are more complicated, studying the 2HDM will show us how multiple Higgs doublet models work and it will help us understand

the key problems that must be addressed.

There are two doublets  $H_1$  and  $H_2$ . They each get vacuum expectation values,  $(v_1, v_2) \equiv v(\cos \beta, \sin \beta)$ . They have subfields

$$H_1 = \begin{pmatrix} \phi_2^+ \\ (v_1 + \rho_1 + i\pi_1)/\sqrt{2} \end{pmatrix} H_2 = \begin{pmatrix} \phi_2^+ \\ (v_2 + \rho_2 + i\pi_2)/\sqrt{2} \end{pmatrix} \quad (3.9)$$

The charged  $\phi^+$  fields mix to form the longitudinal mode of the  $W$  and a charged scalar, the  $\pi$  fields form the  $Z$  longitudinal mode and a neutral pseudoscalar. The  $\rho$  fields mix to form two neutral scalars, one of which should correspond to  $H(125)$ .

As promised we use a theory with a global  $U(1)$  symmetry that allows us to break flavor-universality without introducing FCNCs. The charge assignments are

$$H_2 \mapsto e^{i\theta} H_2 \quad (3.10)$$

$$\begin{pmatrix} \nu_{\mu L} \\ \mu_L \end{pmatrix} \mapsto e^{i\theta/2} \begin{pmatrix} \nu_{\mu L} \\ \mu_L \end{pmatrix} \quad (3.11)$$

$$\mu_R \mapsto e^{-i\theta/2} \mu_R \quad (3.12)$$

All the other fields are neutral under this symmetry. We could include the electron in the symmetry as well without affecting the results of this chapter, but we will not do so now.

The most general scalar potential that respects  $CP$  symmetry and the global  $U(1)$  symmetry above has the form

$$\begin{aligned} V_H = & m_{11}^2 H_1^\dagger H_1 + m_{22}^2 H_2^\dagger H_2 - m_{12}^2 (H_1^\dagger H_2 + \text{h.c.}) \\ & + \lambda_1 (H_1^\dagger H_1)(H_1^\dagger H_1) + \lambda_2 (H_2^\dagger H_2)(H_2^\dagger H_2) \\ & + \lambda_3 (H_1^\dagger H_1)(H_2^\dagger H_2) + \lambda_4 (H_1^\dagger H_2)(H_2^\dagger H_1) \end{aligned} \quad (3.13)$$

The off-diagonal mass coupling  $m_{12}^2$  breaks the global  $U(1)$  softly, which does not spoil the Yukawa couplings or introduce FCNCs.



The mass parameters  $m_{11}^2, m_{22}^2$  can be chosen so the potential has a minimum at  $\langle H_{1,2} \rangle = v_{1,2}/\sqrt{2}$ . The mass matrices for the  $\rho$ ,  $\phi$ , and  $\pi$  fields then become

$$m_\pi^2 = \frac{m_{12}^2 v^2}{v_1 v_2} \begin{pmatrix} \frac{v_2^2}{v^2} & -\frac{v_1 v_2}{v^2} \\ -\frac{v_1 v_2}{v^2} & \frac{v_1^2}{v^2} \end{pmatrix} \quad (3.14)$$

$$m_{\phi^+}^2 = \frac{(m_{12}^2 - \lambda_4 v_1 v_2) v^2}{v_1 v_2} \begin{pmatrix} \frac{v_2^2}{v^2} & -\frac{v_1 v_2}{v^2} \\ -\frac{v_1 v_2}{v^2} & \frac{v_1^2}{v^2} \end{pmatrix} \quad (3.15)$$

$$m_\rho^2 = \begin{pmatrix} m_{12}^2 \frac{v_2}{v_1} + \lambda_1 v_1^2 & -m_{12}^2 + (\lambda_3 + \lambda_4) v_1 v_2 \\ -m_{12}^2 + (\lambda_3 + \lambda_4) v_1 v_2 & m_{12}^2 \frac{v_1}{v_2} + \lambda_2 v_2^2 \end{pmatrix} \quad (3.16)$$

which are non-diagonal. The physical fields are the mass eigenstates of these matrices. The  $\pi$  mass matrix and the  $\phi^+$  mass matrix both have one zero eigenvalue, corresponding to the eaten Goldstone bosons that act as longitudinal modes for the massive gauge bosons. The other eigenvalues are the masses of the physical pseudoscalar  $\eta$  and charged scalar  $h^+$ . Their masses are

$$m_\eta^2 = \frac{m_{12}^2 v^2}{v_1 v_2} \quad (3.17)$$

$$m_{h^+}^2 = (m_{12}^2 - \lambda_4 v_1 v_2) \frac{v^2}{v_1 v_2} = m_\eta^2 - \lambda_4 v^2 \quad (3.18)$$

The matrix

$$T \equiv \begin{pmatrix} \cos \beta & \sin \beta \\ -\sin \beta & \cos \beta \end{pmatrix}, \quad (3.19)$$

rotates the doublets to the basis where only one doublet gets a vev, and also diagonalizes the mass matrices  $m_\pi^2$  and  $m_{\phi^+}^2$ . Hence,

$$\begin{pmatrix} G^+ \\ h^+ \end{pmatrix} = T \begin{pmatrix} \phi_1^+ \\ \phi_2^+ \end{pmatrix}, \quad \begin{pmatrix} G_Z \\ \eta \end{pmatrix} = T \begin{pmatrix} \pi_1 \\ \pi_2 \end{pmatrix} \quad (3.20)$$

On the other hand, the neutral scalar mass matrix requires an additional diagonal-

ization angle,

$$\begin{pmatrix} H_{125} \\ h \end{pmatrix} = W_h T \begin{pmatrix} \rho_1 \\ \rho_2 \end{pmatrix} = \begin{pmatrix} \cos \Theta & \sin \Theta \\ -\sin \Theta & \cos \Theta \end{pmatrix} T \begin{pmatrix} \rho_1 \\ \rho_2 \end{pmatrix} \quad (3.21)$$

where  $\Theta$  is the mixing angle between the mass eigenstate  $H_{125}$  and the scalar mode that has purely Standard Model couplings. The limit where  $\cos \Theta \rightarrow 1$  is the alignment limit, where  $H_{125}$  has exactly the couplings of the Standard Model Higgs boson. Since the 125 GeV Higgs boson does appear to have Standard Model-like couplings, most of our analysis will be very close to the alignment limit. (See section 3.3.1 for a more detailed discussion of  $\Theta$  and Higgs alignment)

We take  $m_\eta = 30$  GeV and  $m_h = 50 - 60$  GeV. We consider the mass of the charged scalar later. The LEP signal will then proceed through  $Z \rightarrow h\eta$ ,  $\eta \rightarrow \mu\mu$ ,  $h \rightarrow bb$ .

The  $Z$  couples to scalars through the terms

$$\mathcal{L}_{Zss} = \frac{2e}{\sin 2\theta_W} Z_\mu \left[ \sin \Theta \left( \eta \overleftrightarrow{\partial}^\mu H_{125} \right) + \cos \Theta \left( \eta \overleftrightarrow{\partial}^\mu h \right) \right] \quad (3.22)$$

This means that in the alignment limit,  $\theta \rightarrow \Theta$ , the decay rate of  $Z$  to  $h\eta$  is given by

$$\Gamma(Z \rightarrow h\eta) = \frac{1}{3} \frac{m_Z}{16\pi} \left( \frac{m_Z}{v} \right)^2 \times \left[ \left( 1 - \frac{(m_h + m_\eta)^2}{m_Z^2} \right) \left( 1 - \frac{(m_h - m_\eta)^2}{m_Z^2} \right) \right]^{3/2} \quad (3.23)$$

corresponding to a branching ratio between  $1.4 \times 10^{-2}$  ( $m_h = 30$  GeV) and  $1.2 \times 10^{-4}$  ( $m_h = 60$  GeV). Recall that the signal corresponds to a branching of approximately  $4 \times 10^{-4}$ . That these branching ratios depend only on the masses of the scalars is the first cause of a problem with the 2HDM that we will see later.

The global  $U(1)$  symmetry makes the Yukawa sector simple; all couplings of fermions to physical scalars are proportional to the mass of the fermion times some mixing angles.

The Yukawa coupling of  $h$  to muons and  $b$  quarks is given by

$$y_\mu(\bar{\mu}_L\mu_R H_2 + \text{h.c.}) \rightarrow \frac{m_\mu}{v_2}(W_h T)_{22} h \bar{\mu} \mu, \quad (3.24)$$

$$y_b(\bar{b}_L b_R H_1 + \text{h.c.}) \rightarrow \frac{m_b}{v_1}(W_h T)_{21} h \bar{b} b \quad (3.25)$$

and the Yukawa couplings of the  $\eta$  are

$$y_\mu(\bar{\mu}_L\mu_R H_2 + \text{h.c.}) \rightarrow \frac{m_\mu}{v_2} T_{22} \eta \bar{\mu} \gamma^5 \mu = \frac{m_\mu}{v} \cot \beta \eta \bar{\mu} \gamma^5 \mu, \quad (3.26)$$

$$y_b(\bar{b}_L b_R H_1 + \text{h.c.}) \rightarrow \frac{m_b}{v_1} T_{21} \eta \bar{b} \gamma^5 b = \frac{m_b}{v} \tan \beta \eta \bar{b} \gamma^5 b \quad (3.27)$$

In general the lepton Yukawa couplings are

$$\begin{aligned} \mathcal{L}_{y_\ell} = & -\frac{m_\mu}{v \sin \beta} \bar{\mu} [v \sin \beta + H_{125} \sin(\beta + \Theta) + h \cos(\beta + \Theta) + i\eta \gamma^5 \cos \beta] \mu \\ & - \sum_{\ell_k=e,\tau} \frac{m_{\ell_k}}{v \cos \beta} \bar{\ell}_k [v \cos \beta + H_{125} \cos(\beta + \Theta) - h \sin(\beta + \Theta) - i\eta \gamma^5 \sin \beta] \ell_k \\ & + h^+ \left[ \frac{\sqrt{2} m_\mu \cot \beta}{v} \bar{\nu}_\mu P_R \mu - \sum_{\ell_k=e,\tau} \frac{\sqrt{2} m_{\ell_k} \tan \beta}{v} \bar{\nu}_{\ell_k} P_R \ell_k \right] + \text{h.c.} \end{aligned} \quad (3.28)$$

The quark Yukawa couplings are

$$\begin{aligned} \mathcal{L}_{Y_q} = & - \sum_{d_k=d,s,b} \frac{m_{d_k}}{v \cos \beta} \bar{d}_k [v \cos \beta + H \cos(\beta + \Theta) - h \sin(\beta + \Theta) - i\eta \gamma^5 \cos \beta] d_k \\ & - \sum_{u_k=u,c,t} \frac{m_{u_k}}{v \cos \beta} \bar{u}_k [v \cos \beta + H \cos(\beta + \Theta) - h \sin(\beta + \Theta) + i\eta \gamma^5 \sin \beta] u_k \\ & - \frac{\sqrt{2} \tan \beta}{v} \sum_{k,l=1} 3 [\bar{u}_k (V M_d)_{kl} P_R d_l h^+ - \bar{d}_k (V^\dagger M_u)_{kl} P_R u_l h^-] + \text{h.c.} \end{aligned} \quad (3.29)$$

where  $M_{u,d}$  are the diagonal up- and down-quark mass matrices and  $V$  is the Cabibbo-Kobayashi-Maskawa matrix.

The angle factors in these these Yukawa couplings arise from the scalar mixing matrices. In particular, the Yukawa coupling of the  $i$ th scalar in  $(H_{125}, h)$  or  $(0, \eta)$

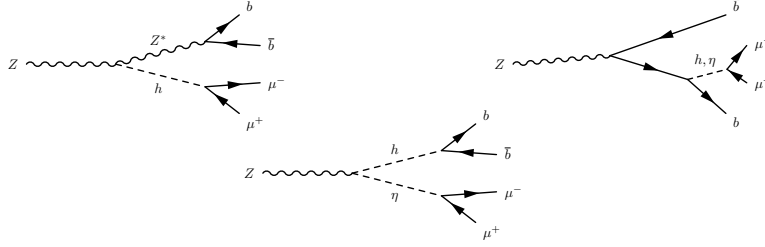


**Figure 3.7:** The possible channels for signal  $Z \rightarrow b\bar{b}\mu\bar{\mu}$  events in the 2HDM, shown schematically (not all possible diagrams are included). We assume that only one of the new scalar particles has a mass of 30 GeV. The  $Z \rightarrow Z^*h$  and  $Z \rightarrow b\bar{b}$  amplitudes are too small to contribute to the observed signal branching ratio. Only the  $Z \rightarrow h\eta$  channel

to a fermion that couples to the  $j$ th doublet is equal to  $m_f/v(W_h T)_{ij}(v/v_j)$  for the scalars and  $m_f/vT_{ij}(v/v_j)$ .

Crucially, in the alignment limit the neutral mixing matrix  $W_h$  reduces to the identity matrix, and so the  $h$  Yukawa couplings are identical to the  $\eta$  couplings. This implies  $B(h \rightarrow X) = B(\eta \rightarrow X)$ . This is the second problem for the model.

### 3.3.1 Replicating the signal

In the 2HDM there are three channels that can potentially produce the signal, illustrated in figure 3.7. We require a 30 GeV resonance that decays to muons, and if the  $b\bar{b}$  pair arises from a resonant particle it must have a mass of  $m_{b\bar{b}} \simeq 60$  GeV. The first channel is  $Z \rightarrow Z^*h$  where  $Z^* \rightarrow b\bar{b}$  and  $h \rightarrow \mu^+\mu^-$ . The second has  $Z \rightarrow b\bar{b}$  where one of the  $b$  quarks radiates an  $\eta$  which subsequently decays into  $\mu^+\mu^-$ . The third is  $Z \rightarrow h\eta$  with  $h \rightarrow b\bar{b}$  and  $\eta \rightarrow \mu^+\mu^-$ . In all cases but the first we take the  $\eta$  to be the 30 GeV particle that decays to muons. In theory we could have that be the scalar  $h$ , but when  $m_\eta < m_h$  it is too easy to violate the unitarity and positivity bounds that we will discuss in section 3.4.3

The  $Z^*$  channel cannot be strong enough to produce the required signal branching

ratio  $B_{\text{signal}} \simeq 3 \times 10^{-4}$ . With  $m_{\mu\mu} = 30$  GeV the  $Z^*$  is far off-shell and so the decay rate is suppressed by factors of the  $Z$  mass. It produces the branching ratio  $B(Z \rightarrow Z^* h \rightarrow b\bar{b}\mu^+\mu^-) = 4.58 \times 10^{-5} \times \sin^2 \Theta \times B(h \rightarrow \mu^+\mu^-)$ . Since  $\sin \Theta$  needs to be small to match the observed couplings of  $H(125)$  we cannot make this channel large enough to explain the signal.

The  $Z \rightarrow b\bar{b}$  channel is also too weak to produce the signal. Generically it yields the branching ratio  $B(Z \rightarrow \bar{b}(b \rightarrow \mu^+\mu^-b)) = 9.36 \times 10^{-8} \times (y_{\eta,bb}v/m_b)^2 \times B(\eta \rightarrow \mu^+\mu^-)$ . Since increasing the  $\eta bb$  Yukawa coupling simultaneously decreases the  $\eta \rightarrow \mu^+\mu^-$  branching ratio, we cannot choose parameters that makes this channel significant.

Only the  $h\eta$  channel can contribute appreciably to the signal. Ideally we would like to find  $B(\eta \rightarrow \mu^+\mu^-) \simeq 1$  and  $B(h \rightarrow b\bar{b}) \simeq 1$  to avoid adding other new  $Z$  decays. However, investigating the Yukawa couplings of the scalar particles to the Standard Model fermions reveals that this is impossible in the 2HDM, as we will now see.

### Yukawa couplings

The decay width of the  $Z$  boson is  $\Gamma_Z = 2.4952 \pm 0.0023$  GeV (Particle Data Group, 2016a). The  $1\sigma$  uncertainty corresponds to a possible additional branching ratio of  $9.2 \times 10^{-4}$ . The ATLAS collaboration has measured the specific decay channel  $Z \rightarrow 4\ell$  where the leptons include  $4e$ ,  $4\mu$ , and  $2e2\mu$  (ATLAS Collaboration, 2014c). The corresponding branching ratio is  $B(Z \rightarrow 4\ell) = (3.2 \pm 0.2) \times 10^{-6}$ , which is in agreement with the Standard Model prediction of  $4.45 \times 10^{-6}$ . This means any additional branching ratio to four muons from our model must be less than  $0.8 \times 10^{-6}$  or so.

On the other hand, we can see that an aligned 2HDM that produces the correct  $2b2\mu$  signal branching rate necessarily violates either the bound on  $4\mu$  decays or the

bound on the total  $Z$  width. This is because, in the alignment limit, all the branching ratios of the  $h$  and  $\eta$  are equal, as in equations (3.24-3.27). The 2HDM contributions to  $Z \rightarrow 2b2\mu$  and  $Z \rightarrow 4\mu$  are

$$B(Z \rightarrow 2b(2\mu)_{30 \text{ GeV}}) = B(Z \rightarrow h\eta)B(\eta \rightarrow 2\mu)B(h \rightarrow 2b) = B_{\text{signal}} \quad (3.30)$$

$$B(Z \rightarrow 4\mu) = B(Z \rightarrow h\eta)B(\eta \rightarrow 2\mu)B(h \rightarrow 2\mu). \quad (3.31)$$

The 2HDM contribution to the total  $Z$  width includes the  $Z \rightarrow 2b2\mu$  and  $Z \rightarrow 4\mu$  channels as well as  $Z \rightarrow 4q$  and  $Z \rightarrow 2q2\mu$ . It is enough for our purposes to consider  $Z \rightarrow 4b$ , which is equal to

$$B(Z \rightarrow 4b) = B(Z \rightarrow h\eta)B(\eta \rightarrow 2b)B(h \rightarrow 2b). \quad (3.32)$$

It follows that

$$B(Z \rightarrow 4b) = B_{\text{signal}} \times \frac{B(\eta \rightarrow 2b)}{B(\eta \rightarrow 2\mu)} \quad (3.33)$$

$$B(Z \rightarrow 4\mu) = B_{\text{signal}} \times \frac{B(h \rightarrow 2\mu)}{B(h \rightarrow 2b)} = B_{\text{signal}} \times \left( \frac{B(\eta \rightarrow 2b)}{B(\eta \rightarrow 2\mu)} \right)^{-1}, \quad (3.34)$$

where in the last line we have used the equality of the  $h$  and  $\eta$  branching ratios. If we are to arrange that  $B_{\text{signal}} = 4.7 \times 10^{-4}$  and  $B(Z \rightarrow 4\mu) < 0.8 \times 10^{-6}$  then we must have  $B(\eta \rightarrow 2b)/B(\eta \rightarrow 2\mu) > 590$ . But this then implies that

$$B(Z \rightarrow \text{all})_{2HDM} > B(Z \rightarrow 4b) > 0.28$$

which is dramatically too large.

There is simply no way to choose couplings in the alignment limit to avoid all the bounds on  $Z$  decays. Note that the argument above did not depend at all on how the Yukawa couplings were chosen. The only way out in the 2HDM is to leave the alignment limit and let  $|\cos \Theta| \neq 1$ . This is constrained, however, by measurements of the

couplings of the  $H_{125}$  signal strengths, which are the ratios of measured cross-sections to their Standard Model predictions,  $\mu = (\sigma \times BR)/(\sigma \times BR)_{SM}$ . Signal strength measurements from the LHC experiments are consistently within one standard deviation of  $\mu = 1$  for all processes. Lower limits are typically  $\mu \gtrsim 0.9$  (see (ATLAS Collaboration, 2014a), (CMS Collaboration, 2015), (Aad et al., 2016) for details.) The 2HDM signal strengths are proportional to  $\cos^2 \Theta$ , meaning  $|\cos \Theta| \gtrsim 0.95$ .

In general

$$\frac{B(h \rightarrow 2b)}{B(h \rightarrow 2\mu)} = \left(\frac{m_b}{m_\mu}\right)^2 \tan^4 \beta \times \left(\frac{\cos \Theta - \sin \Theta \cot \beta}{\cos \Theta + \sin \Theta \tan \beta}\right)^2 \quad (3.35)$$

which differs from  $B(\eta \rightarrow 2b)/B(\eta \rightarrow 2\mu)$  by a factor that depends on  $\Theta$ . However, the bound  $\cos^2 \Theta \gtrsim 0.9$  means this is not enough; The  $h$  term is too close to the  $\eta$  term and in general the same argument as above applies and rules out the theory.

In the next section we will see that in a three Higgs doublet model the  $h$  and  $\eta$  Yukawa couplings are uncorrelated, even in the alignment limit. This extra freedom allows us to produce the correct signal branching ratio while also satisfying the bounds on  $Z$  decays. However, it has another unavoidable problem in the charged scalar sector, as we shall see. The 2HDM has this issue as well, and it is helpful to look at it now before we investigate the more complicated situation in the 3HDM.

### 3.3.2 Charged Higgs Decays

The last new particle of the 2HDM is the charged scalar boson  $h^+$ . There have been extensive searches for the  $h^+$ , as it is one of the most accessible predictions of all multiple Higgs doublet models.

Our model's  $h^+$  is possibly very different from most. Since it has the same mass-mixing matrix as the  $\eta$  it also has Yukawa couplings of the same strength. So if the  $\eta$  decays primarily to  $\mu$ 's then the  $h^+$  will decay mostly to  $\mu\nu_\mu$ .

This is markedly different from standard 2HDMs, where the  $h^+$  decays primarily to either the heaviest possible quark pair or to  $\tau\nu_\tau$ . This means that almost all past searches for a charged Higgs potentially miss ours. Hence, we have some freedom in choosing its mass. If  $m_{h^+} \leq 62.5$  GeV then it will be ruled out by the large decay  $H(125) \rightarrow h^+h^-$ .

If the  $\eta$  and  $h^+$  decay primarily to  $b$  quarks then most of the the standard searches apply and require  $m_{h^+} \gtrsim 300$  GeV, as summarized in the Particle Data Group review of charged Higgs searches (Particle Data Group, 2016b).

On the other hand, the strongest limit on a  $h^+$  that decays mainly to  $\mu^+\nu_\mu$  appears to come from searches at LEP for pair-production of supersymmetric partners of the muon  $\tilde{\mu}^+$ . They limit  $m_{h^+} > 95$  GeV; see (Particle Data Group, 2016a), for example. Also, even when the  $\mu\nu_\mu$  decays dominate,  $h^+ \rightarrow t\bar{b}$  can still be significant when the  $h^+$  is massive enough. It is excluded by a CMS search for  $t(b)h^\pm$  production followed by  $h^+ \rightarrow t\bar{b}$  with large branching ratio (Eysermans et al., 2016). Based on a CMS search we estimate on  $m_{h^+}$  in our model to be  $m_{h^+} \lesssim 200$  GeV.

However, these fermionic decays are almost irrelevant in light of the decisive constraint from LHC searches for off-shell weak bosons muons. The  $h^+$  contributes to this process through diagrams like figure 3-8. The  $W^*$  decays to  $h^+\eta$  or  $h^+h$ . The  $h^+$  then decays further to  $h$  or  $\eta$  plus on-shell  $W$ . The coupling between the  $W$ ,  $h^+$ , and neutral scalars is

$$\mathcal{L}_{Wss} = \frac{m_W}{v} W_\mu^+ \left( \cos \Theta h^- \overleftrightarrow{\partial}^\mu h + \sin \Theta h^- \overleftrightarrow{\partial}^\mu H_{125} + i h^- \overleftrightarrow{\partial}^\mu \eta \right) + \text{h.c.}, \quad (3.36)$$

which means in the alignment limit the  $h^+$  always couples to  $W^+h, W^+\eta$  at maximum strength.

We used the Contur analysis tools (Butterworth et al., 2017) to put limits on the mass of the  $h^+$  using data from LHC experiments, as described in detail by



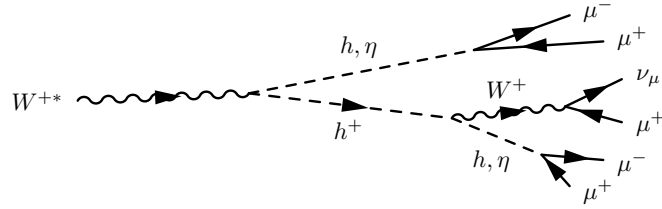


**Figure 3.8:** An example of a  $W^*$  decaying to four leptons through the charged higgs. Though the pairs of muons arising from the neutral scalar vertices may have invariant masses that do not pass the ATLAS cuts ( $50 < M_{\ell\ell} < 120$  GeV for at least one pair), other pairings may. There are enough events of this type that a significant number pass the cuts and constrain the 2HDM.

Butterworth et al. in (Brooijmans et al., 2018a). We generated simulated events in many experimental channels using a Monte-Carlo procedure and the 2HDM model with a range of values for  $m_{h^+}$ . The analysis then compared the number of simulated events to actual data from the same channels. The most constraining channels were events of the type

$$\bar{q}q \rightarrow \gamma^*, Z^* \rightarrow h^+ h^- \rightarrow \mu^+ \mu^- + E_T^{\text{miss}} \quad (3.37)$$

$$\bar{q}q \rightarrow W^* \rightarrow h^\pm h, h^\pm \eta \rightarrow \mu^\pm \mu^+ \mu^- + E_T^{\text{miss}} \quad (3.38)$$

along with a few other processes. The experimental data was taken from an ATLAS 8 TeV measurement (ATLAS Collaboration, 2016), a CMS measurement of  $H \rightarrow WW$  (CMS Collaboration, 2017a), and various 7 TeV ATLAS measurements (ATLAS Collaboration, 2014b) (and see (Brooijmans et al., 2018a) for more). The simulations predicted many more events of these types than were observed in the data.

This data excludes the entire mass range  $95 \text{ GeV} \leq m_{h^+} \leq 200 \text{ GeV}$  at a 99.9% confidence level. The most constraining dataset is the ATLAS four-lepton lineshape. This is surprising at first, since the ATLAS measurement requires at least one lepton

pair relatively close to the  $Z$  mass ( $50 < M_{\ell\ell} < 120$  GeV). However, when  $h$  and  $\eta$  both decay mostly to  $\mu^+\mu^-$ , and we consider that  $W$  has a combined 20% branching ratio to  $e\nu$  and  $\mu\nu$ , we can see that a large portion of the signal events have four or more leptons. So while some pairs of muons come from a narrow, non- $Z$  resonance, pairs selected from different vertices in the decay have no mass peak. The high multiplicity and high cross section then mean that many events pass the fiducial selection of the experiment.

This is a very strong constraint on our scalar models. While the 2HDM was ruled out even before considering this analysis, we will see that it also rules out the 3HDM despite the additional freedom that model has in the charged Higgs sector.

### 3.4 Three Higgs Doublet Model — Trouble with Triples

The two Higgs doublet model cannot explain the Aleph dimuon signal without introducing additional signals that contradict experiment. We have seen two ways it does this: the equality of the  $h$  and  $\eta$  Yukawa couplings introduce too large  $Z$  decays, and the charged Higgs shows up in LHC data even when it evades most direct searches.

A three Higgs doublet model allows us to circumvent the first of these problems, but not the second<sup>1</sup>. We will show how this happens in the 3HDM, which should also suggest how similar problems would arise in even more general models.

Our 3HDM has the muons couple to the third doublet,  $H_3$ , and all the other fermions couple to  $H_2$ .<sup>2</sup> The three doublets all get vevs,

$$(v_1, v_2, v_3) = v(\cos\beta\cos\gamma, \cos\beta\sin\gamma, \sin\beta) \quad (3.39)$$

---

<sup>1</sup>The next simplest model after the 2HDM is one with two Higgs doublets along with a  $SU(2)$  singlet scalar field, but this has exactly the same problems as the 2HDM.

<sup>2</sup>In theory we could let up-type quarks couple to one doublet and down-type quarks couple to the remaining one, but we would then have to choose parameters to suppress both  $\eta \rightarrow \bar{b}b$  and  $\eta \rightarrow \bar{c}c$  instead of just the single parameter choice to suppress all quark decays.

We again introduce a global symmetry that allows the Yukawa structure just outlined. We must have at least a  $U(1)$  symmetry where each doublet has a different charge,  $Y_{H_a}$ . One possible charge assignment is  $Y_{H_1} = 1$ ,  $Y_{H_3} = -1$ ,  $Y_{\mu_R} = 1$ , with all other fields invariant. This protects the coupling structure of  $H_3$  with muons,  $H_2$  with all other fields, and  $H_1$  with none.

Each doublet has subfields

$$H_i \equiv \begin{pmatrix} \phi_i^+ \\ (v_i + \rho_i + i\pi_i)/\sqrt{2} \end{pmatrix} \quad (3.40)$$

that mix to make the physical states. In the symmetry-broken phase there are now two physical charged scalars, two pseudoscalars, and two physical scalars besides the 125 GeV Higgs. The matrix

$$T = \begin{pmatrix} \cos \beta \cos \gamma & \cos \beta \sin \gamma & \sin \beta \\ -\sin \gamma & \cos \gamma & 0 \\ -\sin \beta \cos \gamma & -\sin \beta \sin \gamma & \cos \beta \end{pmatrix} \quad (3.41)$$

rotates the vevs into the basis where only doublet has a non-zero vev. As in the 2HDM, the top row  $T$  also determines the combinations of  $\phi^+$ 's and  $\pi$ 's that form the longitudinal  $W^+$  and  $Z$  modes. The analogous combination of  $\rho$ 's has exactly Standard Model-like couplings, though it is not necessarily a mass eigenstate.

The scalar potential becomes

$$\begin{aligned} V_{\text{3HDM}} = & \sum_{ij} H_i^\dagger m_{ij}^2 H_j + \sum_i \lambda_{ii} (H_i^\dagger H_i)^2 + \\ & + \sum_{i<j} \lambda_{ij} (H_i^\dagger H_i)(H_j^\dagger H_j) + \tilde{\lambda}_{ij} (H_i^\dagger H_j)(H_j^\dagger H_i) \\ & + L_a (H_a^\dagger H_b H_a^\dagger H_c + \text{h.c.}) \end{aligned} \quad (3.42)$$

where  $m_{ij}^2$  is a hermitian matrix. There are three diagonal quartic couplings and six off-diagonal quartic couplings, along with the nine mass parameters. This is again

the most generic CP-invariant potential consistent with a softly-broken global  $U(1)$  symmetry that has different charges for each of the three doublets. The symmetry allows us to couple the doublets to fermions in a non-flavor-universal way without introducing flavor-changing neutral currents.

In the term on the last line only one of  $H_3^\dagger H_1 H_3^\dagger H_2$ ,  $H_1^\dagger H_2 H_1^\dagger H_3$ , or  $H_2^\dagger H_1 H_2^\dagger H_3$  is allowed. This term breaks the  $U(1)^3$  global symmetry of the potential down to a single  $U(1)$  where  $2Y_a = Y_b + Y_c$  (this is still compatible with the Yukawa structure, which allows any  $Y_{H_1} \neq Y_{H_3} \neq 0$  and  $Y_{H_2} = 0$ ). If more than one of those terms is present then all three doublets must have the same charge which means no symmetry protects the Glashow-Weinberg condition and the theory can generate FCNCs. We hence limit ourselves to just one term at most and  $Y_a \neq Y_b \neq Y_c$ . It is fully consistent to have none of the terms appear and for most of the analysis here we will let  $L = 0$  as it makes several calculations much easier. We will consider it again briefly in the section on triple-scalar interactions.

The undiagonalized mass matrices are

$$m_\pi^2 = \begin{pmatrix} 2v_1^2\lambda_{11} + m_{12}^2\frac{v_2}{v_1} + m_{13}^2\frac{v_3}{v_1} & -m_{12}^2 + v_1v_2\lambda_{12} & -m_{13}^2 + v_1v_3\lambda_{13} \\ & \ddots & \end{pmatrix} \quad (3.43)$$

In the 2HDM, the matrix  $T$  was enough to diagonalize the charged and pseudoscalar mass matrices because they were  $2 \times 2$ . Now that all the mass matrices are  $3 \times 3$  the charged and pseudoscalar mass matrices both require an extra mixing angle to fully diagonalize, corresponding to a rotation around the vector  $\vec{v}$ . We write

$$\begin{pmatrix} H_{(125)} \\ h_1 \\ h_2 \end{pmatrix} = W_+ T \begin{pmatrix} \rho_1 \\ \rho_2 \\ \rho_3 \end{pmatrix} \quad (3.44)$$

$$\begin{pmatrix} G_Z \\ \eta_1 \\ \eta_2 \end{pmatrix} = W_- T \begin{pmatrix} \pi_1 \\ \pi_2 \\ \pi_3 \end{pmatrix} \quad \begin{pmatrix} G^+ \\ h_1^+ \\ h_2^+ \end{pmatrix} = W_c T \begin{pmatrix} \phi_1^+ \\ \phi_2^+ \\ \phi_3^+ \end{pmatrix} \quad (3.45)$$

where

$$W_{-,c} = \begin{pmatrix} 1 & 0 & 0 \\ 0 & \cos \theta_{-,c} & -\sin \theta_{-,c} \\ 0 & \sin \theta_{-,c} & \cos \theta_{-,c} \end{pmatrix} \quad (3.46)$$

and

$$W_+ = \begin{pmatrix} c_\Theta & -s_\Theta s_\psi & -s_\Theta c_\psi \\ s_\Theta s_{\psi-\theta_+} & c_{\psi-\theta_+} c_\psi + c_\Theta s_{\psi-\theta_+} s_\psi & c_\Theta s_{\psi-\theta_+} c_\psi - c_{\psi-\theta_+} s_\psi \\ s_\Theta c_{\psi-\theta_+} & c_\Theta c_{\psi-\theta_+} s_\psi - s_{\psi-\theta_+} c_\psi & c_\Theta c_{\psi-\theta_+} c_\psi + s_{\psi-\theta_+} s_\psi \end{pmatrix} \quad (3.47)$$

where  $c_x$  and  $s_x$  stand for  $\cos x$  and  $\sin x$ . The angle  $\Theta$  is again the one that measures the alignment of the  $H_{125}$  couples with those of the Standard Model Higgs boson. When  $\cos \Theta = 1$  then  $W_+$  takes the same form as  $W_-$  and  $W_c$  with  $\theta_+$  as its only remaining mixing angle.

We will again take the 30 GeV resonance to be the lightest pseudoscalar  $\eta_1$ . The signal decay proceeds through  $Z \rightarrow \eta_1 h_1 \rightarrow 2\mu 2b$ , where  $m_{h_1} \simeq 60$  GeV and the  $\eta_1$  decays mostly to muons.

The couplings that control the decay of  $Z$  into  $h, \eta$  now depend on the mass-mixing angles:

$$\mathcal{L}_{Zss} = i \frac{m_Z}{v} Z^\mu \left( h_i \overleftrightarrow{\partial}_\mu \eta_j \right) (W_+ W_-^T)_{ij} \quad (3.48)$$

In the alignment limit this has the form

$$\mathcal{L}_{Zss} = i \frac{m_Z}{v} Z^\mu \begin{pmatrix} H_{125} & h_1 & h_2 \end{pmatrix} \begin{pmatrix} 1 & 0 & 0 \\ 0 & \cos(\theta_+ - \theta_-) & \sin(\theta_+ - \theta_-) \\ 0 & -\sin(\theta_+ - \theta_-) & \cos(\theta_+ - \theta_-) \end{pmatrix} \overleftrightarrow{\partial}_\mu \begin{pmatrix} 0 \\ \eta_1 \\ \eta_2 \end{pmatrix} \quad (3.49)$$

Hence, in the alignment limit, the  $Z \rightarrow h_1 \eta_1$  decay rate picks up a factor of  $\cos^2(\theta_+ -$

$\theta_-$ ) relative to the 2HDM rate in equation (3.23).

### 3.4.1 Yukawa couplings and signal

The advantage of the 3HDM is that in the alignment limit the Yukawa couplings of the  $\eta_1$  and the  $h_1$  are no longer the same. The Yukawa couplings of the  $\eta_1$  are

$$y_{\eta_1,\mu} = \frac{m_\mu}{v_3}(W_-T)_{23} = -\frac{m_\mu}{v} \cot \beta \sin \theta_- \quad (3.50)$$

$$y_{\eta_1,b} = \frac{m_b}{v_2}(W_-T)_{22} = \frac{m_b}{v} (\cos \theta_- \cot \gamma \sec \beta + \sin \theta_- \tan \beta) \quad (3.51)$$

while the  $h_1$  couplings are

$$y_{h_1,\mu} = \frac{m_\mu}{v_3}(W_+T)_{23} \simeq -\frac{m_\mu}{v} \cot \beta \sin \theta_+ \quad (3.52)$$

$$y_{h_1,b} = \frac{m_b}{v_2}(W_+T)_{22} \simeq \frac{m_b}{v} (\cos \theta_+ \cot \gamma \sec \beta + \sin \theta_+ \tan \beta) \quad (3.53)$$

If we choose  $\cos \theta_- \cot \gamma \sec \beta + \sin \theta_- \tan \beta \simeq 0$  so that  $y_{\eta_1,\mu}/y_{\eta_1,b}$  is large then  $\eta_1$  will decay mostly to muons. As long as  $\theta_+$  is not very close to  $\theta_-$  it will still decay mostly to  $b$ 's. Note that attempting to make  $B(\eta_1 \rightarrow \mu\mu)$  large by choosing  $\beta$  small has the same problem as the 2HDM; we need to make use of the extra mixing angles  $\theta_\pm$  to make sure  $h_1$  and  $\eta_1$  have different branching ratios.

In choosing  $\theta_+$  we need to take into account equation (3.49) and make sure that  $\Gamma(Z \rightarrow h_1\eta_1)$  is not too small. We must balance the  $\cos^2(\theta_+ - \theta_-)$  factor there against the fact that if  $\theta_+ = \theta_-$  the  $h_1$  and  $\eta_1$  branching ratios will be the same. Figure 3-9 shows that this is possible. There are regions in the  $\theta_+ - \theta_-$  plane that produces the correct signal branching ratio without exceeding known bounds on  $Z \rightarrow 4\mu$  or the total  $Z$  width. This is true for sizeable ranges of  $\beta$  and  $\gamma$ . For example, with  $\beta = 0.2$ ,  $\gamma = 0.5$ ,  $\theta_+ = 2.7$  and  $\theta_- = 1.6$  we get  $B_{\text{signal}} = 3.58 \times 10^{-4}$ ,  $B(Z \rightarrow 4\mu) = 3.84 \times 10^{-8}$ , and  $B(Z \rightarrow \text{all})_{\text{NP}} = 7.02 \times 10^{-4}$ . Interestingly, meeting all these requirements simultaneously requires  $\eta_1$  to decay to muons and  $b$ -quarks about half and half. With

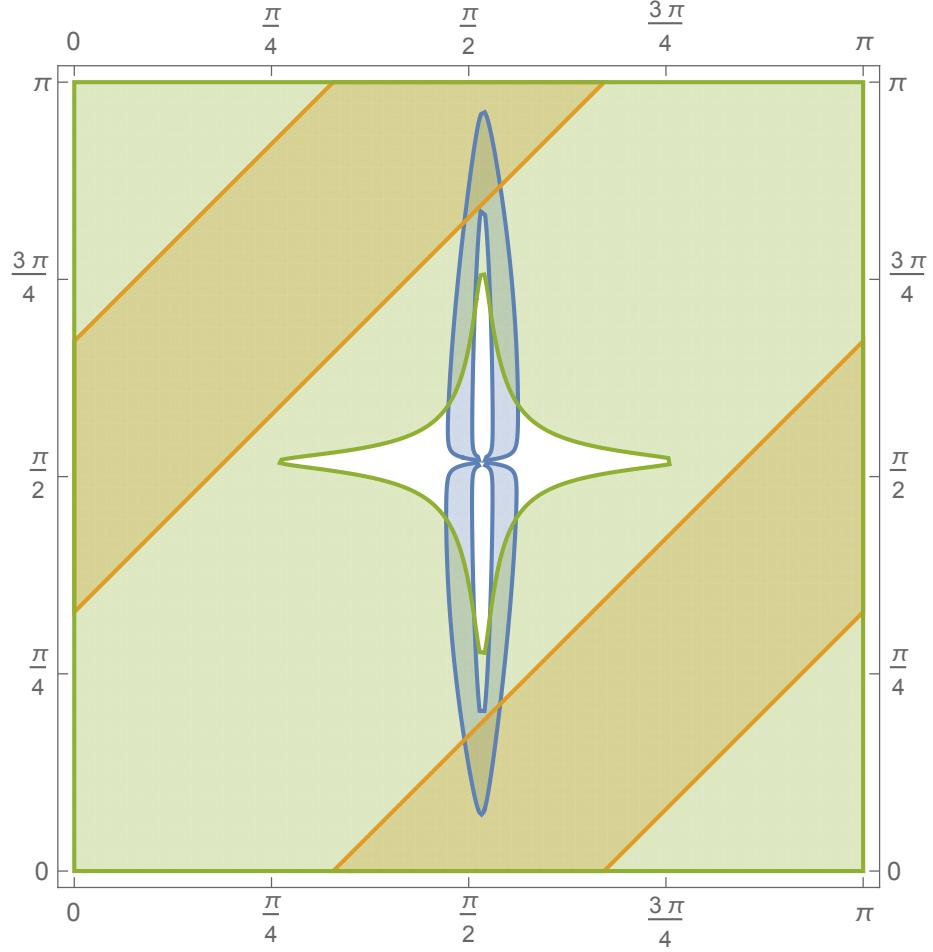


**Figure 3-9:** Constraints on  $\theta_{\pm}$  from bounds on  $Z$  decays for  $\gamma = 0.5$  and  $\beta = 0.1$ . The regions where three constraints are satisfied separately are shown;  $B(Z \rightarrow 4\mu)$  must be less than  $10^{-6}$  (green region), the signal branching ratio  $B(Z \rightarrow 2b2\mu)$  must be in the range  $1 - 9 \times 10^{-4}$  (blue region), and the total  $Z$  branching ratio to new particles must be less than  $9 \times 10^{-4}$  (yellow region). There are two small regions where all three constraints are satisfied.

the numbers above,  $B(\eta_1 \rightarrow \mu^+\mu^-) = 0.51$ , while  $h_1$  goes almost entirely to  $\bar{b}b$ :  $B(h_1 \rightarrow \bar{b}b) > 0.999$ .

### 3.4.2 The charged scalars

There are now two physical charged scalars  $h_1^+$  and  $h_2^+$ , and we must worry about their contribution to the same channel that ruled out the charged Higgs of the 2HDM.

Like in the 2HDM, we have the basic constraint that both charged scalars must have mass greater than half of 125 GeV. Besides this, there are two major possible issues. The extra freedom in the mass mixing angles means that we can possibly avoid the Contur analysis that ruled out the 2HDM, but it also means that one of the charged scalars will not decay predominantly to muons, but more like the charged scalar from a typical 2HDM. The charged scalar that decays to quarks or  $\tau$  leptons is subject to many of the existing searches for a charged Higgs. We will investigate both of these constraints in more detail. Ultimately, the 3HDM is not able to balance the two constraints and so is excluded.

#### Fermionic decays

The charged scalars can decay to lepton-neutrino pairs or to quark pairs. Which fermions each charged scalar decays to is determined by  $\theta_c$ , and  $\beta$  and  $\gamma$ . If  $\theta_c$  is close to  $\theta_-$  then  $h_{1,2}^+$  will have similar fermionic decay rates to  $\eta_{1,2}$ . On the other hand, if  $\theta_c \simeq \theta_- \pm \pi/2$  then  $h_{1,2}^+$  will decay like  $\eta_{2,1}$ .

If one of the charged scalars has large branching ratios to quarks the typical constraints from charged higgs searches apply as in 3.3.2, and it must be quite massive. If it decays largely to  $\mu\nu_\mu$  then its mass must be at least 95 GeV or so, following the same arguments as in the 2HDM case.

However, like in the 2HDM, once the mass of a charged Higgs is above 100 GeV or so the fermionic decays are swamped by decays to  $\eta_1 W^+$  and  $h_1 W^+$ . Figure 3-10



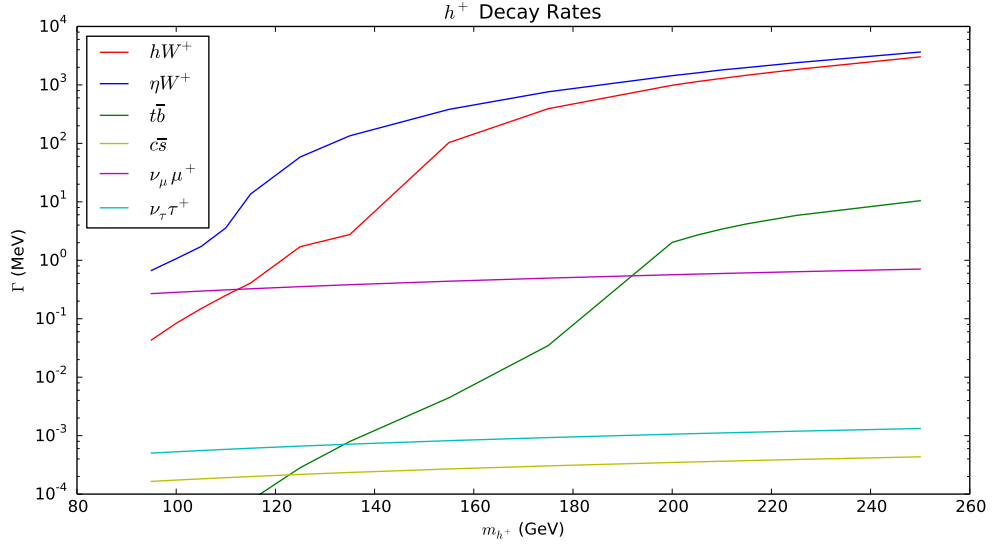


**Figure 3.10:** The decay rates of a charged Higgs  $h^+$  in the 2HDM with  $m_\eta = 30$  GeV,  $m_h = 60$  GeV, and  $\beta$  chosen so that  $h^+$  and  $\eta$  both decay muons much more than other fermions. A charged Higgs heavier than 100 GeV or so decays mainly to a lighter scalar plus a  $W$  boson, despite large muon Yukawa couplings. The situation in the 3HDM is similar for at least one charged scalar.

shows how the fermionic decays become irrelevant for most of the allowed mass range.

This brings us back to the problem of the LHC  $W^*$  data.

### $W^*$ processes

For considering  $h^+ \rightarrow W^+ h$  decays, the relevant couplings in the 3HDM are

$$\mathcal{L}_{Wss} = \sum_{ij} igW^{+\mu} \left( (W_c W_+^T)_{ij} h_i^- \overleftrightarrow{\partial}_\mu h_j + i(W_c W_-^T)_{ij} h_i^- \overleftrightarrow{\partial}_\mu \eta_j \right) \quad (3.54)$$

In the alignment limit this means the  $W$  couples to  $h_1 h_1^+$  and  $h_2 h_2^+$  with the mixing factor  $\cos(\theta_c - \theta_+)$ , and to  $h_2 h_1^+$  etc. with  $\sin(\theta_c - \theta_+)$ , and likewise for the  $\eta$ 's with  $\theta_-$  instead of  $\theta_+$ .

We can use this mixing factor to suppress the processes in the Contur analysis, that depend on  $W^{*+} \rightarrow h_i^+ \eta_j$  and  $h_i^+ \rightarrow \eta_j W^+$ . Assuming that the rate of  $\eta_1 \rightarrow \mu^+ \mu^-$

is sizeable, the worst process is  $W^{+*} \rightarrow \eta_1 h_i^+ \rightarrow \eta_1 \eta_1 W^+$ . For  $h_1^+$  this has a rate proportional to  $\cos^4(\theta_c - \theta_-)$ , and  $\sin^4(\theta_c - \theta_-)$  for  $h_2^+$ .

Generically, if we try to use  $\theta_c$  to tune away one of the  $h_i^+ \rightarrow \eta_1 W^+$  decays the other will still be large, and the Contur analysis will rule out the 3HDM. There are some tricky possibilities. By taking  $\theta_c - \theta_- \simeq \pi/4$  we could reduce both the  $h_1^+$  and  $h_2^+$  contributions to the  $W \rightarrow 4\ell$  process by 1/4. Additionally, since the analysis in section 3.4.2 suggests that  $B(\eta_1 \rightarrow \mu^+ \mu^-)$  the contribution may be lower than assumed for the Contur analysis (Brooijmans et al., 2018a).

We have not used Contur to do an explicit analysis of the 3HDM contribution to  $W^* \rightarrow 4\ell$ , despite these possibilities, for two reasons. The first is that the Contur analysis so thoroughly excluded a  $h^+$  that there is no obvious avenue for exploration; the factors of 1/2 and 1/4 in the previous paragraph offer little to no hope against the theory-to-data ratios of 20 to  $> 100$  discovered in the Contur analysis. Especially when we consider all the possible excluded fermionic decays on the other hand. The second reason is that it hardly matters if we fix this problem — the 3HDM, and all other Higgs doublet models, has another critical flaw in the form of triple scalar decays interactions. We will cover these next.

### 3.4.3 The neutral scalars

The 3HDM has two additional neutral bosons besides  $h_1$  and  $h_2$ . Three of the neutral scalars have their masses fixed by the data —  $m_{\eta_1} = 30$  GeV,  $m_{h_1} \simeq 55$  GeV, and  $m_H = 125$  GeV. The remaining masses are constrained by perturbative unitarity and positivity considerations. We shall see that they both must have mass less than about 200 GeV, which allows them to show up and be excluded by existing searches

## Unitarity and positivity bounds

The quartic couplings of the 3HDM,  $\lambda_{11}$  etc., are determined by the physical masses of the Higgs bosons, along with the mixing angles and vacuum expectation values of the theory. However, for the theory to be sensible they must also satisfy certain other bounds.

Lee, Thacker, and Quigg showed that if the quartic couplings of a Higgs doublet model are too large then they can produce four-scalar scattering amplitudes that violate partial-wave unitarity bounds (Lee et al., 1977). Theories that violate these bounds must either be non-unitary (which is right out!) or non-perturbative, which is certainly beyond the scope of this dissertation, and probably excluded experimentally.

The unitarity constraints on the 3HDM can be generalized by the procedure for the 2HDM found in (Kanemura et al., 1993). A set of discrete symmetries in the scalar potential allows us to reduce the task to constraining the eigenvalues of a few  $3 \times 3$  matrices and  $2 \times 2$  matrices, which are not shown here.

A sensible Higgs theory also requires that the scalar potential be bounded from below. This requires the potential to be positive at large Higgs field strength for all orientations of the three Higgs fields. We can again obtain the 3HDM constraints by generalizing the 2HDM procedure found in (Branco et al., 2012). This requires

$$\begin{aligned}\lambda_{ij} &> \lambda_{ii} + \lambda_{jj} \\ \lambda_{ij} &< 2\sqrt{\lambda_{ii}\lambda_{jj}}\end{aligned}\tag{3.55}$$

for all  $i, j$ .

Figure 3-11 shows the mass ranges allowed by these two constraints. Neither  $m_{h_2}$  or  $m_{\eta_2}$  can be much greater than 100 GeV without violating the bounds. The actual upper bounds depend on the other parameters of the model in ways that are too complicated to investigate in detail, but they are mostly insensitive for the range of

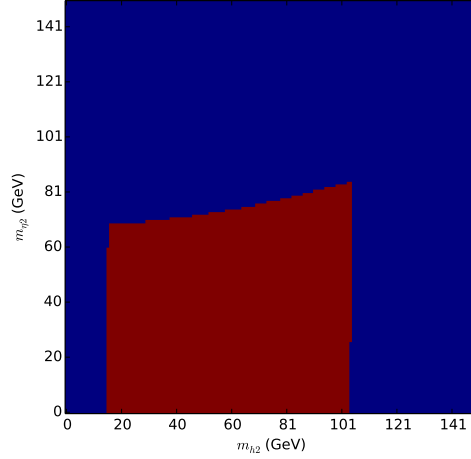


**Figure 3-11:** Bounds on  $m_{h_2}$  and  $m_{\eta_2}$  from the positivity and unitarity conditions on the 3HDM quartic couplings. Neither coupling can be much more than 100 GeV, putting both in reach of current experiments. The other model parameters used are the same as in figure 3-9

parameters that we use.

### Triple scalar interactions

Once the doublets of the 3HDM get a vacuum expectation value the quartic part of the scalar potential generates cubic interactions between the Higgs bosons. These can be quite large, and they are difficult to avoid, especially since we require at least one relatively light neutral boson with  $m = 30$  GeV.

The first dangerous decay is  $H_{125} \rightarrow \eta_1 \eta_1$ , and to a lesser extent,  $H_{125} \rightarrow h_1 h_1$ . As long as  $m_{h_2}, m_{\eta_2} > 0.5 \times 125$  GeV those decays don't happen. In the Standard Model the decay width of Higgs boson is thought to be no more than a few MeV, and current experiments agree (Particle Data Group, 2016a; CMS Collaboration, 2016). Since the Higgs decays to scalars generically have strength

$$\Gamma(H \rightarrow ss) = \frac{m_H}{16\pi} \left( \frac{g_{Hss} v}{m_H} \right)^2 \quad (3.56)$$

if  $\Gamma(H \rightarrow ss) \ll 1 \text{ MeV}$  we must have  $g_{Hss} \ll 1 \times 10^{-2}$  for all pairs of scalars lighter than 61.25 GeV. However, the triple scalar couplings are generically  $\mathcal{O}(1)$  or larger. Scanning carefully over the angles  $\Theta$  and  $\beta$  show that it is possible to choose parameters so that  $g_{H\eta_1\eta_1}$  and  $g_{Hh_1h_1}$  are small enough ( $g_{Hh_1h_1}$  does not need to be quite so small because when  $m_{h_1} \simeq 60 \text{ GeV}$  that decay is also suppressed by phase space). However, it is an extremely small parameter range that successfully suppresses these two decays. This is no sense a natural choice of parameters. As in the 2HDM, there is no symmetry that forces this parameter choice, and both parameters run independently, meaning the two coefficients can only be suppressed at a particular scale — they will be larger when measured at a different scale.

However, There are other dangerous decays. The fact that  $m_{h_2}, m_{\eta_2} > 60 \text{ GeV}$  means that  $h_1$  can decay to  $\eta_1\eta_1$ , and possibly  $h_1h_1$ , while  $\eta_2$  can possibly decay to  $\eta_1h_1$ . The  $\eta_1\eta_1$  is especially dangerous as  $\eta_1$  decays significantly to  $\mu\mu$ , and  $H \rightarrow 4\mu$  was one of the principal search channels for the Higgs boson.

If we do some parameter-counting we can see a problem. The 3HDM potential is specified by 19 parameters: nine mass terms and nine  $U(1)^3$  symmetric quartic couplings, and possibly one  $L$  parameter. The physical parameters of the theory are also 18. There are the three vevs (or  $v$  and the two angles  $\beta$  and  $\gamma$ ). There are two  $\eta$  masses and one  $\eta$  mixing angle, and likewise two charged masses and one  $\eta$  mixing angle. There are also three scalar masses and three mixing angles, making 15 or 16 physical parameters total.

This means that the values of the triple-scalar couplings are fixed in terms of the physical masses and mixing angles. The  $g_{h\eta\eta}$  couplings depend only on the diagonal quartic couplings and the combinations  $\lambda_{ij} + \tilde{\lambda}_{ij}$ , and possibly the  $L$  coupling. Hence the couplings depend only on the neutral masses and mixing angles and the vacuum expectation values.

Three of the five neutral masses are fixed by experiment; 30 GeV,  $\sim 55$  GeV, and 125 GeV. Three of the four mass mixing angles are also highly constrained:  $\Theta$  needs to be near 0 or  $\pi$ , and  $\theta_+$  and  $\theta_-$  are constrained by the signal and  $Z$  width as in section 3.4.1. That leaves the mixing angle  $\psi$ , the two vacuum expectation value angles  $\beta$  and  $\gamma$ , and possibly  $L$  as independent parameters, three or four in total.

On the other hand, we need to tune away at least three triple-scalar couplings. If  $m_{h_2} \geq 120$  GeV or  $m_{\eta_2} \geq 90$  GeV then we likely also need to tune away  $g_{h_2 h_1 h_1}$  and  $g_{\eta_2 h_1 \eta_1}$ . Numerical scans suggest that even if there is a choice of parameters that makes these vanish, it is an extremely narrow range.

### 3.5 Conclusions

At this point we leave off investigating scalar models for the dimuon resonance. The initial appeal of scalar models is their straightforward-ness and how the relationship between fermion masses and couplings make it easy to explain flavor-non-universal effects. But we have seen that even the most minimal scalar models either do not have enough freedom in their couplings to explain the theory, or add too many unobserved particles without means to hide them from experiments.

Extending the 2HDM to a 3HDM added extra degrees of freedom that allowed us to correctly explain the signal without disturbing the  $Z$  width. But it also added too many particles like the  $h_2$  and an extra  $h^+$  that cannot evade detection. As far as we can tell, extending the model further would only make these problems worse.

Scalar models that have light scalars will naturally have upper limits for at least some of their other scalars, as we saw in the 3HDM. Perturbativity and positivity bounds constrain the size of quartic couplings, but quartic couplings are generically expressible in terms of differences of squared masses. Hence, we expect that it is not possible to hide additional scalar states by making them very massive while keeping

the 30 GeV scalar.

What's more, we see no indication that there are other ways to hide the decays of the additional scalars. The triple-scalar interactions exist even with additional symmetries added to the theory, as do the couplings to the weak bosons. And the combined requirements of matching physical observables and avoiding unitarity bounds suggests that there are simply not enough degrees of freedom to tune away all the bad decays.

The experimental results presented in (Heister, 2016) are intriguing, and call for more data. This is especially true in light of the difficulty of devising a simple theoretical model for the result. More data and more theoretical input are required to fully understand it.

## List of Bibliographic Abbreviations

Ann. Rev. Nucl. Part. Sci.	...	Annual Review of Nuclear and Particle Science
Chin. Phys.	...	Chinese Physics
Eur. Phys. J.	...	European Physical Journal
Incl. Instrum. Meth.	...	Nuclear Instruments and Methods in Physics
JHEP	...	Journal of High Energy Physics
Lect. Notes Phys.	...	Lecture Notes in Physics
Nucl. Phys.	...	Nuclear Physics
Phys. Lett.	...	Physics Letters
Phys. Rept.	...	Physics Reports
Phys. Rev.	...	Physical Review
Phys. Rev. Lett.	...	Physical Review Letters
PoS	...	Proceedings of Science



## References

- Aad, G. et al. (2016). Measurements of the Higgs boson production and decay rates and coupling strengths using pp collision data at  $\sqrt{s} = 7$  and 8 TeV in the ATLAS experiment. *Eur. Phys. J.*, C76(1):6.
- ALEPH Collaboration (1990). ALEPH: A detector for electron-positron annihilations at LEP. *Nucl. Instrum. Meth.*, A294:121–178. [Erratum: Nucl. Instrum. Meth.A303,393(1991)].
- Appelquist, T., Soldate, M., Takeuchi, T., and Wijewardhana, L. C. R. (1988). EFFECTIVE FOUR FERMION INTERACTIONS AND CHIRAL SYMMETRY BREAKING. In *12th Johns Hopkins Workshop on Current Problems in Particle Theory: TeV Physics Baltimore, Maryland, June 8-10, 1988*.
- ATLAS Collaboration (2014a). Measurement of Higgs boson production in the diphoton decay channel in pp collisions at center-of-mass energies of 7 and 8 TeV with the ATLAS detector. *Phys. Rev.*, D90(11):112015.
- ATLAS Collaboration (2014b). Measurement of the low-mass Drell-Yan differential cross section at  $\sqrt{s} = 7$  TeV using the ATLAS detector. *JHEP*, 06:112.
- ATLAS Collaboration (2014c). Measurements of Four-Lepton Production at the Z Resonance in pp Collisions at  $\sqrt{s} = 7$  and 8 TeV with ATLAS. *Phys. Rev. Lett.*, 112(23):231806.
- ATLAS Collaboration (2015a). Search for a new resonance decaying to a W or Z boson and a Higgs boson in the  $\ell\ell/\ell\nu/\nu\nu + b\bar{b}$  final states with the ATLAS detector. *Eur. Phys. J.*, C75(6):263.
- ATLAS Collaboration (2015b). Search for high-mass diboson resonances with boson-tagged jets in proton-proton collisions at  $\sqrt{s} = 8$  TeV with the ATLAS detector. *JHEP*, 12:055.
- ATLAS Collaboration (2015c). Search for production of  $WW/WZ$  resonances decaying to a lepton, neutrino and jets in  $pp$  collisions at  $\sqrt{s} = 8$  TeV with the ATLAS detector. *Eur. Phys. J.*, C75(5):209. [Erratum: Eur. Phys. J.C75,370(2015)].
- ATLAS Collaboration (2015d). Search for resonant diboson production in the  $\ell\ell q\bar{q}$  final state in  $pp$  collisions at  $\sqrt{s} = 8$  TeV with the ATLAS detector. *Eur. Phys. J.*, C75:69.

- ATLAS Collaboration (2016). Measurement of total and differential  $W^+W^-$  production cross sections in proton-proton collisions at  $\sqrt{s} = 8$  TeV with the ATLAS detector and limits on anomalous triple-gauge-boson couplings. *JHEP*, 09:029.
- ATLAS Collaboration (2018a). Search for resonant  $WZ$  production in the fully leptonic final state in proton-proton collisions at  $\sqrt{s} = 13$  TeV with the ATLAS detector.
- ATLAS Collaboration (2018b). Searches for heavy  $ZZ$  and  $ZW$  resonances in the  $\ell\ell qq$  and  $\nu\nu qq$  final states in  $pp$  collisions at  $\sqrt{s} = 13$  TeV with the ATLAS detector. *JHEP*, 03:009.
- Bando, M., Kugo, T., Uehara, S., Yamawaki, K., and Yanagida, T. (1985). Is the  $\rho$  meson a dynamical gauge boson of hidden local symmetry? *Phys. Rev. Lett.*, 54:1215–1218.
- Bando, M., Kugo, T., and Yamawaki, K. (1988). Nonlinear realization and hidden local symmetries. *Physics Reports*, 164(4):217 – 314.
- Bardeen, W. A., Hill, C. T., and Lindner, M. (1990). Minimal dynamical symmetry breaking of the standard model. *Phys. Rev. D*, 41:1647–1660.
- Bellazzini, B., Csaki, C., Hubisz, J., Serra, J., and Terning, J. (2012). Composite Higgs Sketch. *JHEP*, 11:003.
- Bellazzini, B., Csáki, C., and Serra, J. (2014). Composite Higgses. *Eur. Phys. J.*, C74(5):2766.
- Branco, G. C., Ferreira, P. M., Lavoura, L., Rebelo, M. N., Sher, M., and Silva, J. P. (2012). Theory and phenomenology of two-Higgs-doublet models. *Phys. Rept.*, 516:1–102.
- Brehmer, J. et al. (2015). The Diboson Excess: Experimental Situation and Classification of Explanations; A Les Houches Pre-Proceeding.
- Brooijmans, G. et al. (2018a). Les Houches 2017: Physics at TeV Colliders New Physics Working Group Report. In *10th Les Houches Workshop on Physics at TeV Colliders (PhysTeV 2017) Les Houches, France, June 5-23, 2017*.
- Brooijmans, G. et al. (2018b). Les Houches 2017: Physics at TeV Colliders New Physics Working Group Report. In *10th Les Houches Workshop on Physics at TeV Colliders (PhysTeV 2017) Les Houches, France, June 5-23, 2017*.
- Brooijmans, M. and Pollard (2015). communication at Les Houches Workshop, *Physics at TeV Colliders*.

- Butterworth, J. M., Grellscheid, D., Krämer, M., Sarrazin, B., and Yallup, D. (2017). Constraining new physics with collider measurements of Standard Model signatures. *JHEP*, 03:078.
- Cheung, K., He, S.-P., Mao, Y.-n., Zhang, C., and Zhou, Y. (2018). Simplest little Higgs model revisited: Hidden mass relation, unitarity, and naturalness. *Phys. Rev.*, D97(11):115001.
- CMS Collaboration. Search for massive WH resonances decaying to  $\ell\nu b\bar{b}$  final state in the boosted regime at  $\sqrt{s} = 8$  TeV. Technical report, CERN.
- CMS Collaboration (2014a). Search for massive resonances decaying into pairs of boosted bosons in semi-leptonic final states at  $\sqrt{s} = 8$  TeV. *JHEP*, 08:174.
- CMS Collaboration (2014b). Search for massive resonances in dijet systems containing jets tagged as W or Z boson decays in pp collisions at  $\sqrt{s} = 8$  TeV. *JHEP*, 08:173.
- CMS Collaboration (2015). Search for a charged Higgs boson in pp collisions at  $\sqrt{s} = 8$  TeV. *JHEP*, 11:018.
- CMS Collaboration (2016). Search for Higgs boson off-shell production in proton-proton collisions at 7 and 8 TeV and derivation of constraints on its total decay width. *JHEP*, 09:051.
- CMS Collaboration (2017a). Measurement of the transverse momentum spectrum of the Higgs boson produced in pp collisions at  $\sqrt{s} = 8$  TeV using  $H \rightarrow WW$  decays. *JHEP*, 03:032.
- CMS Collaboration (2017b). Search for heavy resonances that decay into a vector boson and a Higgs boson in hadronic final states at  $\sqrt{s} = 13$  TeV. *Eur. Phys. J.*, C77(9):636.
- CMS Collaboration (2018a). Search for a heavy resonance decaying to a pair of vector bosons in the lepton plus merged jet final state at  $\sqrt{s} = 13$  TeV. *JHEP*, 05:088.
- CMS Collaboration (2018b). Search for massive resonances decaying into  $WW$ ,  $WZ$ ,  $ZZ$ ,  $qW$ , and  $qZ$  with dijet final states at  $\sqrt{s} = 13$  TeV. *Phys. Rev.*, D97(7):072006.
- Cohen, A. and Georgi, H. (1989). Walking beyond the rainbow. *Nuclear Physics B*, 314(1):7 – 24.
- Cui, Y., Han, Z., and Schwartz, M. D. (2011). W-jet Tagging: Optimizing the Identification of Boosted Hadronically-Decaying W Bosons. *Phys. Rev.*, D83:074023.

- Dercks, D., Moortgat-Pick, G., Reuter, J., and Shim, S. Y. (2018). The fate of the Littlest Higgs Model with T-parity under 13 TeV LHC Data. *JHEP*, 05:049.
- Dimopoulos, S. (1980). Technicolored Signatures. *Nucl. Phys.*, B168:69–92.
- Dimopoulos, S., Raby, S., and Kane, G. L. (1981). Experimental Predictions from Technicolor Theories. *Nucl. Phys.*, B182:77–103.
- Eysermans, J., Morales, M. I. P., and on behalf of the CMS Collaboration (2016). Charged higgs analysis in cms. *Journal of Physics: Conference Series*, 761(1):012030.
- Giudice, G. F. (2013). Naturalness after LHC8. *PoS*, EPS-HEP2013:163.
- Glasgow, S., Smith, D., Pritchett, L., Gardiner, J., and Ware, M. J. (2016). Space-time-resolved quantum electrodynamics: A (1+1)-dimensional model. *Phys. Rev. A*, 93:062106.
- Glashow, S. L. and Weinberg, S. (1977). Natural conservation laws for neutral currents. *Phys. Rev. D*, 15:1958–1965.
- Heister, A. (2016). Observation of an excess at 30 GeV in the opposite sign di-muon spectra of  $Z \rightarrow b\bar{b} + X$  events recorded by the ALEPH experiment at LEP.
- Kanemura, S., Kubota, T., and Takasugi, E. (1993). Lee-Quigg-Thacker bounds for Higgs boson masses in a two doublet model. *Phys. Lett.*, B313:155–160.
- Ko, P., Li, J., and Yu, C. (2016). Implication of the ALEPH 30 GeV dimuon resonance at the LHC.
- Lane, K. (1974). Asymptotic freedom and goldstone realization of chiral symmetry. *Phys. Rev. D*, 10:2605–2618.
- Lane, K. and Martin, A. (2009). An Effective Lagrangian for Low-Scale Technicolor. *Phys. Rev.*, D80:115001.
- Lane, K. and Pritchett, L. (2016). Heavy Vector Partners of the Light Composite Higgs. *Phys. Lett.*, B753:211–214.
- Lane, K. and Pritchett, L. (2017a). The 30 GeV Dimuon Excess at ALEPH.
- Lane, K. and Pritchett, L. (2017b). The light composite Higgs boson in strong extended technicolor. *JHEP*, 06:140.
- Lee, B. W., Quigg, C., and Thacker, H. B. (1977). Weak interactions at very high energies: The role of the higgs-boson mass. *Phys. Rev. D*, 16:1519–1531.
- Marzocca, D., Serone, M., and Shu, J. (2012). General Composite Higgs Models. *JHEP*, 08:013.

- Nambu, Y. and Jona-Lasinio, G. (1961). Dynamical model of elementary particles based on an analogy with superconductivity. i. *Phys. Rev.*, 122:345–358.
- Particle Data Group (2016a). Review of Particle Physics. *Chin. Phys.*, C40(10):100001.
- Particle Data Group (2016b). Review of Particle Physics. *Chin. Phys.*, C40(10):100001.
- Pendleton, B. and Ross, G. (1981). Mass and mixing angle predictions from infra-red fixed points. *Physics Letters B*, 98(4):291 – 294.
- Peskin, M. E. and Takeuchi, T. (1992). Estimation of oblique electroweak corrections. *Phys. Rev. D*, 46:381–409.
- Reuter, J., Tonini, M., and de Vries, M. (2013). Little Higgs Model Limits from LHC - Input for Snowmass 2013. In *Snowmass 2013: Workshop on Energy Frontier Seattle, USA, June 30-July 3, 2013*.
- Schael, S. et al. (2006). Precision electroweak measurements on the  $Z$  resonance. *Phys. Rept.*, 427:257–454.
- Schmaltz, M. and Tucker-Smith, D. (2005). Little Higgs review. *Ann. Rev. Nucl. Part. Sci.*, 55:229–270.
- Sikivie, P., Susskind, L., Voloshin, M., and Zakharov, V. (1980). Isospin breaking in technicolor models. *Nuclear Physics B*, 173(2):189 – 207.
- Takeuchi, T. (1989). Analytical and Numerical Study of the Schwinger-dyson Equation With Four Fermion Coupling. *Phys. Rev.*, D40:2697.
- Veltman, M. (1977). Limit on mass differences in the weinberg model. *Nuclear Physics B*, 123(1):89 – 99.

# CURRICULUM VITAE

